Principles underlying the development and organization of feature maps in the visual cortex

by

Brandon J. Farley

BS Biochemistry
University of Michigan, 1999

Submitted to the Department of Brain and Cognitive Sciences in partial fulfillment of the requirements for the degree of

Doctor of Philosophy in Neuroscience

at the

Massachusetts Institute of Technology

February, 2007

Signature of Author:_____
Department of Brain and Cognitive Sciences
November 30th, 2006

Certified by:_____
Mriganka Sur
Sherman Fairchild Professor of Neuroscience
Head, Department of Brain and Cognitive Sciences
Faculty Advisor

Accepted by:_____
Matt Wilson
Professor of Neuroscience
Chairman, Committee for Graduate Studies

Principles underlying the development and organization of feature maps in the visual cortex

by

Brandon J. Farley

Submitted to the Department of Brain and Cognitive Sciences in partial fulfillment of the requirements for the degree of Doctor of Philosophy in Neuroscience

Abstract

A fundamental question in neuroscience is how sensory information is represented in the brain. In particular, what principles guide the spatial organization of neurons with regard to their receptive field properties, and how is this organization established mechanistically? The visual cortex serves as a model area to address these questions, but whether general principles can explain the layouts of cortical maps, such as those of visual space and of specific response features, remains unresolved. We find that in primary visual cortex of ferret, the layout of each map is inter-dependent with that of the others. First, we find a strong anisotropy in the visual map, such that receptive field positions change more rapidly along one axis of cortex; and importantly, along the axis where visual space changes rapidly, the feature maps of orientation, ocular dominance, and spatial frequency change slowly. Second, orientation, ocular dominance, and spatial frequency maps have local spatial relationships with each other: in areas of cortex where one feature changes rapidly, the other features change more slowly. Each of these relationships are well-explained by a dimension-reduction model of cortex. This suggests that the constraints which drive map formation in the model, continuity (representing each feature smoothly across cortex) and coverage uniformity (representing each feature combination to an equal extent), may play a central role in determining the functional organization of visual cortex. To explore the mechanisms giving rise to the map relationships, we alter the expression of one feature map early in development and measure the impact on the layouts of the remaining maps. We find that alteration of the ocular dominance map, due to neonatal monocular enucleation, does not prevent the formation of the orientation and spatial frequency maps, but it does alter their spatial relationships. The highest gradient regions of the spatial frequency map have a stronger tendency to avoid high gradient orientation regions, and the contours of the two maps have a greater tendency to cross orthogonally. The results are consistent with the predictions of a dimension-reduction model for removing a feature map, suggesting that as a result of altered input patterns, the cortex can rearrange over the time scale of development according to a dimension-reduction strategy.

Thesis supervisor: Mriganka Sur
Title: Sherman Fairchild Professor of Neuroscience

Acknowledgements

I am especially grateful to Mriganka Sur and to the members of his laboratory; these are the people with whom I've spent the most time during graduate school, and they made the experience rewarding on many different levels. Mriganka was an effective advisor and mentor. He gave me room to develop as an independent scientist and thinker, but just as importantly focused my efforts when it was necessary. Our meetings were productive and enjoyable, and I usually left his office with renewed enthusiasm. Mriganka's enthusiasm permeated the laboratory, and it was a positive environment within which to work. I received helpful advice and technical assistance from nearly everyone that passed through the laboratory. I would especially like to thank Hongbo Yu, with whom I performed a majority of my experiments. Hongbo is very talented with experiments and data analysis, and I was lucky to learn from him—he taught me a great deal. Many other members of the lab were of great help. James Schummers provided a significant amount of technical assistance and sound experimental advice. Jitendra Sharma was the first to introduce me to experiments in the lab, and Christine Waite provided invaluable support during my first years. Special thanks also to Beata Jarosiewicz, who arrived in the laboratory as I was nearing completion of graduate school, but provided me very useful advice with my projects. I would also like to acknowledge Alvin Lyckman, Cathy Leamey, Dezhe Jin, Peter Wiesing, David Lyon, and Beau Cronin for effective collaborations, and for helpful advice on experiments and techniques. There were many others that I came into contact with who were supportive and generous, and I am grateful for this.

I would also like to thank Chris Moore, Matt Wilson, and Clay Reid, for agreeing to serve on my committee and for giving me helpful mentoring and career advice. Also, I would like to thank Martha Constantine-Paton and the members of her laboratory, especially Matt Townsend. I worked in Martha's laboratory when I first arrived at MIT, and it was a great experience and introduction to MIT.

The graduate students at MIT were great friends, especially the members of my class. My first couple of years at MIT spent with them were some of the best for me. These and many others at MIT kept me sane, especially during those painful times when experiments were failing! I would especially like to acknowledge Nathan Wilson, Amy Pooler, Emily Hueske, Charlene Ellsworth, Marnie Philips, Beata Jarosiewicz, and Monique Brouillette. They remain great friends and colleagues. Finally, my family has been great support to me during my time at MIT. I wouldn't have made it into graduate school without the tremendous inspiration of my father and the rest of my family; they motivated me and supported me. And though I wish that my visits home could have been more frequent during the past years, they were always enjoyable and provided grounding.

Table of Contents

CHAPTER 1: The coordinated mapping of visual space and stimulus features in visual cortex

SUMMARY

Whether general principles can explain the layouts of cortical maps, such as those of visual space and of specific response features, remains unresolved. We find that in primary visual cortex of ferret, the layout of each map (including visual space) is inter-dependent with that of the others, as predicted by a "dimension-reduction" model. The representation of visual space is anisotropic, with the elevation and azimuth dimensions having different magnification. This anisotropy is reflected in the orientation, ocular dominance, and spatial frequency domains, which are elongated such that the high gradient axes of the visual space and other features maps are orthogonal. The other feature maps are also strongly inter-dependent; their high gradient locations avoid one another on average, but when high gradient regions do coincide, the directions of maximal gradient are orthogonal. Our results demonstrate a clear influence of the visual space map on each feature map. In turn, the local representation of visual space is smooth in the case where many features are mapped within a cortical area.

INTRODUCTION

One of the keys to understanding cortical function is defining the rules that govern the organization of neurons according to their response properties. As some cortical areas are traversed, neuronal response properties change in a regular manner, forming systematic maps with highly stereotyped structures. Additionally, more than one

response property can be mapped simultaneously within an area, as has been shown in visual, somatosensory, and auditory cortex (Hubel and Wiesel, 1963; Sur et al., 1981; Linden and Schreiner, 2003; Friedman et al., 2004). What determines the forms that these maps take? One theoretical proposal is that the structures reflect constraints imposed by "dimension-reduction", or a need to smoothly map several (more than two) response properties onto a two-dimensional cortical surface (Kohonen, 1982b; Durbin and Mitchison, 1990; Obermayer et al., 1990; Swindale, 1991). An explicit goal of dimension-reduction models is to minimize the connection length between neurons that share similar response properties, an approach also used in "elastic net" models (Goodhill and Willshaw, 1990) and "wire-length minimization" algorithms (Koulakov and Chklovskii, 2001) for explaining the structure of cortical columns.

Primary visual cortex (V1) is a model area for examining this issue since neurons in the region are mapped according to several well-understood response properties (i.e., features) including receptive field position, ocular dominance, orientation and spatial frequency. The columnar organization of the area implies that the multiple feature maps are superimposed over a single two-dimensional cortical sheet. To accommodate the representation of all the features, dimension-reduction models predict specific spatial relationships between feature maps (Durbin and Mitchison, 1990; Obermayer et al., 1990). However, recent studies have questioned the relevance of such principles to cortical maps, in particular the map of visual space (Das and Gilbert, 1997; Bosking et al., 2002; Buzas et al., 2003).

A major prediction of dimension-reduction models is that at locations where the value of a given feature changes rapidly across cortex, that of other independent features

should change slowly; that is, there is a negative correlation between the gradient magnitudes of different maps (Obermayer et al., 1992). A corollary to this principle is that at locations where the gradient magnitudes of two features are necessarily high, the contours of the two maps, and hence their gradient directions, are orthogonal. Experimental studies have demonstrated relationships for some pairs of functional maps consistent with these predictions. For example, locations where the preferred orientation map gradient is high, i.e. orientation pinwheels, are situated towards the center of ocular dominance and spatial frequency columns, where the latter maps have low gradients. Additionally, ocular dominance and orientation contours intersect near-orthogonally at the edges of ocular dominance columns, where the ocular dominance gradient is high (Blasdel and Salama, 1986; Bartfeld and Grinvald, 1992; Obermayer and Blasdel, 1993; Hubener et al., 1997).

In contrast, results from experiments that have examined the retinotopic and orientation maps appear inconsistent with the model predictions: whereas the original models (Durbin and Mitchison, 1990; Obermayer et al., 1990) predicted a negative correlation between the gradients of these two maps, such that receptive field locations should change slowly in locations where orientation preferences change rapidly, experimental results show either a positive correlation (Das and Gilbert, 1997) or no correlation (Bosking et al., 2002; Buzas et al., 2003). But the original models included only retinotopy and orientation as mapped features; more recent studies have demonstrated that the predicted relationships between the retinotopic and other maps are dependent on the number of features that are included in the model simulations (Swindale, 2004). It remains to be examined how experimentally-measured relationships

compare to model predictions, when the model simulations include all of the features known to be mapped within the cortical region of question.

We reasoned that an examination of the relationships between the retinotopic and other maps in V1 should address three related questions: (1) does the overall structure of the retinotopic map influence the mapping of other features, in a manner consistent with dimension-reduction principles; (2) are other feature maps related to each other by these principles, and (3) is the mapping of other features in turn reflected in the local structure of the retinotopic map? Since the relationships between the retinotopic and other maps have proven elusive, we examined a case where the dimension-reduction model makes a clear prediction: when the retinotopic map magnification differs for the two axes of visual space, the model predicts clear consequences for the remaining maps. The examination of maps in V1 of ferrets provided a unique opportunity to test this prediction. We found that indeed, the retinotopic map powerfully influences the layout of other maps, as the model predicts, and that the other maps maintain specific local relationships with one another. Finally, the retinotopic map is predicted to be locally smooth, in the case where three other variables are mapped within a cortical area. Our results demonstrate a strong inter-dependence between each visual cortex functional map, including the retinotopic map.

METHODS

Computational model. To simulate the mapping of response features across the cortex we used the Kohonen self-organizing map algorithm (Kohonen, 1982a), as modified by Obermayer (Obermayer et al., 1992). A multi-dimensional feature space is defined, where each stimulus is represented as a multi-component vector

$\mathbf{V}_s = (x_s, y_s, q_s\cos(2\phi_s), q_s\sin(2\phi_s), z_s, \mathrm{f}_s)$ within this space. Here *x* and *y* correspond to azimuth and elevation retinotopic position, respectively, *q* is orientation selectivity, ϕ is orientation preference, *z* is ocular dominance, and *f* is spatial frequency preference. The feature *x* ranges from (0,*X*), *y* from (0,*Y*), *q* from (0,*Q*), ϕ from (0,π), *z* from (0,*Z*), and *f* from (0,*F*). The stimuli are mapped onto a cortical surface, which is represented as a two-dimensional grid of points with size *N* X *N*. Each cortical point $\mathbf{r} = (i, j)$ has a receptive field defined as $\mathbf{W}_r = (x_r, y_r, q_r\cos(2\phi_r), q_r\sin(2\phi_r), z_r, f_r)$. At the beginning of the simulation the maps are initialized as $x_r = i/N$, $y_r = j/N$, $q_r = Q/2$, $\phi_r = \pi/2$, $z_r = Z/2$, and $f_r = F/2$. The maps are formed through iterations (1.5 million) of three steps. (1) A stimulus $\mathbf{V}_s$ is chosen one at a time randomly from the complete feature space, assuming uniform distributions of each feature. (2) The cortical point $\mathbf{r}_c = (i_c, j_c)$, whose preferred features are closest to those of the stimulus, is identified as the "winner". The closeness of the feature is measured with the Euclidian distance between the vectors $|\mathbf{V}_s - \mathbf{W}_r|^2$. (3) The preferred features of the cortical points are updated according to the equation $\Delta\mathbf{W}_r = \alpha h(\mathrm{r})(\mathbf{V} - \mathbf{W}_r)$. Here α is the learning rate, r is the cortical distance between a given cortical point (i, j) and the winner $\mathbf{r}_c$, and $\mathrm{h}(\mathrm{r}) = \exp(-\mathrm{r}^2/\sigma^2)$ is the neighborhood function. The neighborhood function restricts the changes in receptive fields to those cortical points nearby the winner (in cortical distance).

We used the following parameters for the simulations: $N = 513$, $\sigma = 5$, $\alpha = 0.02$, $X = \rho N$, $Y = N$, $Q = 40$, $Z = 60$, $F = 60$. Here ρ is the elevation:azimuth magnification ratio of the retinotopic map, and was chosen to match the magnification anisotropy that exists in the ferret or to simulate an isotropic map. Thus, the anisotropy

was achieved by mapping different extents of azimuth and elevation visual space onto a square cortex. Alternately, a similar anisotropy could be obtained by simulating the mapping of an isotropic visual space onto an oval-shaped model cortex; similar map relationships resulted in both cases (data not shown). The maps displayed and analyzed were derived from a portion of the model cortex that did not include the boundary regions. We found that the gradient vector relationships between pairs of maps persisted for a range of simulation parameters (Q from 30 to 50, Z or F from 50 to 80, and σ from 5.0 to 5.5), while the degree or strength of these relationships systematically varied within these ranges. We were able to produce realistic orientation maps only when the orientation selectivity (q) was allowed to vary across the cortex; a number of parameter and annealing regimes were attempted to achieve a fixed orientation selectivity. The parameters used in the manuscript were chosen so that the relative wavelengths of multiple maps, as well as the orientation pinwheel density, matched between the simulation and experimental data. We found that while the map structures changed significantly during the initial simulation iterations, they did not change greatly between 1.5 million (the number used in this study) and 6 million (the maximum number tested) iterations.

Animals. Ten adult ferrets were used in these experiments. Animals were prepared for acute experiments according to protocols approved by MIT's Animal Care and Use Committee. Details have been described (Rao et al., 1997). Anesthesia was induced with ketamine (25 mg/kg) and xylazine (1.5 mg/kg) and maintained with isofluorane (1.0% to 1.5% in 70:30 mixture of N_2O/O_2) delivered through a tracheal cannula using artificial respiration. Fluid maintenance was achieved with a 50:50 mixture

of 5% dextrose and lactated Ringer's solution, supplemented with Norcuron (0.25 mg/kg/hr) for paralysis. Expired CO_2 was maintained at 4% and the anesthesia level was monitored continuously. A craniotomy and durotomy were performed to expose V1. A chamber was mounted on the skull around the exposed region and filled with agarose (1.5% in saline). This was covered by a cover glass and then silicone oil.

Optical imaging. The details of optical imaging have been described (Dragoi et al., 2000). The cortex was illuminated with 630 nm light. Images of cortical reflectance were obtained (at 70 pixels/mm) using a slow-scan video camera equipped with a tandem macro-lens arrangement, then digitized and fed into a computer (Imager 3001, Optical Imaging, Mountainside, NJ). The camera was focused 500 μm below the cortical surface. Stimuli were generated using CRS (Cambridge Research Systems Ltd., Rochester, Kent, UK) on a CRT monitor that was placed at 57 cm from the eyes and covered 40° (horizontal) × 30° (vertical) of the visual field.

Orientation, spatial frequency, and ocular dominance maps. For orientation and spatial frequency maps, stimuli were presented binocularly, and consisted of drifting, full-field square-wave gratings having one of 4 orientations (separated by 45°), one of four fundamental spatial frequencies (0.08, 0.125, 0.225, or 0.375 cycles/deg), and a temporal frequency of 1Hz. Monocularly presented drifting gratings (4 orientations, spatial frequency of 0.125 cycles/deg) were used to obtain ocular dominance maps. The grating stimuli were presented in pseudorandom order, each for 5 seconds during which cortical images were captured followed by 7 seconds of a blank screen. Single-condition orientation maps were obtained by subtracting the response to all orientations combined ("cocktail blank") from the response to each single orientation. To produce orientation

angle maps, filtered single-condition orientation maps (Gaussian filter, standard deviation of 0.1 mm) were summed at each pixel vectorially; the angle of the resultant vector indicates the preferred orientation at that pixel. To obtain an ocular dominance map, we subtracted the average of all filtered orientation single-condition maps obtained with one eye from those obtained with the other eye. Similarly, the spatial frequency map was calculated by subtracting the average of all filtered orientation single-condition maps obtained with high spatial frequency (0.375 or 0.225 c/deg) stimuli from those obtained with low frequency (0.125 or 0.08 c/deg) stimuli. Given the observation that most cortical locations in ferret respond preferentially to a narrow range of intermediate spatial frequencies (Baker et al., 1998), we favored representing spatial frequency maps as differential maps rather than continuous maps of absolute preference. We found that each pair of high minus low spatial frequency cocktail blanks produced a similar spatial frequency map, and that the map was largely independent of the stimulus orientation used to create it (Supplementary Figure 2A).

Retinotopic maps. To generate retinotopic maps, we used a periodic visual stimulation paradigm (presented to the contralateral eye) combined with continuous data acquisition optical imaging (Kalatsky and Stryker, 2003). For azimuth maps, the stimulus consisted of elongated vertical bars (1°×30°) separated by 20°, which each flashed at 3Hz and shifted their azimuthal location by 0.66° every second. A given location of space was thus stimulated every 30 seconds. Light-reflectance images were captured at 1 Hz. For elevation maps, the stimulus consisted of elongated horizontal bars (1°×40°) separated by 15°, which drifted continuously at a rate of 1°/sec in the elevation dimension. Each location of space was thus stimulated every 15 seconds. Images were captured at 3 Hz.

Each retinotopic stimulus trial consisted of 8-24 cycles of stimulation, after which a blank screen was shown for 25 seconds, and each experiment consisted of 5-15 such trials. The light-reflectance data were averaged in phase over all trials and cycles. Each frame of this averaged response (30 frames total for elevation; 45 for azimuth) thus consisted of the activation pattern resulting from stimulation during a restricted phase the stimulus cycle. To obtain the retinotopic single-condition maps, each frame was subtracted from the mean of all the frames and then filtered (Gaussian filter, standard deviation of 0.06 mm). To determine each pixel's preferred receptive field position, we calculated the phase of the Fast Fourier Transform (FFT) at the stimulation frequency, on the time-course response of each pixel (Kalatsky and Stryker, 2003). Since the optical imaging signals follow the stimulation with an unknown lag time, this method provides maps of relative rather than absolute retinotopy. All of our analyses rely only on relative retinotopy values; for display purposes, we estimated the absolute values based on published maps of retinotopy in ferret (Law et al., 1988).

Analysis of map structures and relationships. We used identical procedures for analyzing our computational and experimental data. Gradient maps were computed from the low-pass filtered maps of retinotopy, orientation, ocular dominance, or spatial frequency as the two-dimensional spatial derivative at each pixel. Let A(x,y) be the value at a pixel (x,y), $dx = (A(x+1, y) - A(x, y))$ and $dy = (A(x, y+1) - A(x, y))$. Then the gradient vector magnitude at (x,y) is $\sqrt{dx^2 + dy^2}$, and the gradient vector angle is $(180/\pi)\text{a}\tan(dy/dx)$ and ranges from -90 to 90. For orientation dx and dy were corrected to take into account circularity. The gradient magnitude describes how much a feature is changing around a given pixel in the map, and the gradient angle indicates the

axis of cortex along which the feature is changing maximally (and is orthogonal to the map contour at that pixel).

Data used to derive orientation, ocular dominance, and spatial frequency gradients. We chose to calculate the orientation gradient (see Experimental Procedures) from the orientation angle map (the map of ϕ), but the gradient could also have been calculated on the full orientation vector (with length q and angle ϕ) map. For the simulation data, the orientation gradient magnitude differs at certain locations of the cortex (such as at orientation pinwheels) according to these two methods, but is strongly correlated overall. Further, similar relationships exist between the orientation and other maps using both methods (data not shown). The ocular dominance and spatial frequency gradient maps were derived from the ocular dominance and spatial frequency preference maps, respectively.

Data used to derive retinotopy gradients. The retinotopy gradient angle at a pixel was defined as being the direction orthogonal to the elevation gradient angle, and approximates the cortical axis along which retinotopy changes maximally. In the following we explain this calculation. The azimuth gradient is on average four times the magnitude of the elevation gradient (Supplementary Table 1). Further, on average the azimuth gradient is strongly orthogonal to the elevation gradient (Supplementary Table 1 and Supplementary Figure 4A). Thus, the overall retinotopy gradient for a pixel can be defined as parallel to the azimuth gradient at that pixel, or orthogonal to the elevation gradient. Using either definition generates similar conclusions regarding the relationships between the gradient angles of retinotopy and other feature maps; e.g. orientation gradients are on average orthogonal to the azimuth gradients, and in turn parallel to the

elevation gradients (Supplementary Figures 4B-C). We chose to define the retinotopy gradient based on the elevation map because this map was obtained in more cases than the azimuth map was, allowing further quantification of map relationships. Thus, the retinotopy gradient angle at a pixel was defined as being the direction orthogonal to the elevation gradient angle, and approximates the cortical axis along which retinotopy changes maximally. To obtain the retinotopy gradient magnitude at each pixel, we calculated the gradient magnitude separately for both the azimuth and elevation maps and summed them.

Calculation of gradient map relationships. The gradient percentile indicates the percentage of pixels within a region whose gradient is at or below the gradient of the pixel in question. The gradient magnitude comparison of two maps, and the associated plots, were obtained by first grouping the pixels within a region into ten equal-sized bins according to the gradient magnitude percentile of one feature map (the x-axis tick marks indicate the mean percentile for each bin). Then, for all pixels of each bin, the average gradient value (or percentile) of the second feature map was calculated. The gradient intersection angle comparisons of two maps, and the associated plots, were obtained by calculating the pixel-by-pixel difference in gradient directions for two feature maps (which range from 0 to 90 degrees). The percent of total pixels from the region falling in each of nine 10° bins (0-10°, 10-20°, …, 80-90°) is plotted.

Electrophysiology. Multi-unit activity was recorded using tungsten electrodes (1 MΩ; FHC, Bowdoinham, ME) and band-pass filtered. Visual receptive fields were measured using the reverse correlation technique. The stimulus consisted of a 3° × 3° square that pseudo-randomly varied its x and y center position (with 1° resolution) and

contrast (bright or dark) within a 12° × 12° stimulus grid (of intermediate contrast) every 50 ms. A stimulus 'movie' consisted of 200 such 50 ms frames. During a recording session, 12 movies with a different sequence of stimulus positions were each presented 5 times. For a small window of time (centered at the approximate stimulus latency, 50ms, of the cells) before all spikes recorded from the electrode, the probability distribution of the stimulus position (the receptive field) was calculated. Responses to bright and dark stimuli were added together, and the center of the receptive field was determined by finding the peak of the distribution. This procedure was repeated for multiple sites whose position was marked on an image of the cortical vasculature. To generate a visual field map, each pixel of cortex was associated with the nearest recording site, using Voronoi tessellation (Matlab, Natick, MA), and was assigned the azimuth and elevation receptive field locations that were determined for that site.

For measuring multi-unit orientation preference, the stimuli consisted of drifting square-wave gratings presented at one of 8 orientations and 2 directions. The orientation preference of a site was defined as the orientation of the stimulus that produced the maximum number of spikes in the post-stimulus time histogram (over 1500 ms). For measuring multi-unit spatial frequency preference we presented square-wave stimuli (having the preferred orientation of the multi-unit cluster) at 8 different fundamental spatial frequencies. The spatial frequency preference of a site was defined as the spatial frequency of the stimulus that produced the maximum number of spikes in the post-stimulus time histogram (over 1500 ms).

RESULTS

The dimension-reduction model

To model how several features could be mapped across the two-dimensional cortical surface, we used the self-organizing feature map algorithm (Kohonen, 1982a; Obermayer et al., 1992). In this algorithm, each possible feature combination within a multi-dimensional response feature space (representing x- and y-axis retinotopic location, orientation, ocular dominance, and spatial frequency) is represented at a location in cortex. In other words, the cortex achieves complete 'coverage' of the feature space. In addition, the algorithm has a mechanism to promote 'continuity' in the cortical representations; i.e., nearby locations on the cortical surface are forced to represent similar features so that orderly feature maps are formed. The constraints of coverage and continuity act in opposition and are commonly employed in some form in many computational models of visual cortex (Erwin et al., 1995; Swindale, 1996). We asked what form the feature mapping was predicted to take given these constraints, and in particular how a global anisotropy in the retinotopic map was predicted to influence the layouts of the other maps. We reasoned that a match between the simulation predictions and *in vivo* experimental observations would suggest that the mapping of visual space and other features occurs in conformity with a dimension-reduction strategy.

Predicted influence of the retinotopic map on the structures of other maps

To determine the predicted influence of retinotopy on the mapping of other features, we compared the results of simulations in which visual space was represented either anisotropically or isotropically. To model an anisotropy, we used a retinotopic map whose magnification was 4 times greater along the elevation axis of visual space

representation than along the azimuth axis (Figure 1A). This degree of anisotropy was chosen because it resembles that found in ferret V1 (see Figure 5). We observed a strong influence of the visual map anisotropy on the layouts of the remaining maps formed in the simulation: domains in the orientation (Figure 1A), ocular dominance (Figure 1B), and spatial frequency (Supplementary Figure 1A) maps were highly elongated. Furthermore, the domains from the latter maps were elongated along a common axis; this axis was parallel to the azimuth (low-magnification) axis of the retinotopic map and orthogonal to the elevation (high-magnification) axis. It follows from these observations that the high gradient axis of retinotopy is orthogonal to the high gradient axis of the other maps.

To quantify this observation, we calculated the gradient vector at every pixel of the orientation map (Figure 2A-B). The direction of this gradient vector indicates the axis of cortex along which orientation changes maximally at that pixel. We found that most orientation gradient vectors pointed along the vertical axis (Figure 2B) of the model cortex. In contrast, most retinotopic gradient vectors (Figure 2C-D) pointed along a horizontal axis of the model cortex, as would be expected from the strong anisotropy in this map. By superimposing the gradient vectors of orientation and retinotopy from corresponding pixels of the model cortex (Figure 2E), a strong bias towards orthogonal intersection angles between the gradients of orientation and retinotopy can be seen. This is quantified in Figure 2F, indicating that on average the orientation and retinotopic gradients had a preponderance of near orthogonal intersection angles. This relationship held between retinotopy and other maps as well. We found a bias towards orthogonal intersection angles between the visual map gradient and the gradients of either the

orientation, ocular dominance, or spatial frequency maps (Figure 3A, dotted lines). Further, in those locations where the latter maps had a high gradient magnitude, there was an even stronger tendency for their gradient direction to be orthogonal to that of the visual map (Figure 3A, solid lines).

In contrast to the above results, when an isotropic visual map was used in the simulation, domains in the resulting orientation (Figure 1C), ocular dominance (Figure 1D), and spatial frequency (Supplementary Figure 1E) maps were not elongated. As a result, there was not a strong bias towards particular intersection angles between the gradient of retinotopic and the gradients of the other maps (Figure 3B). Taking these results together, our model predicts that a global anisotropy in visual space representation will strongly and specifically influence the layouts of other maps.

Predicted gradient relationships between orientation, ocular dominance, and spatial frequency maps

We next examined the relationships between the model's orientation, ocular dominance, and spatial frequency maps. A fundamental prediction of dimension-reduction models, which has previously been described, is that the highest gradient regions of multiple maps should avoid one another. We asked whether this could still occur with a strong anisotropy in the retinotopic map. Orientation, ocular dominance, and spatial frequency gradient maps from the same region of the model cortex were obtained. We found that the anisotropy caused the highest gradient regions of these three maps to align along a common axis of the cortex (Figure 4A; cf. Figure 4F). Nevertheless, the

highest gradient regions were precisely interleaved and appeared to occupy mostly non-overlapping regions of cortex (Figure 4A).

To quantify this relationship, all pixels within each gradient map were assigned a value between 1 and 10, where 1 indicated that the gradient was in the lowest 10^{th} percentile of all gradient values within that map, and 10 the highest 10^{th} percentile. The values from all three maps were averaged together at each pixel in the region, and the standard deviation of this average over the entire cortex was measured. We found that the standard deviation was smaller if the actual gradient maps were used (Figure 4B, red dotted bar) in the calculation, compared to when the pixels in each gradient map were randomly shuffled (Figure 4B, blue histogram). Thus, there is a tendency for the average gradient magnitude of all three maps to remain constant across the cortical surface. This demonstrates that the highest gradient regions of the three maps mutually avoid one another.

To analyze directly whether the high gradient regions of two maps avoid one another, we compared their gradients at corresponding pixels. Pixels were binned into ten groups according to their ocular dominance gradient percentile, and the average orientation gradient over all pixels within each group was determined and plotted (Figure 4C). A negative correlation can be seen, suggesting that the highest gradient regions of these two maps avoid one another. The same relationship exists between the orientation and spatial frequency maps (Supplementary Figure 1B).

These gradient correlations among maps of orientation, ocular dominance, and spatial frequency also held when the initial retinotopic map was isotropic (Figure 4F-H; Supplementary Figure 1F). Thus, a fundamental prediction of dimension-reduction

models is that high gradient regions of multiple maps avoid one another, and it holds whether the retinotopic map is anisotropic or isotropic.

Predicted contour relationships between orientation, ocular dominance, and spatial frequency maps

Above we described a fundamental prediction of dimension-reduction models, that high gradient regions of multiple maps avoid one another. A second major prediction of this class of models, and common to many cortical mapping algorithms, is that contours of different maps should cross at perpendicular angles (Erwin et al., 1995; Swindale, 1996). However, the constraint imposed by the anisotropy in the visual map challenges this prediction. With an anisotropic visual map, the orientation, ocular dominance, and spatial frequency domains are elongated along a parallel axis of cortex (see Figure 4A). This would seem to preclude the contours of these maps from crossing at perpendicular angles.

To examine this issue, we plotted the distribution of the intersection angles, over all map pixels, between the orientation and ocular dominance gradient vectors. When the visual map was isotropic the intersection angles were orthogonal on average, as expected from previous studies (Figure 4J, red line). In contrast, when an anisotropic visual map was used, the intersection angles had no bias towards orthogonality (Figure 4E, red line). Thus, an anisotropy in the visual map precludes an overall orthogonality between the remaining maps.

We next show, however, that the remaining maps have specific local regions where orthogonality is maintained. In the anisotropic case, a clear bias towards

orthogonal intersection angles between the orientation and ocular dominance gradient vectors emerged specifically in those locations where the maps of these features had overlapping high gradients (Figure 4D, gray regions; Figure 4E, blue line). For the isotropic case, the bias towards intersection angles between orientation and ocular dominance gradients similarly became stronger in those locations where the two maps have high gradients (Figure 4I; Figure 4J, blue line). The relationships between the contours of orientation and spatial frequency were very similar to those between orientation and ocular dominance (Supplementary Figures 1C-D, 1G-H). The results suggest that the overall orthogonality between orientation and ocular dominance (or spatial frequency) maps can vary, based on the nature of the retinotopic map. But the model predicts that regardless of the nature of the retinotopic map, orthogonality will consistently occur between the remaining maps in their high gradient overlap regions.

Together, the relationships we have described reflect the model's strategy for smoothly accommodating several features simultaneously on the two-dimensional cortical surface. In particular, they predict what influence the retinotopic map should have on other maps if the mapping of visual space is inter-dependent with that of other features. Whether the visual space and other maps in visual cortex demonstrate these relationships requires experimental examination. We next compared these modeling predictions to the results we obtained experimentally in ferret V1.

Experimental results from ferret visual cortex: an anisotropy in the V1 retinotopic map

We determined the layout of the retinotopic map in ferret V1 (Figure 5, inset) using optical imaging of intrinsic signals (see Experimental Procedures). The

presentation of a vertical bar activated a narrow, medio-laterally elongated strip of cortex in V1, which represents an iso-azimuth contour (Figure 5A). As the vertical bar shifted from central to more peripheral regions of the visual field, the region of activation in V1 shifted posteriorly. A horizontal bar, on the other hand, activated a strip of cortex that was elongated along the antero-posterior axis of the cortex (Figure 5B). This strip represents an iso-elevation contour. Downward movement of the horizontal bar across the visual field caused the activated region to shift from lateral to medial across cortex (Figure 5B).

With our retinotopy stimulation paradigm, the stimulus passes over the receptive field of each cortical location periodically, and causes a periodic activation pattern across time (data not shown) for each pixel. A pixel's relative receptive field location can be determined by its relative phase of activation within the stimulus cycle (Engel et al., 1994; Sereno et al., 1995; Kalatsky and Stryker, 2003; Mrsic-Flogel et al., 2003). We calculated the phase of the Fourier Transform of each pixel's response time course, in response to stimulation by a horizontally or vertically drifting bar, and constructed maps for relative horizontal (Figure 5C) and vertical (Figure 5D) visual space, respectively.

While the general layout we show for the visual space map is in agreement with previous reports (Law et al., 1988; White et al., 1999), we additionally find a pronounced anisotropy in the representation of visual space (Figure 5). A much greater amount of cortex is devoted to the representation of a given amount of visual field elevation than for the equivalent amount of azimuth. In general, for the region of ferret V1 accessible to optical imaging, the magnification factor for the elevation axis of visual space was approximately 3 to 5 times greater than that for azimuth (Supplementary Table 1).

The magnification anisotropy was confirmed by electrophysiological recordings. Receptive field positions and sizes were determined using the reverse correlation method of receptive field mapping. A representative case is shown in Figure 4. On- and off-subfields were summed to calculate the aggregate receptive field at each recording site (Figures 6A-B). The distribution of the receptive fields recorded at multiple sites (Figure 6A) revealed a wide range of azimuth position preferences (within a small antero-posterior extent of cortex), and a narrower range of elevations (Figure 6C). The composite retinotopic map confirmed that the magnification for the elevation axis of visual space was much greater than that for the azimuth axis (Figures 6D and 6E; note similarity to optical imaging-derived maps in Figures 5C and 5D).

Influence of the global visual map anisotropy on feature maps

Given the pronounced anisotropy of the retinotopic map in ferret visual cortex, we examined whether it would impact the layout of other functional maps, as the dimension-reduction model predicted. We first examined the map of orientation in V1, which was obtained by comparing the cortical activation pattern in response to grating stimuli presented at four different orientations. Though this map has been previously been described in ferret (Rao et al., 1997; White et al., 2001a), a salient feature that we noticed was an anisotropy of the orientation domains. They were often elongated along the antero-posterior dimension of cortex (Figures 7A-F). This was also true for the ocular dominance domains. The ocular dominance map in the binocular portion of V1, located at the most postero-lateral edge of cortex (Law et al., 1988; Redies et al., 1990; White et al., 1999) contains ocular dominance columns that interleave similarly to those in V1 of

the cat and macaque. In this part of V1, ocular dominance domains were anisotropic: they were elongated along the antero-posterior dimension of cortex (Figure 7G), similarly to the iso-orientation domains. Finally, we examined whether spatial frequency is mapped in ferret visual cortex (see Experimental Procedures), and in what manner. We found that alternating high and low spatial frequency domains exist in V1, and they are elongated along the antero-posterior dimension of cortex (Figure 7H and Supplementary Figure 2A). The mapping of spatial frequency was verified in one animal by multi-unit electrophysiological recordings (Supplementary Figures 2B-D). Taken together, these results match those predicted by our model, suggesting that an anisotropy of the visual map is indeed accompanied by an anisotropy in the domains of the orientation, ocular dominance, and spatial frequency maps (cf. Figure 1A-B and Supplementary Figure 1A).

We next directly compared the layout of the retinotopic map with that of other maps. By examining retinotopic contours superimposed on the orientation map (Figures 7E-F and 8A), it can be seen that the high gradient axes of these two maps are orthogonal. To quantify this relationship, we calculated the pixel-by-pixel intersection angles between the retinotopic gradient and the gradients of the other maps (see Experimental Procedures). Across the cortex, the percentage of pixels having a 60-90° intersection angle would be 33.3% for a random distribution into the three bins of 0-30°, 30-60° and 60-90°. For the retinotopic and orientation maps the number was 44.1 ± 4.5%, significantly high than the chance level ($p<0.005$, t-test, n = 8 animals). For retinotopy and ocular dominance the number was 48.0 ± 2.8% of pixels ($p<0.005$, t-test, n = 4 animals), and for retinotopy and spatial frequency the number was 51.2 ± 4.9% of pixels ($p<0.005$, t-test, n = 4 animals). Thus there was a preponderance of near orthogonal

intersection angles between the retinotopic gradient and the gradients of the other maps, which reflects the global relationship between the anisotropy of the retinotopic map and the elongation of feature map domains.

Quantifying this in another way, we grouped pixels into nine 10° bins (0-10°, 10-20°, …, 80-90°) according to the intersection angle between the retinotopic gradient and either the orientation, ocular dominance, or spatial frequency gradient. In all three cases, the percent of pixels per bin increased with intersection angle (orientation: Figure 8B, red line, r = 0.91, slope = 0.11 percent/deg; ocular dominance: Figure 8C, red line, r = 0.96, slope = 0.16 percent/deg; spatial frequency: Figure 8D, red line, r = 0.88, slope = 0.16 percent/deg).

The relationship between the retinotopic and orientation map gradients became even more robust if the analysis was performed only for those pixels of the cortex where the orientation gradient was within the highest 30^{th} percentile of all values within the map (Figure 8A, gray regions). In this case, the percent of pixels per bin increased even more steeply with intersection angle (Figure 8B, blue line, r = 0.93, slope = 0.17 percent/deg). Similarly, the relationships between retinotopy and either ocular dominance or spatial frequency maps became stronger in the highest gradient regions of the latter maps (ocular dominance: Figure 8C, blue line, r = 0.96, slope = 0.27 percent/deg; spatial frequency: Figure 8D, blue line, r = 0.89, slope = 0.35 percent/deg). These observations suggest a local influence of retinotopy on the layouts of other feature maps.

In summary, domains in the orientation, ocular dominance, and spatial frequency maps were anisotropic, and were elongated specifically along the high gradient axis of the retinotopic map. This implies that on average, the high gradient axis of the retinotopic

map is orthogonal to that of other maps. The dimension-reduction model, which works under the assumption that the visual and other feature maps in visual cortex are inter-dependent, predicted just this effect (cf. Figure 3A).

Gradient relationships between orientation, ocular dominance, and spatial frequency maps

The results above suggest that the visual space map constrains the mapping of other features. We next determined whether, given this constraint, the remaining feature maps were coupled by specific spatial relationships. We first examined the gradient relationships between orientation, ocular dominance, and spatial frequency. In Figure 9A, we superimpose the gradient maps of these three features. The figure shows that while the high gradient regions of each map are stretched along a similar axis of cortex, they interleave so as to avoid overlapping. To quantify this, each pixel from each gradient map was assigned a value between 1 and 10, where 1 indicated that the gradient was in the lowest 10^{th} percentile of all gradient values within that map, and 10 the highest 10^{th} percentile. The values from all three maps were averaged at each pixel in the region, and the standard deviation across the cortex of this averaged value was calculated. We found that the standard deviation was smaller if the actual gradient maps were used (Figure 9B, red dotted bar) compared to when the pixels in each gradient map were randomly shuffled (Figure 9B, blue histogram, $p<0.0001$). This occurred in all three animals tested, and indicates that the averaged gradient over all three maps stays relatively constant across the cortex.

We next compared the gradient magnitudes at corresponding pixels in orientation and ocular dominance maps. We found that the average orientation gradient calculated

over all pixels whose ocular dominance gradient was within the highest 20th percentile was significantly lower than that calculated for pixels whose ocular dominance gradient was within the lowest 20th percentile (average difference of 1.9 ± 0.6 deg/pixel; means of 6.6 and 8.5 deg/pixel, respectively; paired t-test, $p<0.001$, n = 5 animals). In addition, all the pixels within a region were binned into ten groups according to their ocular dominance gradient percentile, and the average orientation gradient within each group was determined. We found a strong negative correlation between the mean orientation gradient and the ocular dominance gradient percentile (Figure 9C, r = -0.77, slope = -0.03 deg/pixel/percentile).

The gradient relationships also held between orientation and spatial frequency maps. The average orientation gradient calculated for pixels whose spatial frequency gradient was within the highest 20th percentile was significantly lower than that calculated for pixels whose spatial frequency gradient was within the lowest 20th percentile (average difference of 2.1 ± 0.8 deg/pixel; means of 6.3 and 8.4 deg/pixel, respectively; paired t-test, $p<0.001$, n = 5 animals). There was a strong negative correlation between the mean orientation gradient and the spatial frequency gradient percentile, which held throughout the cortex (Figure 9F, r = -0.71, slope = -0.02 deg/pixel/percentile).

The results demonstrate that in ferret V1, where the retinotopic map imposes a strong constraint on the remaining maps, the latter maintain specific relationships with one another. Their highest gradient regions avoid one another, so that their combined gradient remains constant across the cortical surface. These relationships closely match

the predictions of our dimension-reduction model (cf. Figures 4B-C and Supplementary Figure 1B).

Contour relationships between orientation, ocular dominance, and spatial frequency maps

We next examined whether the contours of orientation, ocular dominance, and spatial frequency maps tend to intersect at near perpendicular angles. Previous studies have shown that this occurs in cat and monkey V1. But it may not occur in ferret V1 since (as noted above) the domains of orientation, ocular dominance, and spatial frequency maps are elongated along a parallel (rather than perpendicular) axis of cortex, reflecting the visual map anisotropy (see Figure 9A).

The contour lines of a superimposed orientation and ocular dominance map are illustrated in Figure 9D. Across the cortex, we found no significant tendency for the gradient vectors of the two maps to intersect at near perpendicular angles. Quantification revealed that 36.2 ± 1.8% of pixels had gradients that intersected at an angle between 60-90°, which is not significantly different from the chance percentage of 33.3% ($p > 0.1$, t-test, n = 5 animals). By grouping the pixels into nine 10° bins according to their intersection angles, the percent of pixels per bin did not increase greatly with intersection angle (Figure 9E, red line, r = 0.76, slope = 0.037 percent/deg). However, for the pixels of the cortex where both the orientation and ocular dominance gradients were within the highest 30th percentile, a clear tendency for orthogonal intersection angles between gradient vectors of the two maps emerged (Figure 9D, gray region; Figure 9E, blue line, r = 0.89, slope = 0.20 percent/deg). Considering this region, 49.3 ± 5.0% of pixels had gradient vector intersection angles within 60-90° ($p<0.01$, t-test, n = 5 animals).

The relationships between the orientation and spatial frequency contours (Figure 9G) were similar. Across the cortex, there was only a weak tendency for orthogonal intersection angles between the gradients of the two maps, with 34.3 ± 2.8% of pixels having gradient intersection angles within 60-90° ($p > 0.1$, t-test, n = 5 animals). By grouping the pixels into nine 10° bins according to their intersection angles, the percent of pixels per bin did not change greatly with intersection angle (Figure 9H, red line, r = 0.28, slope = 0.011 percent/deg). In contrast, for the pixels of the cortex where both the orientation and spatial frequency gradients were within the highest 30th percentile, there was a clear tendency for orthogonal intersection angles between the gradient vectors of the two maps (Figure 9G, gray regions; Figure 9H, blue line, r = 0.77, slope = 0.16 percent/deg). In that case, 47.1 ± 1.4% of gradient vectors had intersection angles within 60-90° ($p<0.005$, t-test, n = 5 animals).

The results demonstrate, as our model predicted, that the visual map anisotropy decreases the overall tendency for perpendicular intersections between gradients of orientation and ocular dominance (and spatial frequency) maps. But the maps maintain strong orthogonal relationships in those locations where they have overlapping high gradients (cf. Figure 4 and Supplementary Figure 1).

Influence of feature maps on local retinotopy: model and experiment

We showed above that the structure of the retinotopic map is reflected in the layouts of other feature maps. We lastly wanted to determine whether, in turn, the local structure of the retinotopic map is influenced by the mapping of these other features. Previous simulation studies predicted that the orientation map would have a strong

influence on the retinotopic map (Durbin and Mitchison, 1990; Obermayer et al., 1990), but those simulations included only orientation and retinotopy as mapped features. We compared the predictions of simulations using only orientation and retinotopy to those that included additional features known to be mapped in ferret V1, and examined how the predictions in each case related to experimental relationships.

In the retinotopy-orientation simulation (the retinotopic map was anisotropic), we found that the retinotopic contours were distorted (Figure 10A). Iso-elevation lines were, in general, more widely spaced than average at pinwheel centers (dots in Figure 10A) and extremes of the orientation gradient map (although some counter-examples exist). We plotted the retinotopic gradient percentile as a function of the orientation gradient percentile (Figure 10C, red line) and found a clear negative correlation. Thus, in the retinotopy-orientation simulation, the detailed structure of the retinotopic map is visibly influenced by the orientation map, as has been shown previously with isotropic retinotopy (Durbin and Mitchison, 1990; Obermayer et al., 1990).

The results differed when the simulations included, besides orientation and retinotopy, the additional features of ocular dominance and spatial frequency (4 components total, as in Figures 1-4). In this case, we did not find distortions in the retinotopic map that correlated with orientation pinwheels (Figure 10B), and there was no strong relationship between the gradient magnitudes of orientation and retinotopy (Figure 10C, blue line). Further, the retinotopy contours were smoother in this simulation (consistent with the smooth averaged background gradient; Figure 10B) than in the retinotopy-orientation simulation.

We compared these predictions to experimentally-measured relationships in ferret V1, where optical imaging was used to obtain retinotopic and orientation maps (see Figure 7). We found no strong correlation between the gradient magnitudes of retinotopy and orientation (Figure 10C, black line), or between the gradient magnitudes of retinotopy and either ocular dominance or spatial frequency (data not shown). We additionally measured the local relationships between the retinotopic and orientation maps using electrophysiological techniques (Supplementary Figure 3), and found no strong correlation between the orientation gradient and either the receptive field gradient or the degree of receptive field overlap. These experimentally-measured relationships between retinotopy and orientation were thus similar to the predictions of the four-component simulation, and suggest that the retinotopic map may not be visibly distorted locally by the orientation map, in the case where several features are mapped within a cortical area.

DISCUSSION

Our study presents a comprehensive description of the mapping of visual space and of multiple other features within a cortical area. By directly comparing modeling and experimental results we show that the spatial relationships between cortical maps, including those between visual space and other features, occur in conformity with a dimension-reduction strategy. This suggests that the constraints which drive map formation in the model, continuity (representing each feature smoothly across cortex) and coverage uniformity (representing each feature combination), may play a central role in determining the functional organization of visual cortex.

The retinotopic map and other feature maps are inter-dependent

Recent experimental studies have come to conflicting conclusions regarding whether the structure of the retinotopic map is inter-dependent with that of other maps. In ferret V1, we find evidence for an inter-dependence: the retinotopic map in this species is strongly anisotropic, and the anisotropy is reflected in the layouts of other maps. Specifically, the gradient vectors of the orientation, ocular dominance, and spatial frequency maps align along a specific axis of the retinotopic map, so that the highest gradient of axis of retinotopy is orthogonal to the highest gradient axes of the remaining feature maps. Our model suggests that these relationships play a role in coordinating the mapping of visual space along with multiple additional features within a single cortical area.

While we suggest that retinotopy influences the layouts of other feature maps, some other factors have also been implicated. A role for the V1/V2 border is suggested by observations that ocular dominance columns in primates run perpendicular to this border (LeVay et al., 1985; Florence and Kaas, 1992). Since the retinotopic map and the V1/V2 border often have a specific relationship with one another, it can be difficult to distinguish between the influences of these two factors on the layouts of feature maps. However, in some cortical regions retinotopy and the V1/V2 border are not aligned. In macaque V1, for example, they can deviate from each other, and here it was found that ocular dominance patterns follow local changes in the axis of the retinotopic anisotropy (Blasdel and Campbell, 2001). This favors the hypothesis that retinotopy itself has a direct relationship with other feature maps. Simulation studies have demonstrated that the

shape of a cortical area is an additional factor that may influence the structures of feature maps (Bauer, 1995; Wolf et al., 1996). However, the shape of a cortical area also likely influences the degree of anisotropy of the retinotopic map; thus, cortical area shape may influence feature maps directly, or indirectly via its influence on the retinotopic map, which in turn influences the other feature maps.

The local pattern of retinotopy

Whether local distortions exist in the retinotopic map (at a sub-columnar scale) that relate to the mapping of other features, such as pinwheel centers of the orientation map, has remained a question of particular interest. Early dimension-reduction models predicted specific local relationships between retinotopy and orientation (Durbin and Mitchison, 1990; Obermayer et al., 1990) whereas experimental measurements failed to confirm the predictions (Das and Gilbert, 1997; Bosking et al., 2002; Buzas et al., 2003). However, a recent modeling study suggested that predictions of dimension-reduction models, regarding the relationships between retinotopy and other feature maps, are dependent on how many features are mapped within a cortical area (Swindale, 2004). In agreement with this, our studies suggest that the local relationships in ferret V1 between retinotopy and orientation maps are in close agreement with model predictions when a realistic number of features are simulated in the model.

For example, we show that low gradient retinotopy regions are predicted to coincide with high gradient orientation regions, when these are the only two features mapped within an area. But if ocular dominance and spatial frequency maps also exist, then low retinotopic gradient regions should coincide with high gradient regions of these

additional maps as well. Given our observation that the high gradient regions of orientation, ocular dominance, and spatial frequency maps occur in non-overlapping locations of cortex, each of these feature maps should have opposing effects on the retinotopic map, and smooth out the distorting effects of one another. In this case, the local retinotopic map is predicted to be smooth and to have no visible distortions that correlate with any other single map. These local relationship predictions are in agreement with our experimental results as well as those recently measured in other species (Bosking et al., 2002; Buzas et al., 2003). It remains possible that local distortions exist in the retinotopic map that cannot be detected by intrinsic-signal optical imaging or electrophysiological methods.

Contour relationships between multiple maps

Mapping variables along orthogonal axes of cortex has long been suggested as a means to accommodate a smooth representation of multiple variables within a single cortical area (Hubel and Wiesel, 1977). However, since it is not possible for the domains of more than two maps to be mutually orthogonal, this cannot represent a general solution to the problem. In a modeling study (Obermayer et al., 1992), a relationship was suggested that could hold between more than two maps: that orthogonality occurs between any two maps when the high gradient regions of those maps coincide. Our data directly confirm this prediction with experimental evidence. We find that although ocular dominance and orientation are not mapped along orthogonal axes (their domains are often elongated along a parallel axis), the contours of these maps intersect at perpendicular

angles when high gradient regions of the two maps coincide (and similarly for spatial frequency and orientation).

The general prediction, that two features are mapped orthogonally in their high gradient overlap regions, may relate to previous observations in cat V1 that ocular dominance and orientation contours intersect at orthogonal angles in ocular dominance border regions (Bartfeld and Grinvald, 1992; Hubener et al., 1997). It may also relate to the finding in macaque V1 that orthogonality between orientation and ocular dominance contours increases in "linear" regions of the orientation map (Obermayer and Blasdel, 1993).

In some cases, two features can be mapped orthogonally throughout the cortex, not only locally. For example, orientation domains run along a specific axis of the retinotopic map in cat V2 (Cynader et al., 1987), and our results shown that orientation, ocular dominance, and spatial frequency domains do the same in ferret V1. We suggest that this occurs due to the strong anisotropy in retinotopy within these two cortical areas; in these cases, the strong retinotopy gradient, which points along a constant axis of cortex, will cause the high gradient regions and in turn the domains in other feature maps to be elongated along a constant axis.

While one recent study suggested that no orthogonal relationships exist between orientation and ocular dominance maps in ferret visual cortex (White et al., 2001a), we found strong relationships. We suggest that the difference lies in the part of visual cortex examined: White and colleagues analyzed the V1/V2 border region, which has very large monocular domains. We analyzed the region containing interleaving ocular dominance

columns, and we detect relationships consistent with those found in functionally similar regions of cat and primate.

Separability of response maps in V1

An assumption implicit in our study, that separable maps of multiple response properties exist in V1, is supported by numerous studies. It has previously been demonstrated that the orientation map (in binocular regions of cortex) is not dependent on the eye to which stimuli are presented; conversely, the map of ocular dominance is invariant to stimulus orientation (Blasdel, 1992). Further, the overall structure of the retinotopic map is not dependent on stimulus orientation (Blasdel and Campbell, 2001). While the receptive field of a neuron can differ for the two eyes, this relationship does not lead to systematic changes in retinotopic magnification, which implies that within binocular regions of cortex the overall pattern of retinotopy is not dependent on the eye to which stimuli are presented. Thus, we suggest that the maps of orientation, ocular dominance, and retinotopy are separable.

Whether orientation and spatial frequency maps can be approximated as separable from one another has also been examined. It has been shown, using sine-wave gratings, that the structure of the orientation map is not altered by the stimulus spatial frequency (Issa et al., 2000). On the other hand, the preferred spatial frequency of some neurons can change with orientation (Webster and De Valois, 1985). While one study suggests that the spatial frequency map has some dependence on stimulus orientation (Issa et al., 2000) our results suggest that the structure of the differential spatial frequency map in the region of ferret V1 we examined remains largely invariant to orientation.

Responses to texture stimuli are also consistent with separable maps of orientation and spatial frequency. An optical imaging study (Basole et al., 2003) showed, using texture stimuli composed of short line segments, that changing the bar length or axis of motion causes changes in the cortical population response. In particular, an activation pattern produced by long bars (gratings) moving orthogonally was reproduced by short bars moving obliquely. Such equivalence has been previously described using inter-digitating gratings composed of short line segments, which can elicit patterns of cortical activity that resemble activity patterns due to orthogonal gratings (Sheth et al., 1996). But compared to gratings, short line segments contain a broader range of spatial frequencies and orientations in their Fourier spectrum, and the population response to short segments in these studies is fully compatible with both the known spatiotemporal responses of V1 neurons (Mante and Carandini, 2003) and the existence of separable maps of orientation and spatial frequency (Baker and Issa, 2005; Mante and Carandini, 2005).

Note: Portions of the data from this chapter have been previously published.
Reprinted from Neuron, Vol 47, Yu H, Farley BJ, Jin DZ and Sur M. The coordinated mapping of visual space and response features in visual cortex, pp. 267-280, Copyright 2005, with permission from Elsevier (Yu et al., 2005).

FIGURES

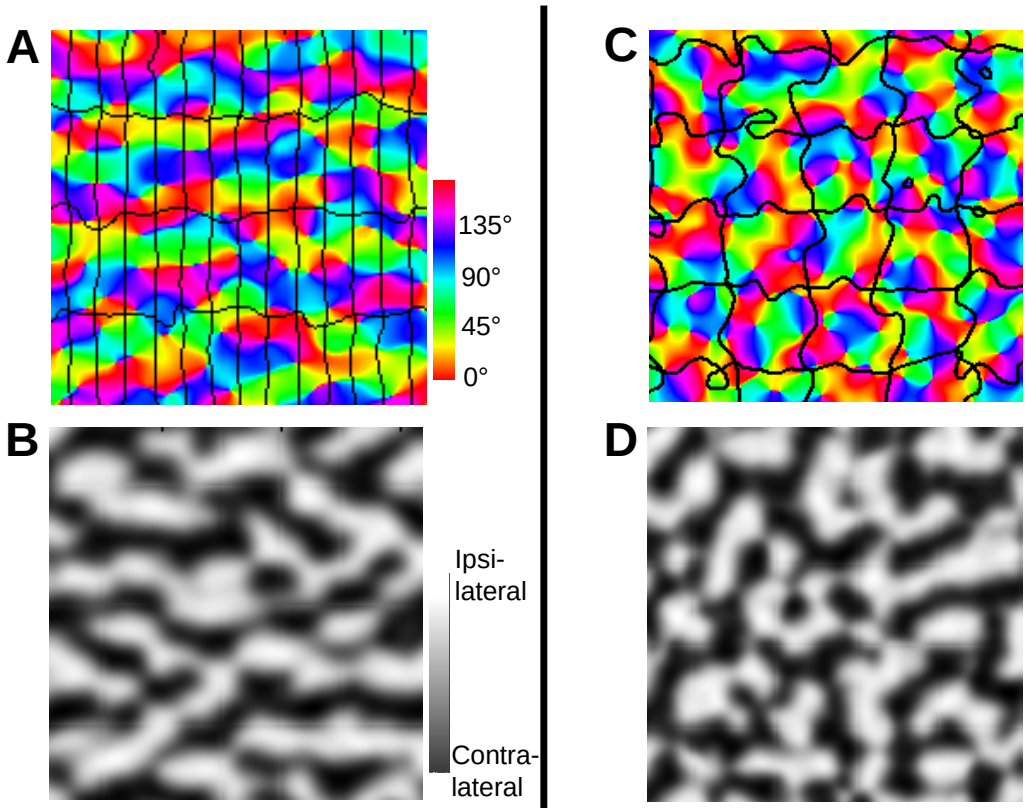

Figure 1. Effect of visual space anisotropy on the layouts of other feature maps, as predicted by a dimension-reduction model. Results from simulations run with a retinotopic map that was either anisotropic (A-B) or isotropic (C-D); the retinotopic map is illustrated in (A) and (C) by iso-elevation (horizontal in figure) and iso-azimuth (vertical in figure) contours; all contour intervals are identical. **(A, C)** The orientation map, denoted by color-coding each pixel according to its preferred orientation. **(B, D)** The ocular dominance map.

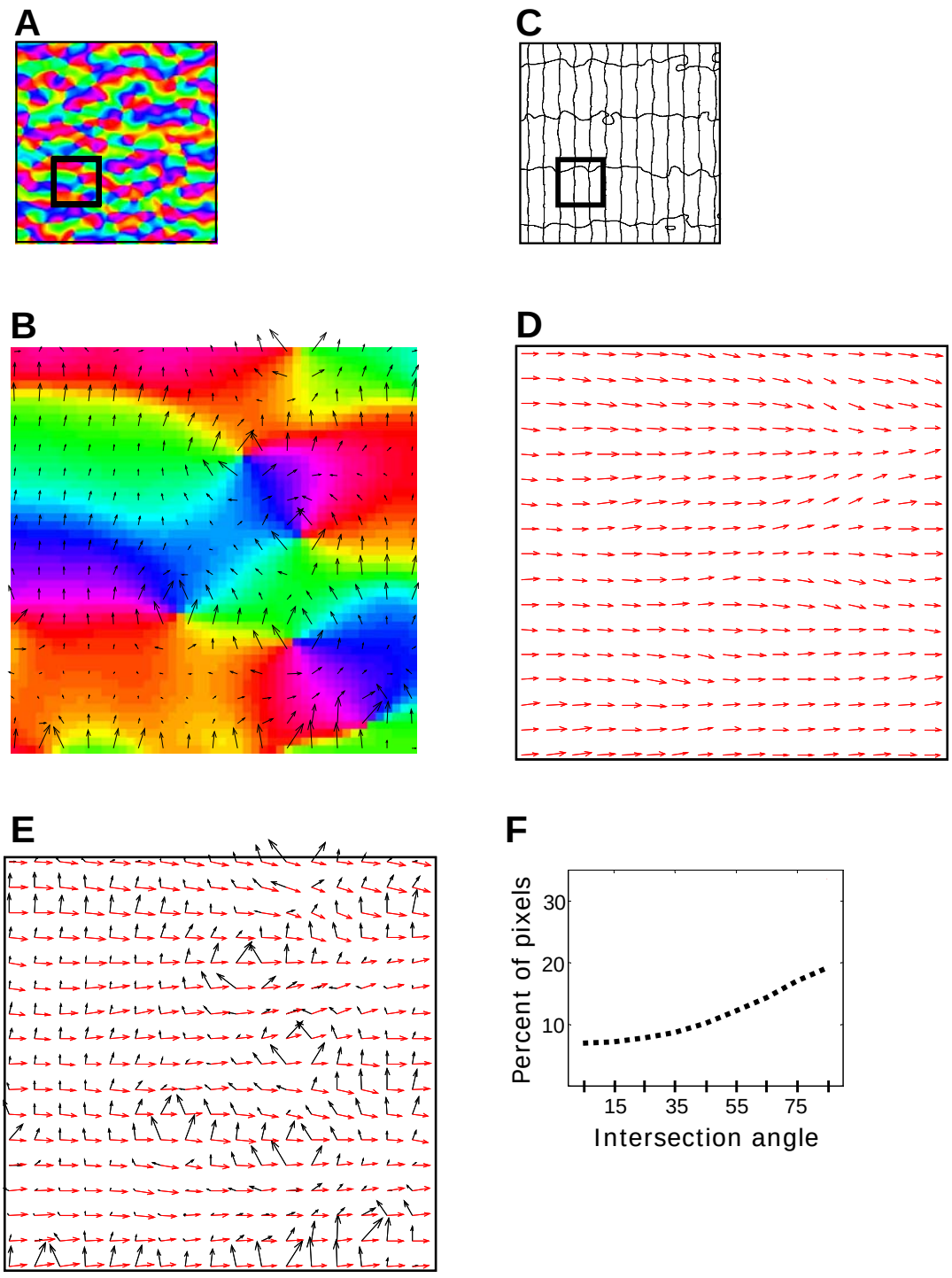
A
C
B
D
E
F
Percent of pixels
30
20
10
15
35
55
75
Intersection angle

Figure 2

Figure 2. Measuring the relationships between maps by calculating gradient intersection angles. The maps in this figure come from the simulation where the retinotopic map was anisotropic (see Figure 1A-B). **(A)** The orientation map produced by the simulation, denoted by color-coding each pixel according to its preferred orientation. **(B)** A higher magnification view of the outlined portion of the orientation map from (A). The orientation gradient vectors are displayed for every one out of 9 pixels of the orientation map. The length of the vector indicates the magnitude of the orientation gradient at that pixel; the angle of the vector indicates the axis of cortex along which orientation is changing maximally at that pixel. The direction in which the arrow points, forwards or backwards, is arbitrary—the vector angles effectively range from 0°-180° (where 0° is horizontal in the figure and 90° is vertical). **(C)** The retinotopic map, illustrated by iso-elevation (horizontal in figure) and iso-azimuth (vertical in figure) contours; all contour intervals are identical. **(D)** A higher magnification view of the outlined portion of the retinotopic map shown in (C), with the retinotopic gradient vectors displayed for every one out of 9 pixels. **(E)** The orientation gradient vectors and retinotopic gradient vectors are superimposed. **(F)** Percent of pixels that have an intersection angle, within each 10° range whose center is indicated by the x-tick mark, between the retinotopic gradient vector and the orientation gradient vector.

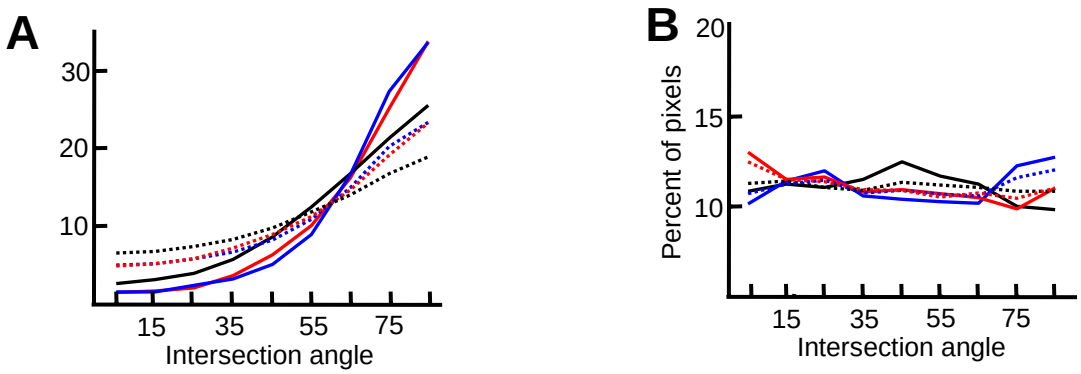

Figure 3. The gradient relationships between the retinotopic map and the maps of orientation, ocular dominance, and spatial frequency. Results come from simulations where the retinotopic map was initialized as either anisotropic (A) or isotropic (B). **(A, B)** Percent of pixels that have an intersection angle, within each 10° range whose center is indicated by the x-tick mark, between the retinotopic gradient and the gradient of the orientation (black lines), ocular dominance (blue lines) or spatial frequency (red lines) map. Dotted lines indicate the calculation over all pixels of the cortex. Solid lines indicate the calculation over only those pixels whose orientation, ocular dominance or spatial frequency gradients were within the highest 30th percentile.

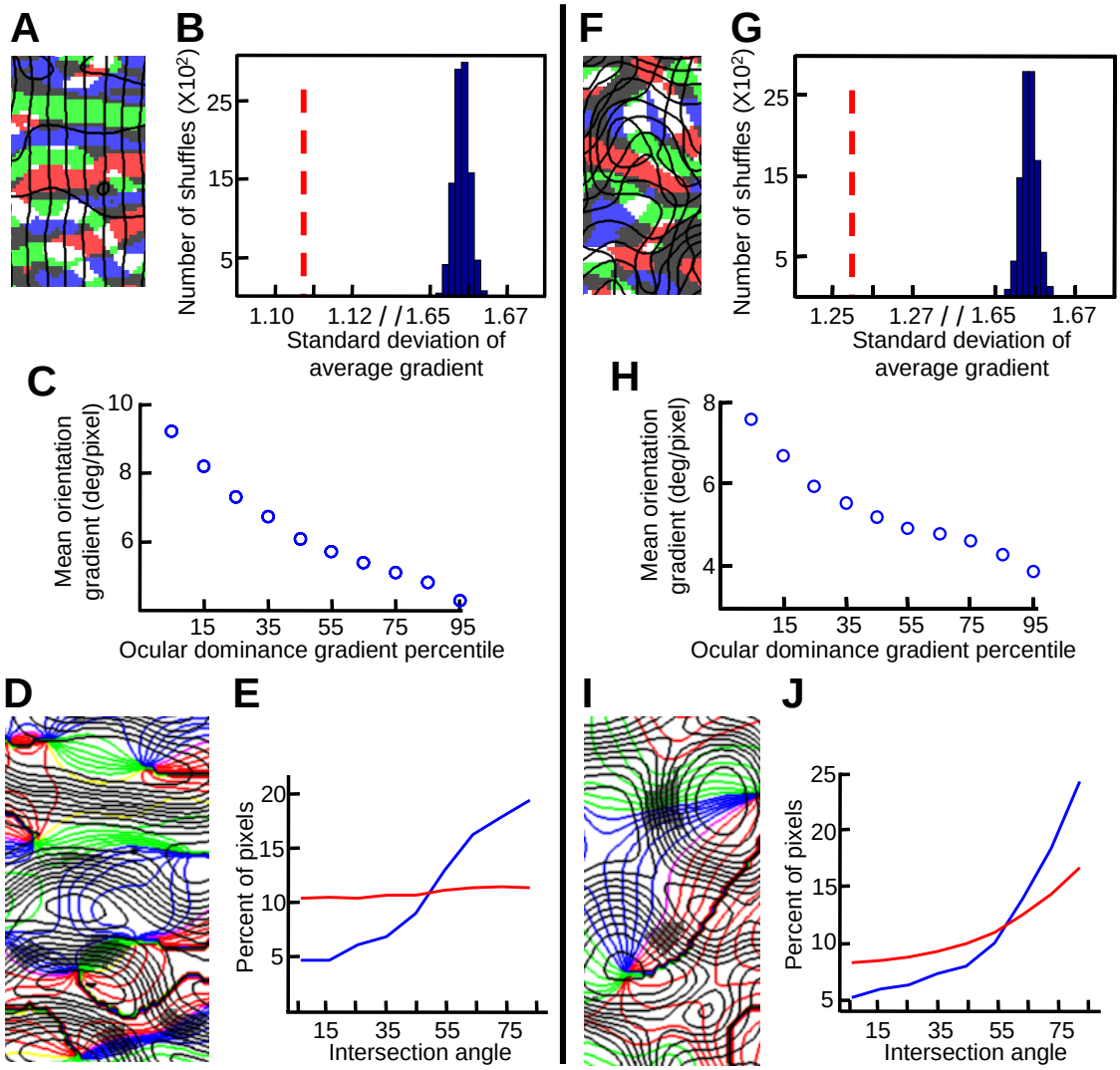
A
B
Number of shuffles (X10²)
25
15
5
1.10
1.12 / / 1.65
1.67
Standard deviation of
average gradient
F
G
Number of shuffles (X10²)
25
15
5
1.25
1.27 / / 1.65
1.67
Standard deviation of
average gradient
C
Mean orientation
gradient (deg/pixel)
10
8
6
15
35
55
75
95
Ocular dominance gradient percentile
H
Mean orientation
gradient (deg/pixel)
8
6
4
15
35
55
75
95
Ocular dominance gradient percentile
D
E
Percent of pixels
20
15
10
5
15
35
55
75
Intersection angle
I
J
Percent of pixels
25
20
15
10
5
15
35
55
75
Intersection angle

Figure 4

Figure 4. Predicted effect of visual space map anisotropy on the relationships between other feature maps. The retinotopic map was either anisotropic (A-E) or isotropic (F-J). **(A, F)** High gradient regions (pixels with gradients within the top 30th percentile) of orientation (blue), ocular dominance (green), spatial frequency (red), or two or more maps (white) are indicated. **(B, G)** Standard deviation across cortex of the average gradient magnitude of the orientation, ocular dominance, and spatial frequency maps (red dotted line). Histogram of this standard deviation calculation after pixels within each map were randomly shuffled, in 10,000 cases (blue histogram). **(C, H)** Pixels are grouped into ten bins according to their ocular dominance gradient percentile, and the mean orientation gradient for each group is indicated. **(D, I)** Orientation (color) contours superimposed on ocular dominance (black) contours. Gray pixels indicate locations where the gradient of both the orientation and ocular dominance maps are within the highest 30th percentile. **(E, J)** Percent of pixels that have an intersection angle, within each 10° range whose center is indicated, between the orientation and ocular dominance gradients. Red line shows the calculation over all pixels. Blue line indicates the calculation for those pixels where the gradients of both maps are within the highest 30th percentile.

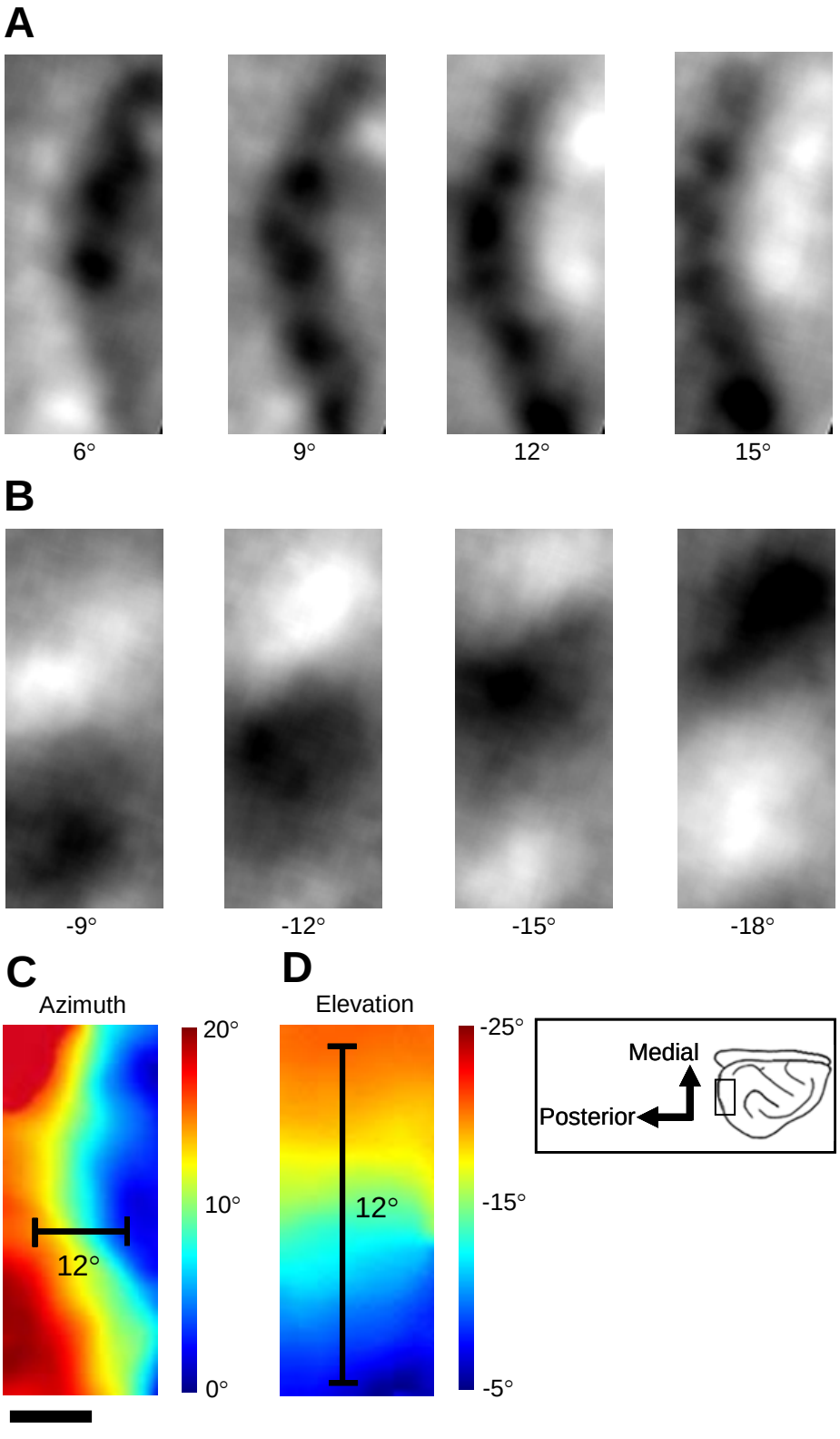
A
6°
9°
12°
15°
B
-9°
-12°
-15°
-18°
C
Azimuth
20°
10°
0°
12°
D
Elevation
-25°
-15°
-5°
12°
Medial
Posterior

Figure 5

Figure 5. Optical imaging reveals that the retinotopic map in ferret V1 is anisotropic. *Inset:* Dorsal view of right hemisphere of ferret brain, indicating the orientation of the functional maps for all figures; outlined area indicates the region of cortex imaged. **(A-B)** 'Single-condition' retinotopic maps. **(A)** Cortical activity pattern (activated pixels are darker) elicited by a flashing vertical bar. The stimulus position differed by 3° in horizontal space between successive panels, as indicated. **(B)** Activity elicited by a horizontal bar. The stimulus position differed by 3° in vertical space between successive panels. **(C)** Azimuth position preference map. Each pixel is color coded according to its preferred relative azimuth position in visual space. 12° of horizontal space was represented over 1.1 mm of cortex. **(D)** Elevation position preference map. 12° of vertical space was represented over 4.1 mm. Scale bar in (C) 1 mm, and also applies to (A-B) and (D).

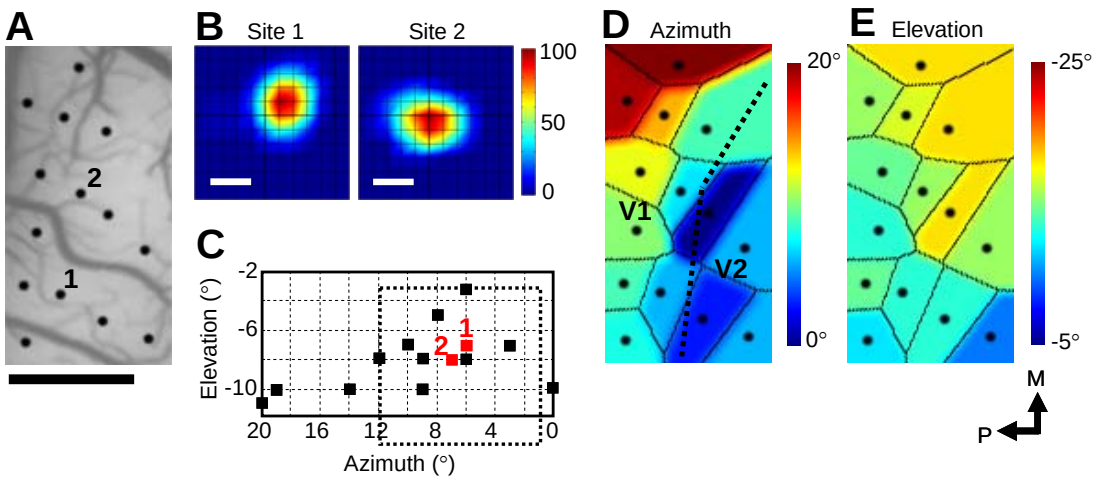

Figure 6. Multi-unit electrophysiological recordings confirm the anisotropy of the retinotopic map in ferret V1. (A) Image of cortical vasculature showing 14 recording sites. **(B)** Example multi-unit receptive fields recorded at the two sites indicated in (A). The strength of the response to stimuli presented in each location of the stimulus grid (dotted box in C) is indicated (as percent maximum response). **(C)** Receptive field locations for all recording sites shown in (A). **(D, E)** Azimuth (D) and elevation (E) position preference map for the region of cortex shown in (A) (see Experimental Procedures). The dotted line in (D) indicates the approximate location of the V1/V2 border. Scale bar in (A) 1 mm, and also applies to (D-E); bar in (B) 3˚.

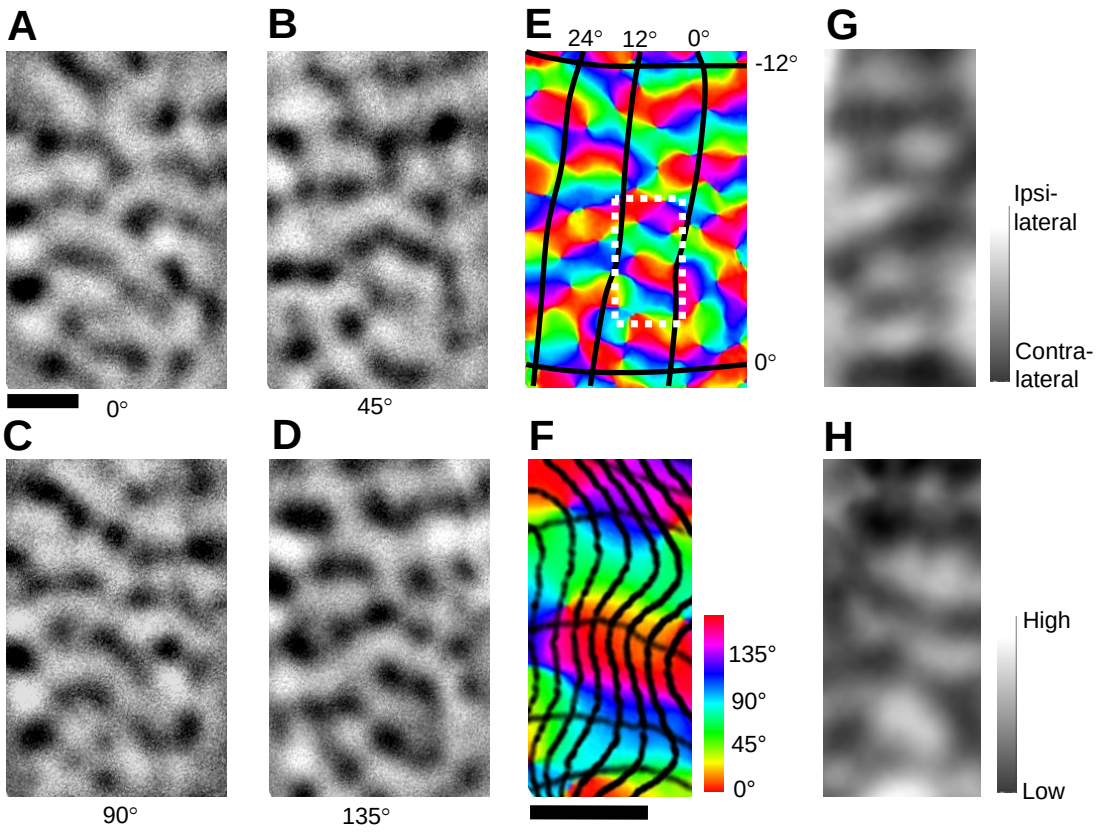

Figure 7. Orientation, ocular dominance, and spatial frequency domains are anisotropic. (A-D) Cortical activity patterns elicited by the presentation of grating stimuli that had the orientation indicated. **(E)** Orientation preference map with retinotopic contours superimposed. Vertical lines represent iso-azimuth contours and horizontal lines are iso-elevation contours. **(F)** Detailed view of the region from (E) that is outlined. All contour intervals are 1.5°. **(G)** Ocular dominance preference map. **(H)** Spatial frequency preference map. Scale bars are 1 mm. Scale bar in (A) applies to (A-E), (G), and (H). Orientation, ocular dominance, and spatial frequency maps in this figure were obtained from different animals.

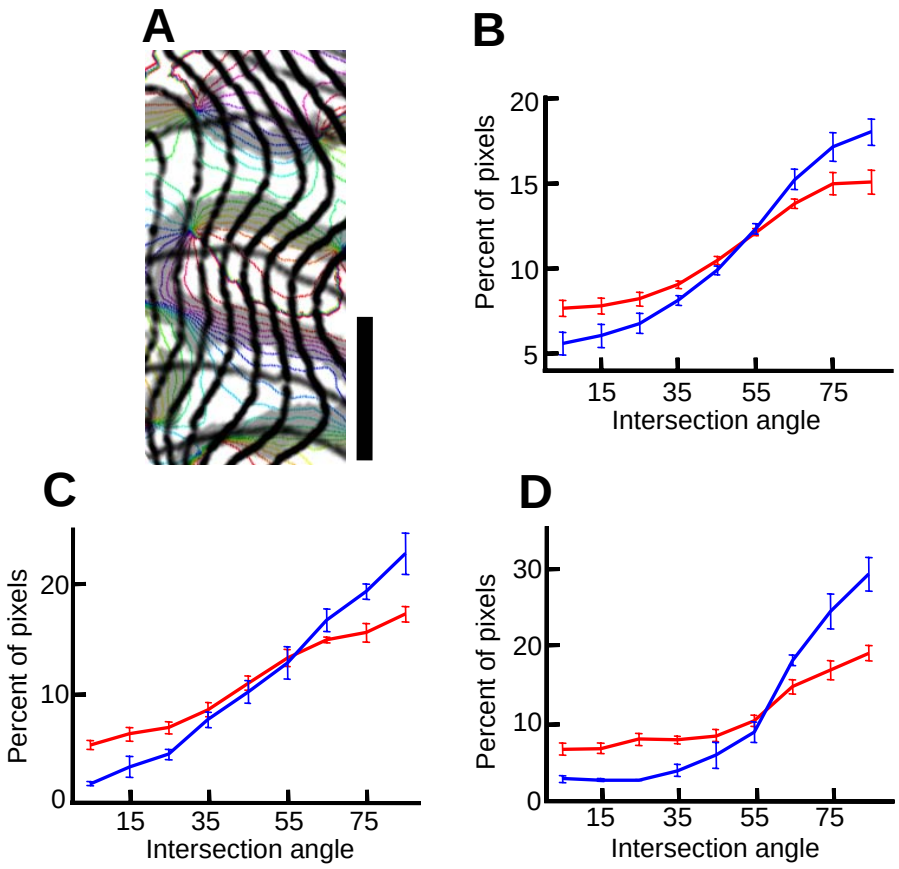

Figure 8. Relationships between the map of retinotopy and the maps of orientation, ocular dominance and spatial frequency. (A) Orientation contours (color) superimposed with retinotopic contours (black), for the outlined region from Figure 5E. The gray regions are the high gradient (top 30th percentile) regions of the orientation map. **(B-D)** Percent of pixels that have an intersection angle, within each 10° range whose center is indicated, between the retinotopic gradient and the gradient of the orientation (B), ocular dominance (C) or spatial frequency (D) map. Calculation over all pixels, red lines. Calculation restricted to pixels whose orientation (B), ocular dominance (C), or spatial frequency (D) gradient is within the highest 30th percentile, blue lines. Scale bar in (A) 1 mm. Error bars denote standard error of the mean percentages over 8 ferrets (B) or 4 ferrets (C-D).

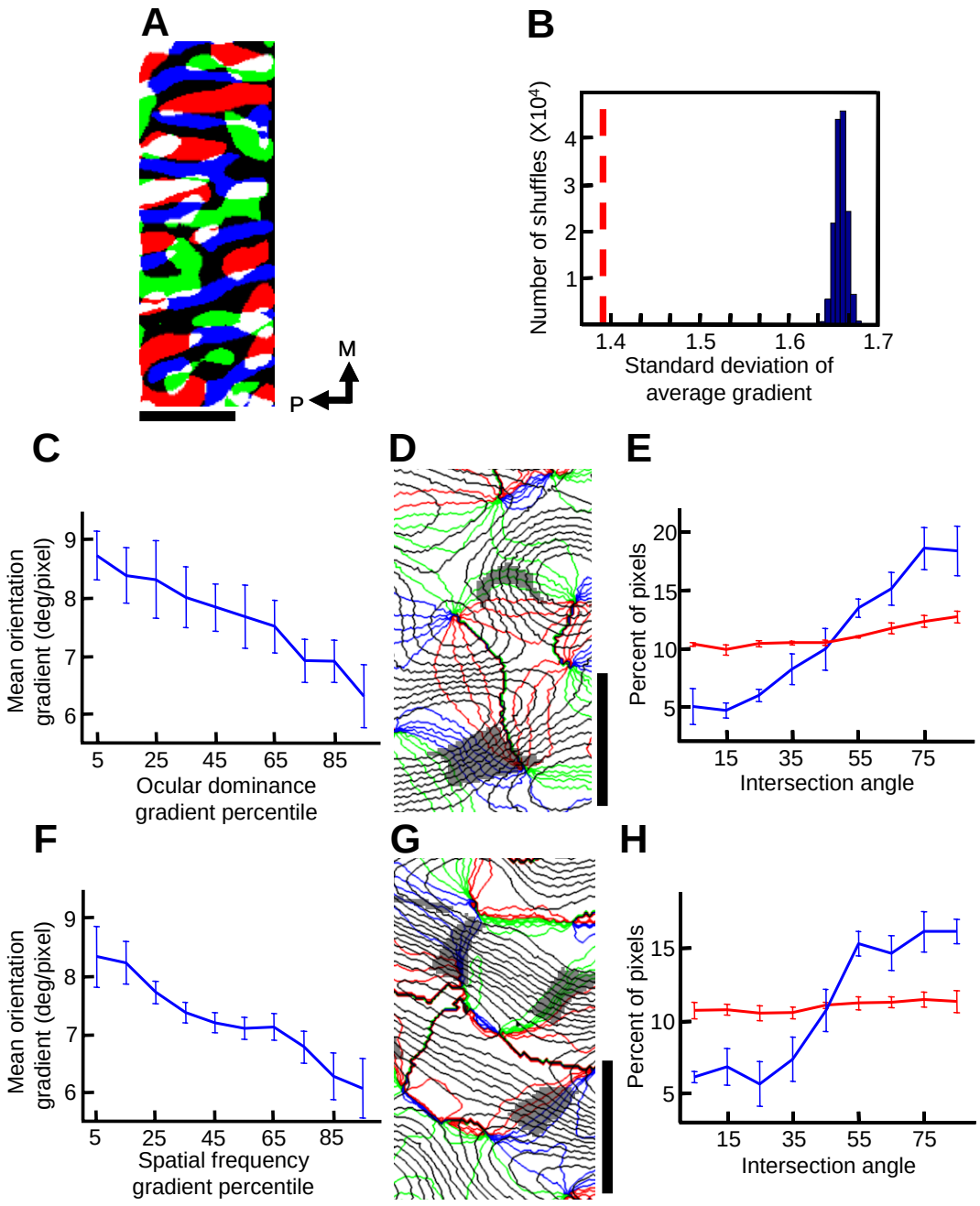
A
M
P
B
Number of shuffles (X10^4)
4
3
2
1
1.4
1.5
1.6
1.7
Standard deviation of
average gradient
C
Mean orientation
gradient (deg/pixel)
9
8
7
6
5
25
45
65
85
Ocular dominance
gradient percentile
D
E
Percent of pixels
20
15
10
5
15
35
55
75
Intersection angle
F
Mean orientation
gradient (deg/pixel)
9
8
7
6
5
25
45
65
85
Spatial frequency
gradient percentile
G
H
Percent of pixels
15
10
5
15
35
55
75
Intersection angle

Figure 9

Figure 9. Relationships between the orientation, ocular dominance, and spatial frequency maps. (A) High gradient regions (top 30th percentile) of orientation (blue), ocular dominance (green), spatial frequency (red), or two or more maps (white). **(B)** Standard deviation across cortex of the average gradient magnitude of the orientation, ocular dominance, and spatial frequency maps (red dotted line). Histogram of standard deviations after pixels within each map were randomly shuffled, in 150,000 cases (blue histogram). **(C, F)** Pixels are grouped into ten bins according to their ocular dominance (C) or spatial frequency (F) gradient percentile, and the mean orientation gradient for each group is indicated. **(D, G)** Colored lines representing orientation contours are superimposed on black lines representing ocular dominance (D) or spatial frequency (G) contours. Gray regions indicate locations where high gradient regions (top 30th percentile) of the orientation and ocular dominance (D) or spatial frequency (G) maps coincided. **(E, H)** Percent of pixels that have an intersection angle, within each 10° range whose center is indicated, between the orientation gradient and the ocular dominance (E) or spatial frequency (H) gradients. Average over all pixels, red line. Calculation for high orientation and ocular dominance (E) or spatial frequency (H) gradient overlap regions, blue line. Scale bar in (A) 1 mm, bars in (D) and (G) 0.5 mm. Error bars (in C, E, F, H) denote standard error of the mean values over 5 ferrets.

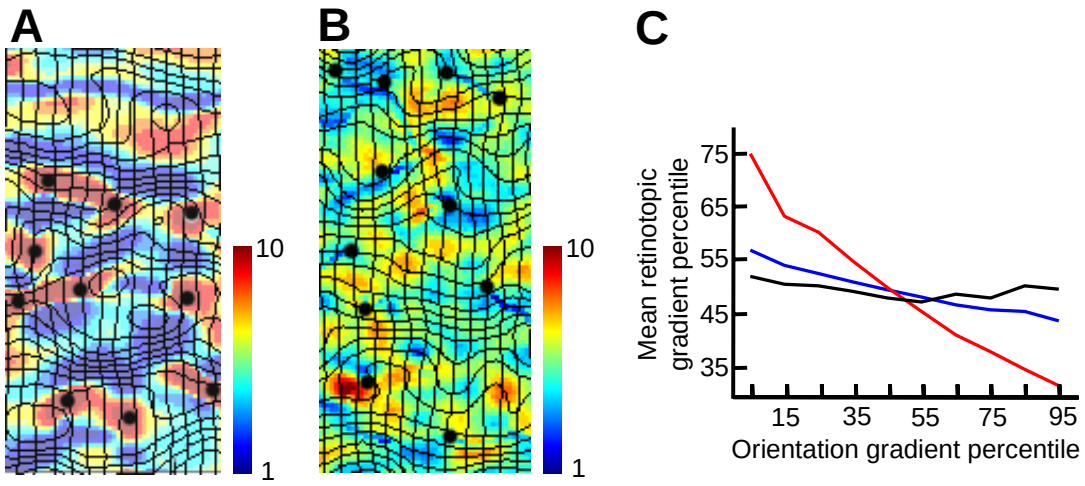

Figure 10. Local gradient relationships between the retinotopic and other feature maps. (A) Retinotopic contours are shown at high-resolution from a two-component (retinotopy and orientation) simulation (retinotopic azimuth contour intervals represent 4 times the extent of visual space than elevation contour intervals). The background represents the normalized orientation gradient (10 indicates that a pixel is within the highest 10^{th} percentile gradient, and 1 the lowest 10^{th} percentile). Black dots represent orientation pinwheels. **(B)** Retinotopic contours are shown at high-resolution from a four-component (retinotopy, orientation, ocular dominance, spatial frequency) simulation, as used throughout the manuscript (except in Figure 8A). Retinotopic contour intervals same as in (A). Background represents the average normalized gradient over the orientation, ocular dominance, and spatial frequency maps. Black dots represent orientation pinwheels. **(C)** Pixels are grouped into ten bins according to their orientation gradient percentile, and the mean retinotopic gradient percentile for each group is indicated. Red line, from two-component simulation; blue line, from four-component simulation; black line, from optical imaging experimental data.

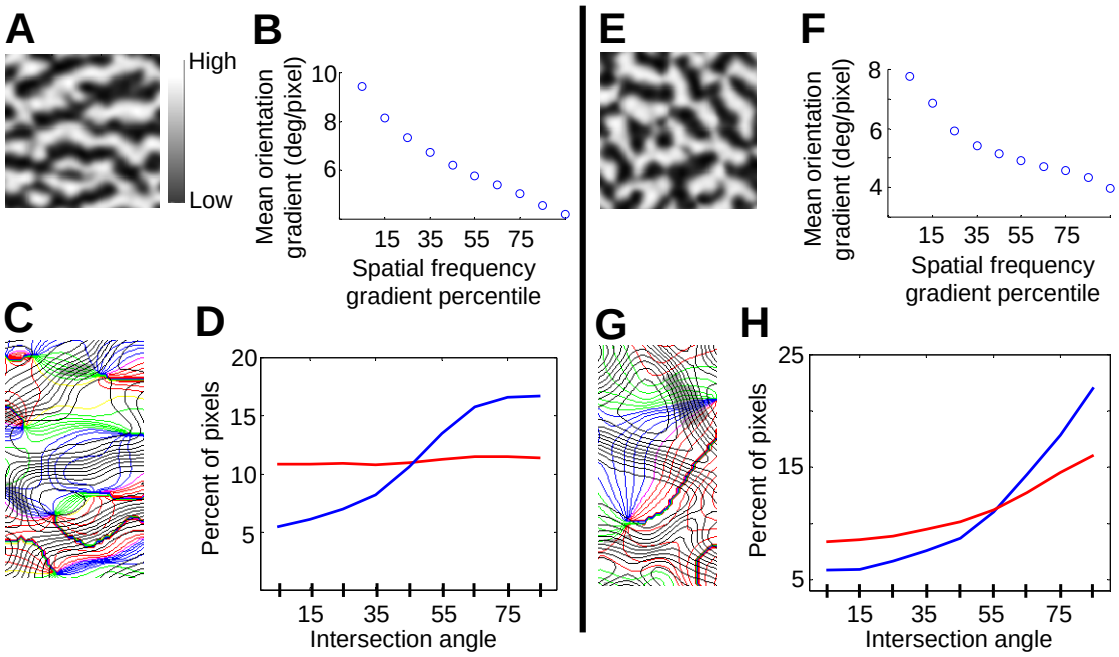

Supplementary Figure 1. Effect of visual space anisotropy on the spatial frequency map, as predicted by a dimension-reduction model. The retinotopic map was either anisotropic (A-D) or isotropic (E-H). **(A, E)** The spatial frequency map. **(B, F)** Pixels are grouped into ten bins according to their spatial frequency gradient percentile, and the mean orientation gradient for each group is indicated. **(C, G)** Orientation (color) contours superimposed on spatial frequency (black) contours. Gray pixels indicate locations where the gradient of both the orientation and spatial frequency maps are within the highest 30th percentile. **(D, H)** Percent of pixels that have an intersection angle, within each 10° range whose center is indicated by the x-tick mark, between the orientation and spatial frequency gradients. Red line shows the calculation over all pixels. Blue line indicates the calculation for those pixels where the gradients of both maps are within the highest 30th percentile.

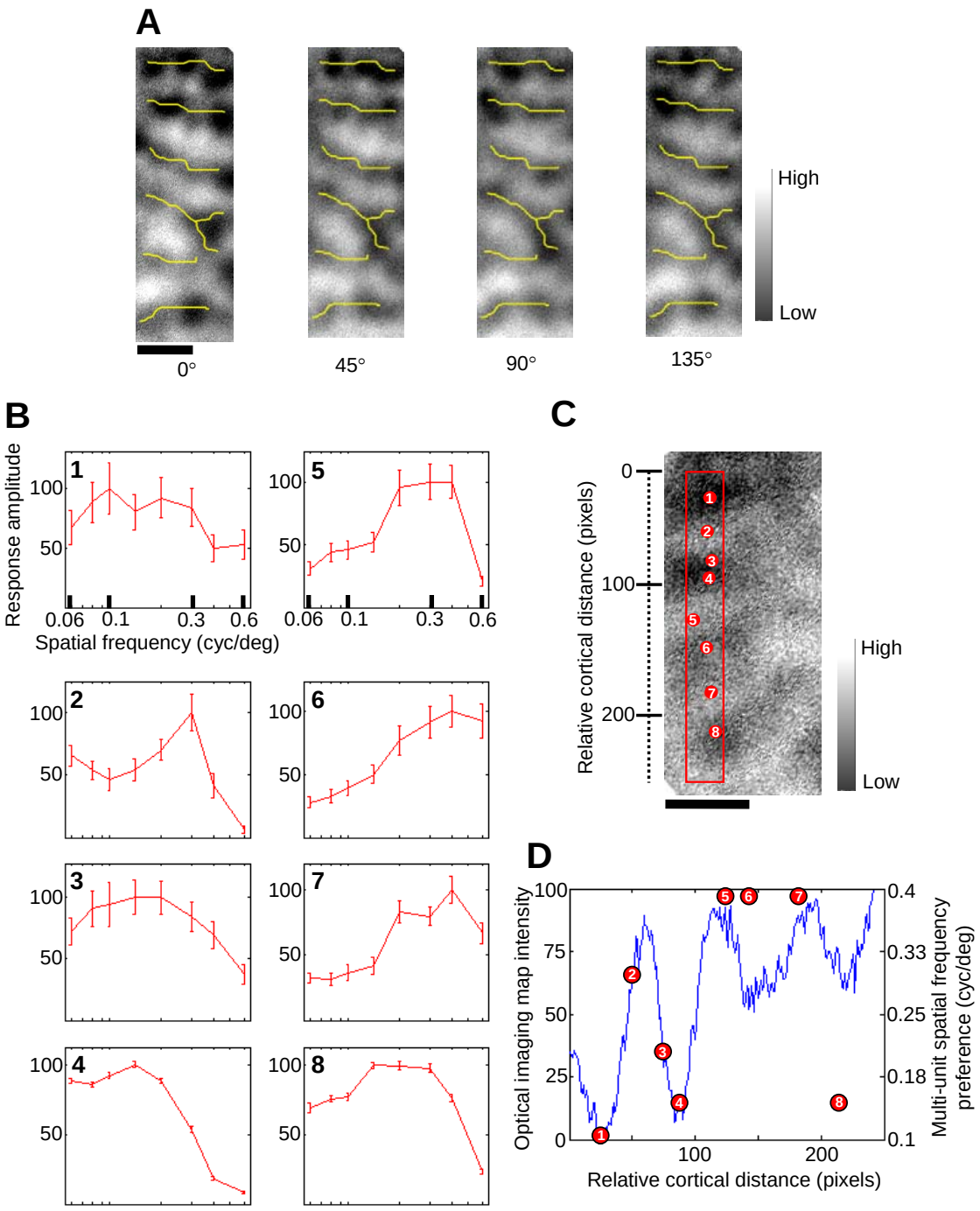

Supplementary Figure 2

Supplementary Figure 2. The spatial frequency map is largely independent of the orientation of the stimulus used to create it, and can be verified by electrophysiological recordings. (A) Spatial frequency preference maps. Each map was created using drifting gratings of a single orientation (indicated below each panel). The cortical response to high spatial frequency gratings (0.225 c/deg) was subtracted from that obtained with low frequency gratings (0.08 c/deg). The yellow marks were hand drawn to indicate those regions most strongly activated by low spatial frequencies in the first panel; the same marks are superimposed on each of the remaining panels. **(B)** Each panel indicates the spatial frequency tuning curve, measured by multi-unit electrophysiological recordings, of the cortical location whose position within an optical imaging-derived spatial frequency map is shown in (C). Responses are shown as percent maximal response along with the standard error of the mean (over repeated trials). **(C)** A spatial frequency preference map. The cortical response to high spatial frequency gratings (0.375 c/deg), summed over all orientations, was subtracted from that obtained with low frequency gratings (0.125 c/deg). **(D)** Comparison between optical imaging and electrophysiological spatial frequency measurements at corresponding cortical locations. The image intensity, for the outlined region in the map displayed in (C), was summed across all pixels for each relative cortical distance. The line plot indicates the summed image intensity plotted as a function of relative cortical distance within the outlined region. For comparison, the 8 red dots indicate the electrophysiologically-measured spatial frequency preference for the 8 sites whose position within the map is shown in (C). Scale bars in (A) and (C) 1 mm.

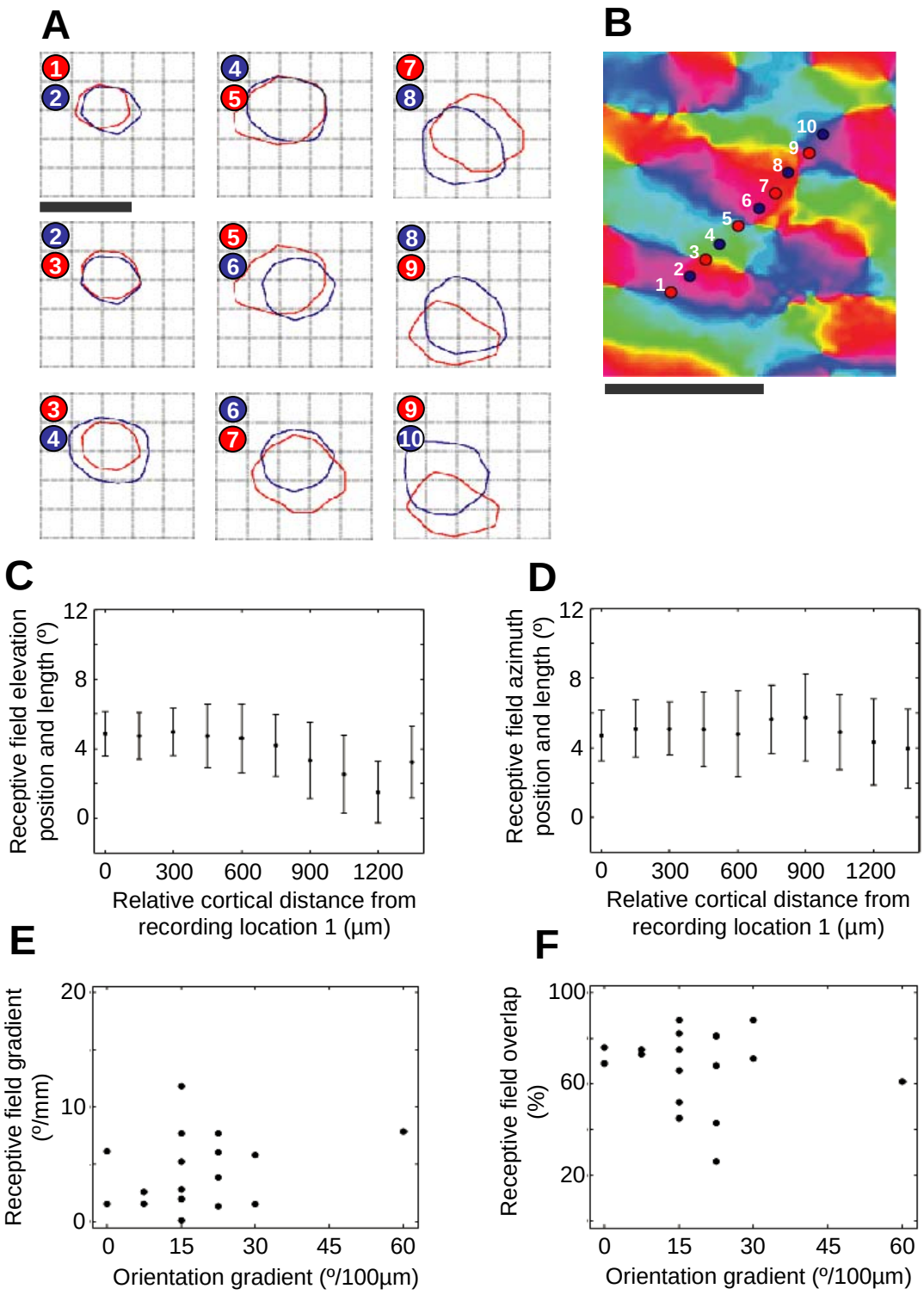

Supplementary Figure 3

Supplementary Figure 3. The local mapping of visual space and its relationship to the orientation map, as measured by multi-unit electrophysiological recordings. (A, B) Each panel in (A) indicates the receptive fields (at half-height) of two adjacent cortical locations (separated by 150 μm), whose position within the orientation map is marked in (B). Receptive fields were measured using the reverse-correlation method. Based on the global structure of the visual map in the ferret, the receptive fields for this line of recordings (proceeding from 1 to 10) are expected to approximately follow an iso-azimuth contour, and to move downwards in visual space. Note that adjacent cortical locations have largely overlapping receptive fields, regardless of their position within the orientation map. **(C, D)** The relative receptive field locations, in the elevation (C) or azimuth (D) dimension of visual space, of the 10 successive cortical penetrations indicated in (B). The extent of each receptive field along the same dimension of space is indicated by the bar. We found a relatively smooth progression of receptive field locations across the cortex. **(E, F)** Graphs comparing the receptive field gradient (E) or receptive field overlap (F) between nearby (150 or 300 μm) recording location pairs to the orientation gradient between the pair. We found no strong correlation between the orientation gradient and either the receptive field gradient or the degree of receptive field overlap. Scale bar in (A) 5˚; bar in (B) 1 mm.

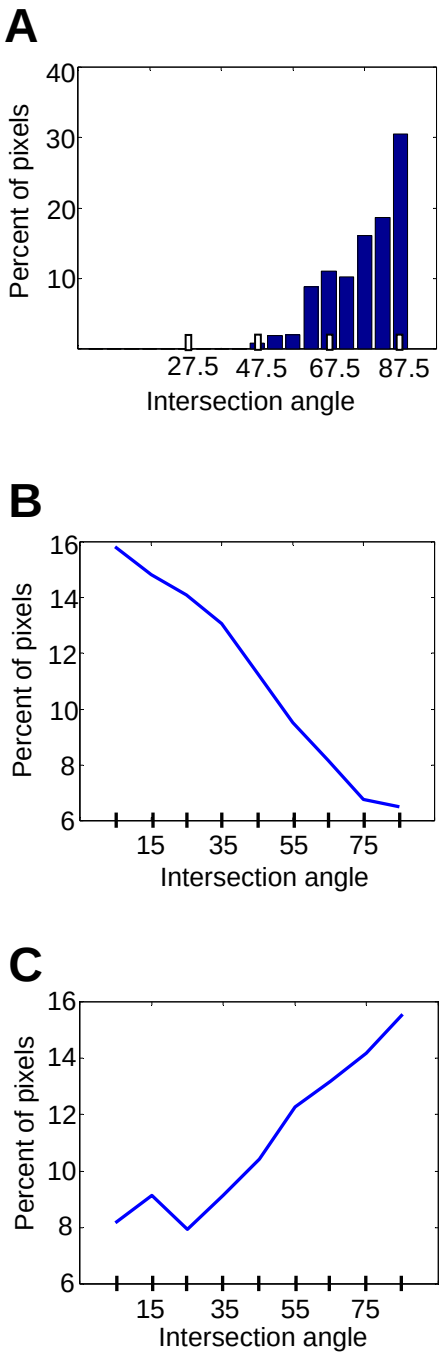

Supplementary Figure 4. The relationship between iso-azimuth and iso-elevation contours. (A) Percent of pixels that have an intersection angle, within each 5° range whose center is indicated, between the retinotopic elevation gradient and the retinotopic azimuth gradient from V1 in a ferret. **(B, C)** Percent of pixels that have an intersection angle, within each 10° range whose center is indicated, between the orientation gradient and the retinotopic elevation (B) or azimuth (C) gradient from the same ferret.

Animal #	1	2	3	4	5	6	7	Mean ± STD
Elevation magnification (mm/deg)	0.26	0.31	0.29	0.27	0.31	0.24	0.30	0.28 ± 0.027
Azimuth magnification (mm/deg)	0.068	0.098	0.062	0.063	0.094	0.067	0.074	0.075 ± 0.015
Magnification anisotropy (elevation:azimuth)	3.8	3.2	4.7	4.2	3.3	3.6	4.1	3.8 ± 0.53
Peak elevation-azimuth intersection angle (deg)	87	90	87	85	85	89	82	86 ± 2.7

Supplementary Table 1. Retinotopy data from 7 ferrets. Elevation and azimuth magnification (mm cortex per degree of visual space) were measured from retinotopic single-condition maps, and represent the mean magnification over the entire region of V1 accessible to imaging; to calculate the magnification we measured the cortical distance between the peaks in the activation patterns due to stimuli that were separated by a known distance in visual space. The magnification anisotropy is the ratio of the elevation magnification to the azimuth magnification. To determine the peak elevation/azimuth intersection angle, all pixels within a region were grouped into ninety 1° bins according to the intersection angle between the elevation and azimuth map gradients at that pixel. The peak was defined as the intersection angle bin containing the most pixels. The last column in the table indicates the mean and standard deviations of the measurements, averaged over all seven ferrets.

CHAPTER 2: The local spatial relationships among visual space and other feature maps in cat area 18

SUMMARY

Although spatial relationships between many pairs of feature maps in visual cortex have been described, the local relationships between the retinotopic and other maps are poorly understood. We examined whether local distortions exist in the retinotopic map, and if so whether they correlate with features in other functional maps, such as orientation pinwheels. We used the combined methods of intrinsic signal optical imaging along with multi-unit electrophysiological recordings in cat area 18 targeted to specific areas of functional maps. Using optical imaging, we found that orientation and ocular dominance maps have clear spatial relationships, similar to those found in other areas and species. In contrast, we did not detect clear local spatial correlations between the retinotopic and orientation map. Two paradigms were used to look for correlations. In the first, a linear series of recordings were made across the tangential dimension of cortex, and the receptive field and orientation preference were measured at each location. As the distance between recording pairs increased, receptive field overlap decreased. However, this trend was only apparent over larger distances; significant scatter existed more locally. Further, for more localized recordings (pairs < 450 μm apart), we did not detect a relationship between the degree of receptive field overlap and the orientation difference. In a second paradigm, a matrix of electrodes was targeted to the orientation map such that the individual electrodes surrounded an orientation pinwheel or were positioned within an orientation domain. We did not detect a clear relationship between

the receptive field gradient and orientation gradient for pairs of recordings from the electrode array. Thus, while the orientation and ocular dominance maps are correlated on a local scale in cat area 18, we do not find similar correlations between the orientation and retinotopic maps.

INTRODUCTION

Spatial relationships between pairs of feature maps are a robust feature of visual cortex. For example, stereotyped relationships between the orientation and ocular dominance maps are found in the monkey, cat, and ferret. Further, in species in which a tangential map of spatial frequency has been observed, relationships between this map and that of orientation exist. The relationships that have been described between the maps mentioned are consistent with the dimension-reduction model of cortex, suggesting that the principles guiding this model may generally underlie cortical organization. If this were the case then all pairs of maps should have relationships consistent with dimension-reduction. But it has remained a matter of contention whether the retinotopic map follows the same principles. Specifically, while the more global relationships described between the retinotopic and other maps are consistent with the principles, reports on local correlations are in disagreement (see Chapter 1). The original dimension-reduction models predicted a negative local correlation between the retinotopic and orientation maps, such that in positions of cortex where orientation changes rapidly, receptive fields were predicted to change more slowly. However, early experimental reports found a positive correlation, and later groups reported no correlation (see Chapter 1).

We chose a model system and experimental techniques that would maximize our chances of finding local correlations between the retinotopic and orientation maps. Some experimental techniques may not have the resolution to detect local relationships between the retinotopic and orientation maps, even if they do exist. For example, the large cortical point image size derived from intrinsic signal optical imaging may preclude allowing one to detect local distortions in the retinotopic map (Das and Gilbert, 1995; Bosking et al., 2002). The point image size measured with electrophysiology is significantly smaller (Das and Gilbert, 1995). Further, of current methods, electrophysiology provides the best chance to measure the precise structures of receptive fields, particular when objective, automated techniques such as reverse correlation are used (Jones and Palmer, 1987; DeAngelis et al., 1993). We further reasoned that the best chance of finding local correlations between the retinotopic and orientation maps would come from looking in an area where the orientation map pinwheel density is low: similarly spaced electrode penetrations will sample a low pinwheel density orientation map with greater resolution than a higher pinwheel density orientation map. Further, if retinotopic map distortions exist on the scale of the orientation map, then they will be more pronounced in a cortical area where the orientation map has a lower pinwheel density. Cat area 18 has a relatively low orientation pinwheel density, compared to cat area 17 (Bonhoeffer et al., 1995) or ferret area 17 and 18 (Muller et al., 2000). We asked whether local relationships between retinotopy and orientation were detectable using electrophysiological mapping methods combined with intrinsic signal optical imaging in cat area 18.

METHODS

Animals. Five adult cats were used in these experiments. Animals were prepared for acute experiments according to protocols approved by MIT's Animal Care and Use Committee. Details have been described (Rao et al., 1997). Anesthesia was induced with ketamine (15 mg/kg) and xylazine (1.5 mg/kg) and maintained with isofluorane (1.0% to 1.5% in 70:30 mixture of N_2O/O_2) delivered through a tracheal cannula using artificial respiration. Fluid maintenance was achieved with a 50:50 mixture of 5% dextrose and lactated Ringer's solution, supplemented with vecuronium bromide (0.2 mg/kg/hr) for paralysis. Expired CO_2 was maintained at 4% and the anesthesia level was monitored continuously. A craniotomy and durotomy were performed to expose V1. A chamber was mounted on the skull around the exposed region and filled with agarose (1.5% in saline). This was covered by a cover glass and then silicone oil.

Optical imaging. The details of optical imaging have been described (Dragoi et al., 2000). The cortex was illuminated with 630 nm light. Images of cortical reflectance were obtained (at 70 pixels/mm) using a slow-scan video camera equipped with a tandem macro-lens arrangement, then digitized and fed into a computer (Imager 3001, Optical Imaging, Mountainside, NJ). The camera was focused 500 μm below the cortical surface. Stimuli were generated using CRS (Cambridge Research Systems Ltd., Rochester, Kent, UK) on a CRT monitor that was placed at 57 cm from the eyes and covered 40° (horizontal) × 30° (vertical) of the visual field.

Orientation and ocular dominance maps. For orientation maps, stimuli were presented binocularly, and consisted of drifting, full-field square-wave gratings having one of 4 orientations (separated by 45°), with a spatial frequency of 0.25 cycles/degree and temporal frequency of 2 cycles/second. Monocularly presented drifting gratings were

used to obtain ocular dominance maps. The grating stimuli were presented in pseudorandom order, each for 5 seconds during which cortical images were captured followed by 7 seconds of a blank screen. Single-condition orientation maps were obtained by subtracting the response to all orientations combined ("cocktail blank") from the response to each single orientation. To produce orientation angle maps, we performed vector summation at each pixel of the filtered (Gaussian filter, standard deviation of 0.1 mm) single-condition orientation maps; the angle of the resultant vector indicates the preferred orientation at that pixel. To obtain an ocular dominance map, we subtracted the average of all filtered orientation single-condition maps obtained with one eye from those obtained with the other eye.

Analysis of map structures and relationships. The procedures used to analyze the relationships between optical imaging-derived functional maps is identical to that described in Chapter 1 (see Chapter 1 Methods).

Electrophysiology. Multi-unit activity was recorded using tungsten electrodes (1 MΩ; FHC, Bowdoinham, ME) and band-pass filtered. Visual receptive fields were measured using the reverse correlation technique (Jones and Palmer, 1987; DeAngelis et al., 1993). The stimulus consisted of a single 1.5° × 1.5° square that pseudo-randomly varied its x and y center position (with 0.75° resolution) every 30 ms within a 11° × 11° stimulus grid. A stimulus 'movie' consisted of 100 such 30 ms frames along with 4 blank frames, so that each position was played once during each movie. Twelve different movies were presented with bright spots on a dark background, and twelve with dark spots on a light background. During a recording session, each movie was presented 4 times, so that each bright and dark spot was presented 48 total times. The multi-unit

receptive field was defined as the probability distribution of the stimulus position 30 ms before each spike. We chose a 30 ms delay because it approximates a typical response latency for neurons in the cat visual cortex. The background firing rate was subtracted. Responses to bright and dark stimuli were added together, and the center of the receptive field was determined by finding the centroid of the distribution. For measuring receptive field overlap, the receptive fields included all positions that elicited at least 50% of the maximum response. The position of the recording electrodes was marked on an image of the cortical vasculature. To generate a visual field map, each pixel of cortex was associated with the nearest recording site, using Voronoi tessellation (Matlab, Natick, MA), and was assigned the azimuth and elevation receptive field locations that were determined for that site.

For measuring multi-unit orientation preference, the stimuli consisted of drifting square-wave gratings presented at one of 8 orientations and 2 directions (with a spatial frequency of 0.25 cycles/degree and a temporal frequency of 2 cycles/second). The orientation preference of a site was defined as the orientation of the stimulus that produced the maximum number of spikes in the post-stimulus time histogram (over 1500 ms).

RESULTS

We first determined whether feature maps had spatial relationships in cat area 18 that are found in other species. We used intrinsic signal optical imaging to measure the layouts of the orientation and ocular dominance maps. The orientation map measured would also serve as a guide for electrode penetrations targeted to specific functional

regions of the cortex. An orientation map obtained from cat area 18 is shown in Figure 1B. The structure of this map has previously been reported. In the same region, we measured an ocular dominance map (Figure 1A). The ocular dominance map consisted of mostly isotropic contralateral and ipsilateral domains. To measure the spatial relationships between the orientation and ocular dominance maps, we calculated the two-dimensional spatial gradient at each pixel of each map. We grouped the pixels in the imaged region according to their ocular dominance percentile, and calculated the mean orientation gradient (raw value) for each group. We found a negative correlation between the gradients in the two maps (Figure 1C). We next calculated the intersection angle, between the gradient of the orientation map and the gradient at the corresponding pixel of the ocular dominance map. We found a tendency for the intersection angles between the gradients of the two maps to be near perpendicular (Figure 1D). These results indicate that the maps of orientation and ocular dominance in cat area 18 are inter-dependent, with spatial relationships of a similar nature to those found in area 17 of the cat, monkey and ferret.

We next explored the nature of the retinotopic map in cat area 18, using multi-unit electrophysiological recordings to record the receptive fields at multiple locations across cortex. The distance between adjacent recordings was on average approximately 500 μm (Figure 2A). We used the reverse correlation method of receptive field mapping to measure the two-dimensional structure of the receptive fields, where the stimuli consisted of sparse noise. In Figures 2A-B, we show the structure of the azimuth and elevation retinotopic maps constructed with this method. An overall progression of both azimuth and elevation receptive field positions across the cortex is apparent from the maps.

However, at a more local scale, significant scatter in receptive field centers is apparent. In the same cortical region, we performed optical imaging to measure the orientation preference map (Figure 2C). No spatial relationship between the maps of orientation and either elevation or azimuth retinotopy is apparent based on visual inspection of the maps. In particular, it is not clear whether the local scatter in receptive field positions relates to features of the orientation map, such as orientation pinwheels.

To uncover a local relationship between retinotopic and orientation maps, it is necessary to measure the maps at a finer scale. We next made a row of closely spaced (150 μm) recordings across the tangential dimension of cat area 18, measuring the receptive field structure (Figures 3A-B) and orientation preference (Figure 3C) at each position. A relatively smooth progression of receptive field position for both the azimuth and elevation axes of space can be observed. Orientation preference changes little between most pairs of nearby recordings, and the overall progression of orientation preference is smooth, although there is a more pronounced jump at some locations. However, a systematic relationship between orientation difference and receptive field movement is not apparent from visual inspection of the line of recordings.

We next analyzed the local relationships between retinotopy and orientation more quantitatively. We determined the relationship between the orientation gradient and the retinotopic gradient or the degree of receptive field overlap. Receptive field overlap may be a more appropriate measure than receptive field movement in the context of comparing map relationships. The degree of receptive field movement (or gradient) between nearby recording locations is dependent on the local retinotopic magnification for the area. Since retinotopic magnification changes systematically across the map, then

areas of the map with high magnification will have small receptive field movement on average, and areas with low magnification will have large receptive field movement. If receptive field movement is compared with orientation movement from recordings made in areas of the retinotopic map with different overall magnification, then the effect of this overall magnification could cancel any local correlations that might be present between the orientation and retinotopic maps. Receptive field overlap does not suffer from this problem, however, because the measure more naturally scales with magnification.

We plotted the degree of receptive field overlap as a function of cortical distance between pairs of recording locations (Figure 4A). As expected, the degree of receptive field overlap decreased as recording distance increased, and there was a relatively strong correlation between the measures ($r^2 = 0.45$). However, for a constant value of cortical distance, receptive fields could be either highly overlapping or nearly non-overlapping, indicating scatter in the local structure of the retinotopic map.

We reasoned that if the retinotopic map had a spatial relationship with the orientation map, then the degree of receptive field overlap for nearby cortical locations could be more accurately predicted by also taking into account the differences in preferred orientation for the cortical locations. Before making the electrode penetrations, we measured the orientation preference map using intrinsic signal optical imaging. A blood vessel reference map was also collected, which could be aligned with the orientation map. By marking the location of each electrode penetration on the blood vessel map, we could estimate the preferred orientation for that location as measured by optical imaging. We found no correlation between receptive field overlap and orientation

difference (measured by optical imaging) for nearby (< 400 μm) recording pairs (r^2 = 0.01; Figure 4B).

The lack of a correlation could have arisen from the fact that we measured the orientation preference of the cortical sites by aligning the electrode penetrations with the optical imaging maps. We could have incorrectly estimated the position of the electrode penetrations in the blood vessel map; further, the orientation map measured by optical imaging could be poorly correlated with orientation measured by electrophysiology. Since we measured the orientation preference for each location with electrophysiology as well, however, we could test these possibilities. First, we directly compared the orientation preference measured with both optical imaging and electrophysiology. We found that there was a strong correlation between the orientation preference measured by these two methods (r^2 = 0.83; Figure 4C). This indicates that the targeting of electrode penetrations to specific functional regions of the optical imaging-derived maps was effective, and that the lack of a correlation between receptive field overlap and orientation difference did not arise because orientation preference was being incorrectly estimated from the optical imaging maps. We also compared the degree of receptive field overlap to the orientation difference, using the orientation preference measured from electrophysiology (Figure 4D). Again, no clear relationship was present between the two measures (r^2 = 0.002).

The lack of a relationship between the retinotopic and orientation maps could have arisen from a number of different methodological pitfalls. When a series of recordings is made along a linear track of the cortex, the orientation difference between most nearby recording pairs is small. Thus, a lack of relationship between the retinotopic

and orientation maps may arise from not sampling enough high gradients regions of the orientation map. Further, because recordings at different locations are made at different times, then any eye movements of the animal in between recordings would artificially increase the amount of scatter in the measurement and confound the true receptive field differences between different locations.

To alleviate these potential problems, we employed a second recording paradigm. We fabricated a rectangular 2 by 3 matrix of 6 total electrodes, where the spacing between adjacent electrodes was 350 μm. We targeted the matrix to specific functional regions of the orientation map, measured by optical imaging, such that a grid of electrodes either spanned an orientation pinwheel or was positioned within an orientation domain. An example is shown in Figure 5. It can be seen that the receptive field positions for most of the six recording locations were similar; but clear jumps in receptive field position were present between some adjacent recording pairs (Figure 5A). This is similarly true for orientation preference: the orientation preference of most of the locations was similar, but there were also some jumps in orientation preference for nearby pairs (Figure 5B).

We analyzed the relationships between receptive field movement and orientation difference quantitatively in multiple ways. For nearby recording pairs (electrodes < 475 μm apart), we compared the degree of receptive field overlap to the orientation difference (or orientation gradient), as measured by electrophysiology (Figure 6A). In this figure, the results are pooled over multiple matrix electrode penetrations within one cortical hemisphere. We found no clear relationship between receptive field overlap and orientation difference ($r^2 = 0.004$). For the same recording pairs, we also measured the

receptive field gradient and orientation gradient; we similarly found no correlation between these measures ($r^2 = 0.02$; Figure 6B).

DISCUSSION

The local structure of the retinotopic map in visual cortex is poorly understood. Dimension-reduction models, which have done well to explain the relationships found between certain feature maps in visual cortex, predict that the local structure of the retinotopic map should have correlations with other maps. But to date, experimental evidence consistent with this prediction does not exist. Further, some of the experimental studies that have analyzed the local structure of the retinotopic map are in disagreement with each other. In cat area 18, we find significant scatter in the local structure of the retinotopic map, and we fail to find any systematic local relationships between retinotopy and other feature maps. We discuss how our findings relate to those of other investigators, the factors that contribute to the difficultly in measuring the local relationships between the retinotopic and other maps, and what principles may govern the local structure of the retinotopic map.

Experiments analyzing the local relationships between retinotopy and other feature maps

Two groups have measured the local structures of the orientation and retinotopic maps in cat area 17 using electrophysiological recordings, but came to largely different conclusions regarding the relationships between these maps (Das and Gilbert, 1997; Buzas et al., 2003). The spatial receptive fields and orientation preferences of single

neurons were measured using hand mapping techniques based on electrophysiological responses. The first group (Das and Gilbert, 1997) found that receptive fields shifted more rapidly than average near orientation pinwheel regions compared to orientation domain regions in cat area 17. A strong positive correlation ($r^2 = 0.71$) was measured between receptive field shift and orientation shift, for pairs of nearby recording locations. Similarly, a positive correlation was found between the retinotopy gradient (the receptive field shift normalized by the distance between the pair of recorded neurons) and the orientation gradient.

Buzas et al. (Buzas et al., 2003) used similar methods as Das and colleagues, but did not find any location correlations between the two maps. The correlation that they measured between receptive field shift and orientation shift ($r^2 = 0.09$) was very weak and largely different from that measured by Das and colleagues (Das and Gilbert, 1997). Buzas and colleagues did observe a positive correlation between the *gradient* of retinotopy and orientation, but they suggested that this was a spurious correlation that arises from systematic errors in estimating the position of the neurons being recorded from. Measuring the gradient of a feature between two neurons requires dividing the difference of the preferred features of each neuron by the distance between the neurons being recorded from. But when using electrophysiology, the position of the recorded neurons relative to the recording electrode is unknown, and must be estimated. If this distance is overestimated, the gradients of both orientation and retinotopy will be underestimated by the same amount. If this distance is underestimated, the gradients of both orientation will both be overestimated. Since the error in the estimated distance between the neurons affects the measured orientation and retinotopy gradients in the

same direction, the error leads to a spurious positive correlation between the gradients of the two features. Buzas et al. showed using Monte Carlo simulations that these measurement errors accounted for the measured positive correlations, and concluded that *no correlation* exists between the retinotopy and orientation gradient maps.

Thus, different results and conclusions regarding the relationships between the retinotopic and orientation maps were reached by these two groups. More recent experimental and modeling results, including our own, support the results of Buzas et al. (Buzas et al., 2003) and further argue against those of Das et al. (Das and Gilbert, 1997).

First, Bosking and colleagues have analyzed the relationships between the retinotopic and orientation maps in the visual cortex of the tree shrew (Bosking et al., 2002). Retinotopy was analyzed using both intrinsic signal optical imaging and electrophysiology, and orientation was measured with optical imaging alone. The mapping of receptive fields by electrophysiological methods was automated, rather than based on hand mapping. The authors failed to find any local correlations between the structures of the retinotopic and orientation maps, when either electrophysiological or imaging methods were used to measure the retinotopic map.

Second, we measured the relationships between retinotopy and orientation maps in cat area 18 (and ferret area 17; see Chapter 1). Like Bosking and colleagues, we used automated methods of mapping receptive fields with electrophysiological recordings. For mapping orientation preference, we used both electrophysiological recordings and optical imaging. We also failed to find systematic local distortions in the retinotopic map that correlated with distortions in other functional maps, either in cat area 18 (this chapter) or in ferret area 17 (Chapter 1).

The challenge of measuring the local structure of the retinotopic map

Numerous methodological issues could contribute to the difficulty in measuring the local structure of the retinotopic map, and could lead to the discrepancies between the results of Das and colleagues and the results from other groups, including our own. First, Das et al. and Buzas et al. used hand-mapping techniques to measure the structures of receptive fields (Das and Gilbert, 1997; Buzas et al., 2003). The subjective nature of this method would seem to make it inappropriate for measuring the retinotopic map at a fine scale. Automated methods of recording are less subjective and preferred.

Other problems also confound measurements of the retinotopic map when using electrophysiological mapping methods. For example, any eye movements that occur in between different recording locations could contribute to noise in the estimation of the receptive field gradient between sites. At the least, paralysis of the animal is necessary to prevent eye movement; further, the sclera can be physically demobilized. But to ensure that this source of noise does not exist, it is necessary to either compare receptive field movement only for those pairs of recordings that are performed at the same time, or to have a second reference electrode in the cortex throughout all of the recordings that are compared. Our matrix electrode recordings (Figures 5 and 6) utilized the first method, whereas both Das et al. and Buzas et al. used the second method (Das and Gilbert, 1997; Buzas et al., 2003). Bosking et al. did not control for eye movement artifacts in either way. An additional problem, mentioned briefly above, is that the actual spatial location of a neuron recorded with an electrode is unknown; this will affect the measurement of the receptive field gradient (which relies on knowing the physical distance between the

recorded neurons) and will also affect the estimation of the position of the recorded neurons in the orientation map. Finally, as mentioned in the results section, magnification changes systematically across the visual cortex; receptive field gradients will be smaller on average for areas of high magnification compared to areas of low magnification. Thus, if measurements of receptive field gradient and orientation gradient are made in areas with different magnification, and the measurements are pooled in order to look for a systematic relationship between the two measures, the effect of magnification on the receptive field gradient between nearby electrodes may be stronger than the effect of orientation gradient, and smear any relationships that exist between receptive field gradient and orientation gradient. We used the measure of receptive field overlap to avoid this confound, but most other groups have relied on measuring the receptive field gradient.

To our knowledge, relationships between any two feature maps have yet to be demonstrated with electrophysiological mapping techniques. Indeed, the demonstration of the relationships between the orientation and ocular dominance maps, which has been repeated by many groups, awaited optical imaging methods (Blasdel and Salama, 1986). Thus, it may be unrealistic to expect to find relationships between the retinotopic and other maps with these electrophysiological mapping methods, unless new and improved mapping techniques are utilized. One possibility is to use many-electrode arrays that have been employed in other systems; these would permit the simultaneous recording of receptive fields and orientations from many locations within a local area of cortex. Uncovering the relationships may, on the other hand, necessitate using imaging techniques. The technique employed in most studies, however, intrinsic signal optical

imaging, suffers from having a large cortical point image size, which may preclude the detection of local distortions in the retinotopic map (Das and Gilbert, 1995; Bosking et al., 2002). An extremely promising emerging imaging technique that is free of many of the above-mentioned problems is two-photon calcium dye imaging (Ohki et al., 2005; Ohki et al., 2006); if receptive fields can be mapped in fine detail with this method, and if the cortical point image size due to the calcium signal is on the scale of the spiking point image size, this technique has the potential to resolve the fine structure of the retinotopic map and to uncover any local relationships that may exist between the retinotopic and other feature maps.

Principles governing the local structure of the retinotopic map and the relationships between this map and other feature maps

With the exception of Das et al. (Das and Gilbert, 1997), our study and previous studies have reported a lack of a relationship between the retinotopic and other feature maps (Das and Gilbert, 1997; Bosking et al., 2002; Buzas et al., 2003; Yu et al., 2005). Further, most studies have reported a significant amount of scatter in receptive field positions within local areas of cortex (Cynader et al., 1987; Bosking et al., 2002; Buzas et al., 2003; Yu et al., 2005). The methodological problems described above could be contributing to these conclusions; but it is equally plausible that the local spatial structure of the retinotopic map is truly noisy, and that no local relationships exist between this and other feature maps.

The expectation that local relationships might exist between retinotopic and other maps derives from the predictions of dimension-reduction models; these models have

successfully predicted the local relationships between many pairs of feature maps, and the original models also predicted similar relationships between retinotopy and other maps (Durbin and Mitchison, 1990; Obermayer et al., 1990). However, we have suggested that the predictions of these original simulations may not have been realistic. Indeed, if retinotopy and orientation are the only two features that are mapped onto a two-dimensional surface using the Kohonen algorithm, significant distortions exist in the retinotopic map and a strong negative correlation is predicted between the gradients of retinotopy and orientation (see Chapter 1). But if additional features maps, which are known to exist in the real visual cortex, are included in the simulations, then the coupling between the retinotopic and orientation maps is predicted to be significantly weaker (see Chapter 1). These results indicate that a lack of local relationships between retinotopy and other feature maps would not be inconsistent with the notion that dimension-reduction principles guide cortical map organization. Further, the predictions of dimension-reduction models, regarding the local relationships between the retinotopic and other feature maps, are dependent on the local structure of the retinotopic map that is simulated, including the amount of scatter present in the map. To date, simulations have not been careful about including a realistic amount of scatter in this map. Thus, it remains difficult to confidently predict what relationships are expected between the retinotopic and other maps by dimension-reduction models.

FIGURES

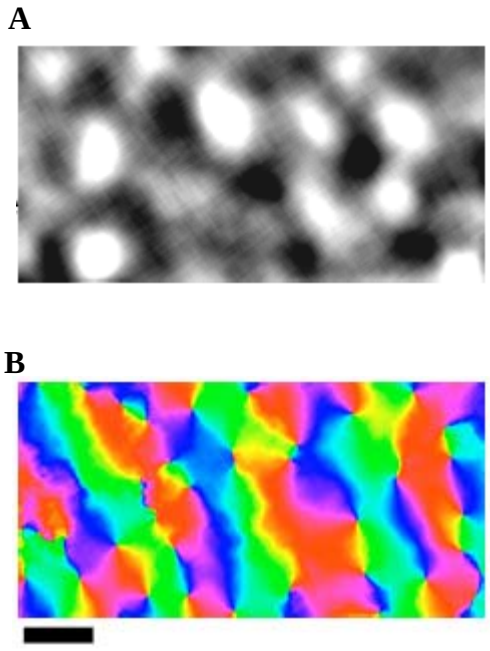
A
B
C
Orientation gradient (°/pixel)
6.2
5.6
5.0
15
35
55
75
95
Ocular dominance gradient percentile
D
Percent of pixels
13
11
9
5
25
45
65
85
Intersection angle (°)

Figure 1.

Figure 1. Orientation and ocular dominance maps have specific spatial relationships in cat area 18. **(A)** An ocular dominance map from cat area 18 measured with intrinsic signal optical imaging. **(B)** An orientation preference map obtained from the same region as the ocular dominance map. **(C)** Pixels are grouped into ten bins according to their ocular dominance gradient percentile, and the mean orientation gradient for each group is indicated. **(D)** Percent of pixels that have an intersection angle, within each 10° range whose center is indicated by the x-tick mark, between the orientation gradient and the ocular dominance gradient. Scale bar in (B) 1 mm, and applies to (A-B).

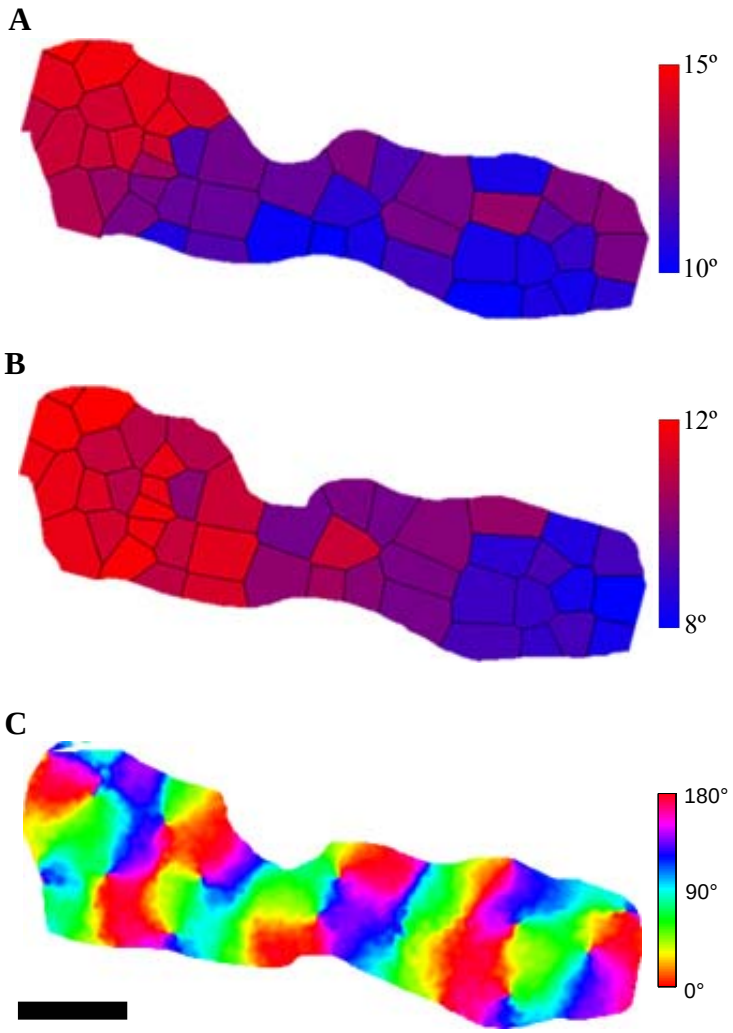

Figure 2. Multiple electrophysiological recordings reveal the global progression of receptive field locations, and local scatter in these locations, across the tangential dimension of cat area 18. (A-B) At 47 tangential locations within cat area 18, we measured the multi-unit two-dimensional spatial receptive fields. The image pixels are color-coded according to the azimuth (A) or elevation (B) component of the receptive field measured nearest that pixel. A clear progression of receptive field locations is evident across the cortex, although significant local scatter exists. **(C)** An orientation preference map from the same region, obtained by an intrinsic signal optical imaging session before the electrophysiological recordings. Scale bar in (C) 1 mm, and applies to (A-C).

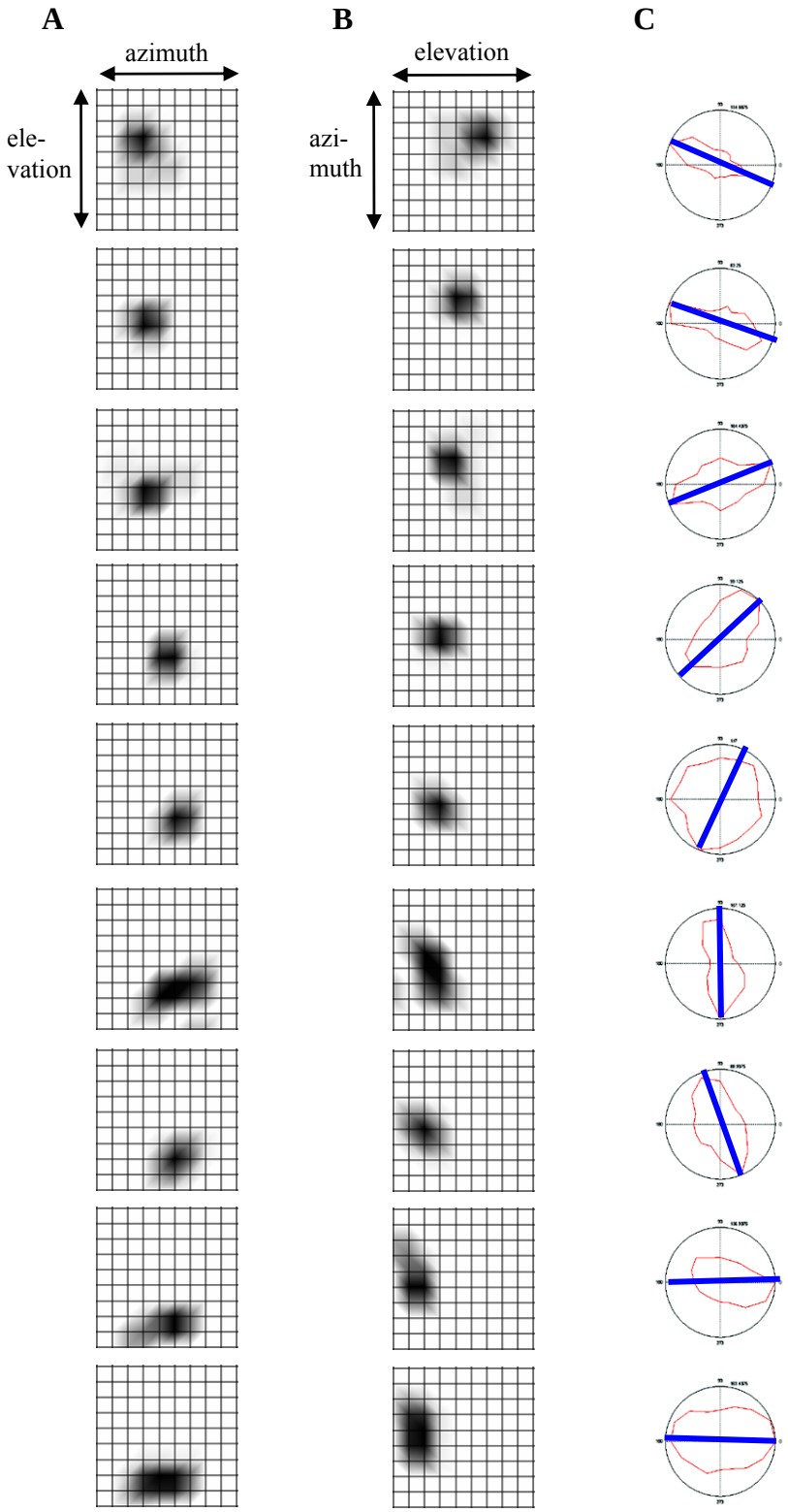

Figure 3.

Figure 3. Mapping the precise local progression of receptive field locations and orientation preferences, with electrophysiological recordings, along a linear tangential track of cat area 18. (A-B) At each of 9 recording locations, we measured the multi-unit two-dimensional spatial receptive field structure using reverse correlation. The neighboring recording locations are separated by 150 μm in the cortex. The strength of the response to stimuli presented in each location of a stimulus grid is indicated (as percent maximum response). The position of the stimulus grid was constant for all recordings. Each square in the grid represents 0.75º of visual space. The same two-dimensional spatial receptive fields are shown in (A) and (B), but in (B) each plot is rotated by 90º relative to (A) so that the receptive field movement along the elevation dimension of space can be appreciated. A relatively smooth progression of receptive field locations is observed. **(C)** The orientation tuning curve (red, polar plot) and preferred orientation (blue bar) of the same 9 recording locations. A smooth progression of orientation preferences between nearby recording locations is punctuated by 1 recording pair that exhibits a large (67.5º) orientation shift.

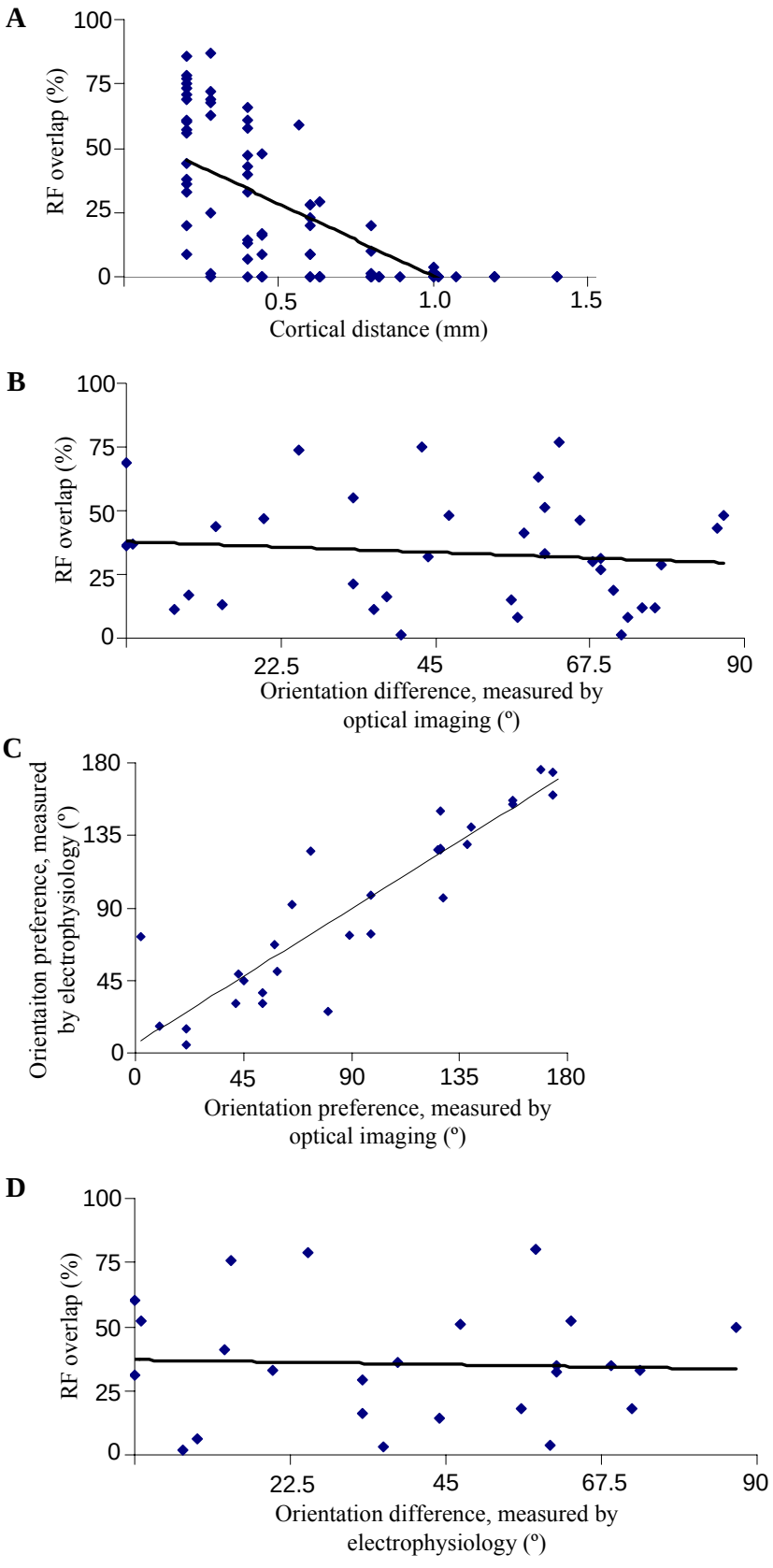
A
100
75
50
25
0
RF overlap (%)
0.5
1.0
1.5
Cortical distance (mm)
B
100
75
50
25
0
RF overlap (%)
22.5
45
67.5
90
Orientation difference, measured by optical imaging (º)
C
180
135
90
45
0
Orientaiton preference, measured by electrophysiology (º)
0
45
90
135
180
Orientation preference, measured by optical imaging (º)
D
100
75
50
25
0
RF overlap (%)
22.5
45
67.5
90
Orientation difference, measured by electrophysiology (º)

Figure 4.

Figure 4. The local relationships between the retinotopic and orientation maps measured with electrophysiological multi-unit recordings along a linear tangential track. (A) The percent of overlap between pairs of receptive fields recorded at nearby locations is plotted as function of the distance between the recordings. The average degree of overlap decreases with cortical distance, but for any one distance a wide degree of overlap measures can exist. **(B)** The percent of receptive-field overlap between nearby (<400 μm apart) recording pairs as a function of the orientation preference difference, measured by optical imaging, for the pair. **(C)** The orientation preference of a recording location, measured by electrophysiology, as a function of the orientation preference measured from optical imaging for the same location. A close correspondence between the two measures is evident. **(D)** The percent of receptive-field overlap between nearby (<400 μm apart) recording pairs as a function of the orientation preference difference, measured by electrophysiology, for the pair.

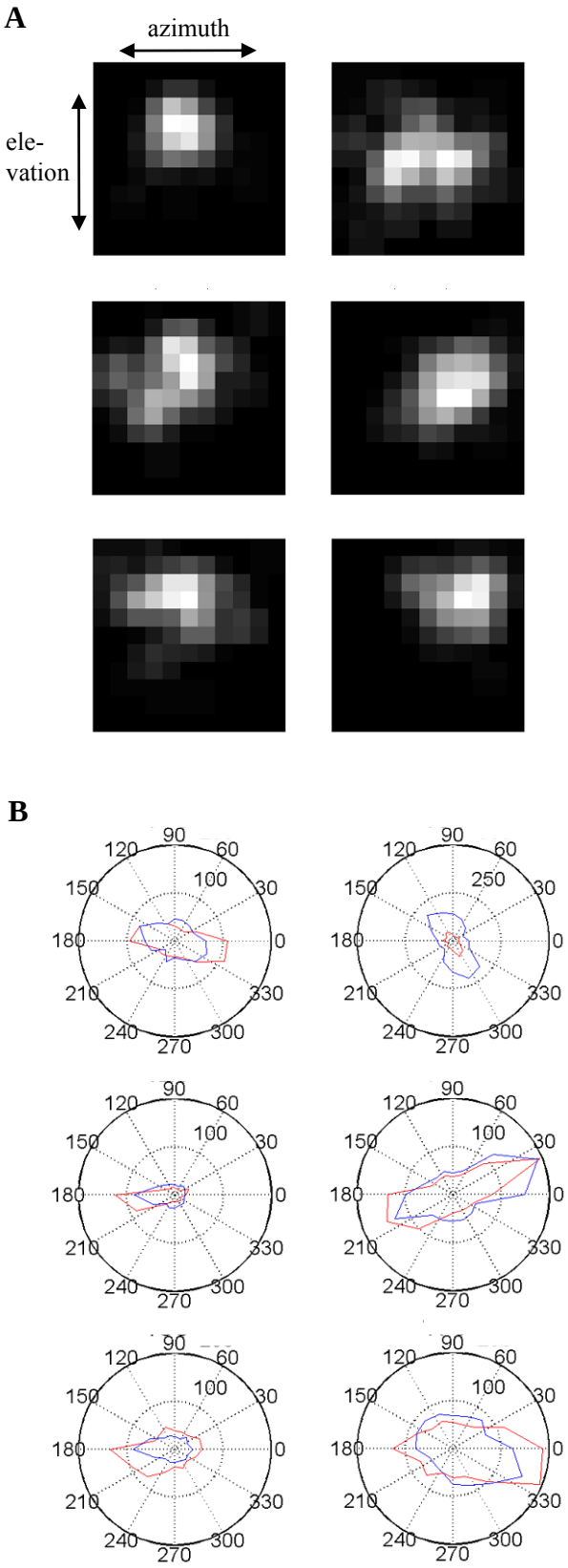
A
azimuth
ele-
vation
B
90
120
60
150
30
180
0
210
330
240
300
270
100
250

Figure 5.

Figure 5. Simultaneous measurement of receptive field structure and orientation tuning for multiple cortical locations using a matrix of electrodes. (A) At each of 6 recording locations (adjacent locations separated by 375 μm) we measured the multi-unit two-dimensional spatial receptive field structure using reverse correlation, where stimuli were presented to the contralateral eye. Each square in the grid represents 1.0º of visual space. **(B)** For the same sites the orientation tuning curve was measured from the contralateral (red) and ipsilateral (blue) eye; all of the analyses in the successive figure are performed on measurements from the contralateral eye.

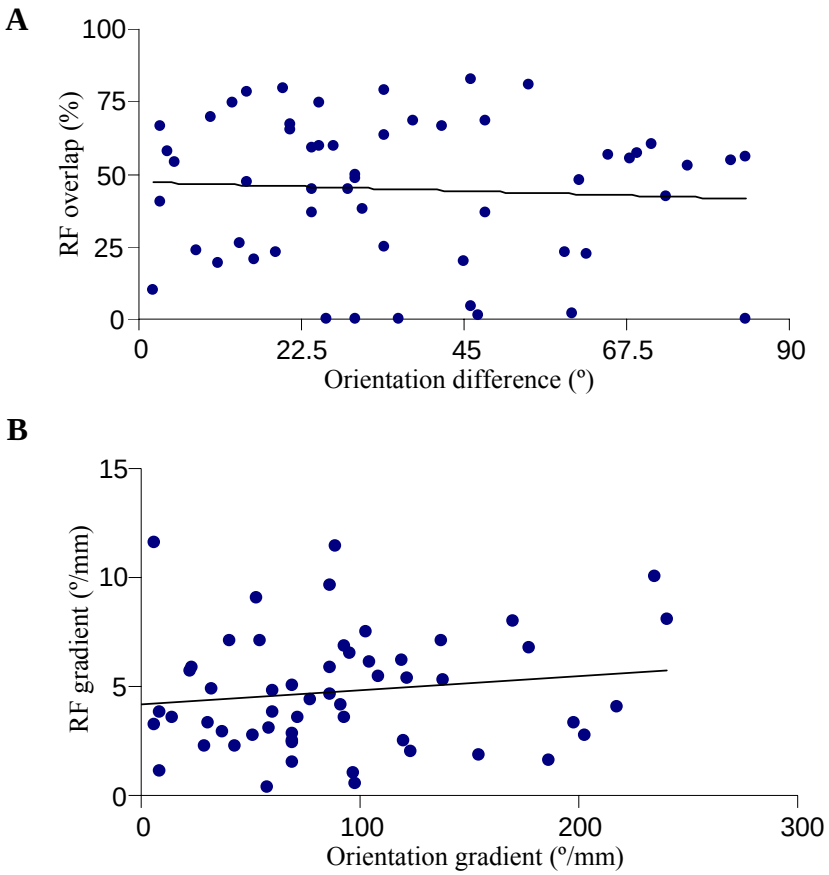

Figure 6. The local relationships between the retinotopic and orientation gradients measured using a matrix of electrodes. (A-B) A matrix of six electrodes was lowered into the cortex and for each electrode, the multi-unit two-dimensional receptive field and orientation preference were measured. **(A)** For pairs of recordings (spaced apart by either 350 μm or 475 μm), the percentage of receptive field overlap between the pair is plotted as a function of orientation difference. **(B)** For pairs of recordings, the receptive field gradient is plotted as a function of the orientation gradient.

CHAPTER 3: Testing the dimension-reduction model of visual cortex development by altering the expression of a cortical map

SUMMARY

In the adult visual cortex, multiple feature maps exist and have characteristic spatial relationships with one another, but the mechanisms responsible for the development of the maps or their relationships are not well understood. We explored whether map relationships are dynamic, such that an altered pattern of input to cortex which is known to change one feature map results in coordinated rearrangements of multiple feature maps; or whether changing one map has no effect on other feature maps. We performed monocular enucleations in newborn ferrets to remove one of the cortical maps, that of ocular dominance. Visual stimulation through the remaining eye in enucleated ferrets caused a more uniform spatial activation pattern than stimulation through one eye in normal ferrets, suggesting that enucleation did successfully alter the ocular dominance map. In the monocular animals, cortical maps of orientation and spatial frequency still formed, but their structures and spatial relationships differed from those in normal ferrets, supporting the hypothesis that altered input results in coordinated rearrangements of multiple maps. The mean orientation gradient across V1 decreased, most prominently in high gradient regions of the spatial frequency map. Further, the orientation and spatial frequency contours intersected each other at more orthogonal angles. The results were consistent with the predictions of a dimension-reduction model of cortical map development.

INTRODUCTION

The mechanisms responsible for the development of cortical feature maps and the spatial relationships between them are not well understood. One possibility is that intrinsic mechanisms are responsible for establishing the maps (Crowley and Katz, 2000), and that related mechanisms may underlie their spatial relationships. On the other hand, self-organization mechanisms dependent on the patterns of spontaneous or visually driven input to the system can also, in principle, account for the development of both the maps and their relationships (Erwin et al., 1995; Swindale, 1996). Finally, these mechanisms could act in combination, where each is responsible for some aspect of cortical map organization.

The spatial relationships between feature maps have similarities across species and mechanisms proposed to account for map development must be able to explain these relationships. For example, orientation pinwheels tend to be located in ocular dominance column centers or in the low gradient regions of the ocular dominance map (Blasdel and Salama, 1986; Bartfeld and Grinvald, 1992; Crair et al., 1997b; Hubener et al., 1997; Yu et al., 2005). Further, contours of these two maps cross orthogonally, particularly in the high gradient regions of the ocular dominance map. Similar spatial relationships have been shown for the maps of orientation and spatial frequency (Hubener et al., 1997; Issa et al., 2000; Yu et al., 2005). Finally, the global layout of the retinotopic map is correlated with that of the ocular dominance (Blasdel and Campbell, 2001) and orientation and spatial frequency (Yu et al., 2005) maps.

Numerous computational models of cortical organization can reproduce the structures of and spatial relationships between cortical maps (Erwin et al., 1995;

Swindale, 1996). Although implemented by different algorithms, the models that have been successful have common characteristics. Namely, they are "dimension-reduction" models driven by two competing constraints: *continuity*, or a smooth representation of each feature, and uniform *coverage*, or a complete and equal representation of each feature combination (Erwin et al., 1995; Swindale, 1996). This observation has led to the hypothesis that continuity and coverage principles underlie the structures of cortical maps and their spatial relationships; but it does not explain the mechanisms that give rise to the maps or their relationships.

It is unknown whether the spatial relationships between maps are encoded rigidly, or whether they are dynamic, such that the relationships can change based on altered input patterns to the cortex. If the mechanisms that produce the relationships are rigid, then altering one feature map early in development should not affect the layouts of other maps. If they proceed dynamically during development, then altering one feature map by altering the input patterns to cortex should cause concomitant changes to other maps; further, if they proceed according to a dimension-reduction strategy, the changes to the other maps should occur in predictable direction.

Conclusive evidence to distinguish between these alternatives has not yet been shown. Following monocular deprivation, the ocular dominance domains belonging to the deprived eye shrink. In these animals, pinwheels locate preferentially to the centers of the deprived eye's domains (Crair et al., 1997a). However, pinwheels locate to domain centers of each eye's domains in normal animals as well (Crair et al., 1997b; Hubener et al., 1997). Further, if deprived eye domains shrink uniformly around their original peak, the relationship observed after the manipulation would result even if the orientation map

had remained static following changes to the ocular dominance map. In strabismic animals, the borders of ocular dominance columns sharpen, and orientation and ocular dominance contours have a similar bias towards orthogonal intersection angles as found in normal animals (Lowel et al., 1998). Again, however, this relationship would be expected even if the orientation map had not rearranged. Thus, these experiments do not provide evidence that maps can change in a coordinated manner over the time course of development. Indeed, these experiments demonstrate that rigid developmental programs might allow for the preservation of continuity and coverage principles following minor changes to the structure of one map, even without coordinated rearrangement of multiple maps.

Comparing the structures of maps, and the spatial relationships between them, in adult animals that have developed with different numbers of feature maps may be a more straight-forward way to test whether development proceeds dynamically according to dimension-reduction principles. Different relationships between maps are predicted by dimension-reduction models when different numbers of features are mapped to cortex (Swindale, 2004; Carreira-Perpinan et al., 2005). We reasoned that it may be possible to remove, or at least the alter expression of, the ocular dominance map by performing early monocular enucleation in the ferret. This manipulation has been shown, at the level of the LGN, to result in the absence of the deprived eye layers and expansion of the non-deprived layers (Guillery et al., 1985). Thus, the substrate of the ocular dominance map at the level of the LGN is fundamentally altered. The cortical effects of this manipulation have not yet been examined. But significant potential for plasticity exists because the thalamocortical afferents in postnatal day zero ferrets have not yet reached the input

layers of cortex (Johnson and Casagrande, 1993; Herrmann et al., 1994). We tested whether early monocular enucleation in the ferret removes the cortical map of ocular dominance, and whether removal of this map has the effects on the remaining feature maps that are predicted by dimension-reduction models.

METHODS

Computational model. We used the Kohonen self-organizing feature map algorithm to simulate the mapping of multiple features across a two-dimensional surface. This model was used because it was successful in reproducing the relationships found between feature maps in the adult ferret visual cortex (see Chapter 1). To simulate the effects of removing a feature map on cortical organization, we compared the results of simulations run with different numbers of feature maps, but with otherwise identical parameters. In the "5-feature" case, the parameters of the simulations were the same as those in Chapter 1 (see Chapter 1 Methods). In the 4-feature case, the parameters were the same as those in the 5-feature case, except for the range of the ocular dominance input values, *z*. In the 5-feature case the range was (0,60), but in the 4-feature case the range was (0,0) or completely uniform. Thus, in the 4-feature case the ocular dominance component did not affect the simulations, and no ocular dominance map formed. For all other details of the simulations, see Chapter 1 Methods.

Neonatal monocular enucleations. Monocular enucleations were performed on postnatal day zero ferrets (within 24 hours of birth). The ferrets were anesthetized by deep hypothermia. The analgesics proparacaine and lidocaine were applied locally to the

eye to be enucleated. The eyelids were separated, the rectus muscles were separated from the sclera, and the optic nerve tied off with suture. The antibiotic cephalothin was applied to the eye orbital, and the orbital was then packed with sterile gelfoam. The eyelids were closed with 6-0 suture. Following recovery from surgery, the animals were returned to their mother in their home cage. Animals were allowed to grow to adulthood (>4 months) before experiments were performed.

Preparation for acute physiology. The preparation for acute physiology is described in Chapter 1 (see Chapter 1, Methods).

Optical imaging. The details of optical imaging have been described previously (Dragoi et al., 2000). The cortex was illuminated with 630 nm light. Images of cortical reflectance were obtained (at 70 pixels/mm) using a slow-scan video camera equipped with a tandem macro-lens arrangement, then digitized and fed into a computer (Imager 3001, Optical Imaging, Mountainside, NJ). The camera was focused 500 μm below the cortical surface. Stimuli were generated using CRS (Cambridge Research Systems Ltd., Rochester, Kent, UK) on a CRT monitor that was placed at 57 cm from the eyes and covered 40° (horizontal) × 30° (vertical) of the visual field.

Orientation, spatial frequency, and monocular response maps. For orientation and spatial frequency maps, stimuli were presented binocularly, and consisted of drifting, full-field square-wave gratings having one of 4 orientations (separated by 45°), one of four fundamental spatial frequencies (0.08, 0.125, 0.225, or 0.375 cycles/deg), and a temporal frequency of 1Hz. The grating stimuli were presented in pseudorandom order, each for 5 seconds during which cortical images were captured, followed by 7 seconds of a blank screen to allow the reflectance to return to a baseline condition. Single-condition

orientation maps were obtained by subtracting the response to all orientations combined ("cocktail blank") from the response to each single orientation. To produce orientation angle maps, filtered single-condition orientation maps (Gaussian filter, standard deviation of 0.1 mm) were summed at each pixel vectorially; the angle of the resultant vector is an estimate of the average preferred orientation at that pixel. The spatial frequency map was calculated by subtracting the average of all filtered orientation single-condition maps obtained with high spatial frequency (0.375 or 0.225 c/deg) stimuli from those obtained with low frequency (0.125 or 0.08 c/deg) stimuli. For monocular response maps, stimuli of four orientations (0.125 c/deg) were presented to the contralateral eye. The response to the stimulus was subtracted from the response to the preceding blank screen condition. The resulting spatial activation pattern, summed over the four orientation conditions, was termed the "monocular response map", and represents the cortical spatial activation pattern due to stimulation of one eye. For the "binocular response map", the same procedure was performed, except that stimuli were presented binocularly.

Analysis of map structures and relationships. We used identical procedures for analyzing our computational and experimental data. Gradient maps were computed from spatially low-pass filtered maps of retinotopy, orientation, ocular dominance, or spatial frequency as the two-dimensional spatial derivative at each pixel. Let A(x,y) be the value at a pixel (x,y), $dx = (A(x+1, y) - A(x, y))$ and $dy = (A(x, y+1) - A(x, y))$. Then the gradient vector magnitude at (x,y) is $\sqrt{dx^2 + dy^2}$, and the gradient vector angle is $(180/\pi)\text{a}\tan(dy/dx)$ and ranges from -90 to 90. The gradient magnitude describes how much a feature is changes around a given pixel in the map, and the gradient angle

indicates the axis of cortex along which the feature changes maximally (and is orthogonal to the map contour at that pixel).

RESULTS

Effects of removing a feature map on cortical organization as predicted by a dimension-reduction model

We employed a computational model, based on the Kohonen self-organizing feature map algorithm, to simulate the mapping of either 5 or 4 features onto a two-dimensional cortical surface. The parameters of the 5-feature simulation were chosen such that the maps produced closely resembled the layouts of the same five maps (elevation retinotopy, azimuth retinotopy, orientation, spatial frequency, and ocular dominance) found in the normal ferret visual cortex (see Chapter 1). We used identical parameters for the 5- and 4-feature simulations, except for the exclusion of the ocular dominance map in the 4-feature case (see Methods). Comparing the results of the two simulations allows us to explicitly determine the predicted effects of removing a feature map on the layouts of the remaining maps.

The overall structures of the individual maps produced by the Kohonen model were largely similar for the 5- and 4-feature simulations (Figure 1A-H); however, there were differences in their details. We focus on the orientation and spatial frequency maps. The wavelengths of these two maps were slightly larger in the 4-feature case (Figure 1I), and the mean orientation gradient was slightly lower in the 4-feature case (Figure 1J). We next analyzed the relationships between the orientation and spatial frequency maps in the 5- and 4-feature simulations. To do this, we calculated the pixel-by-pixel gradient of each

map (see Methods), and then compared the gradients of two maps at corresponding image pixels. We first compared the gradient magnitudes. In the 5-feature case, there was a clear tendency for the high gradient pixels of the orientation and spatial frequency maps to avoid one another; in other words, there was a negative correlation between the gradients (Figure 1K). We found that when going from 5 to 4 features, the gradient correlation became even more strongly negative, although not in a linear way (Figure 1K). We next compared the gradient directions. In the 5-feature case, a similar percent of image pixels had near parallel (1-30º) intersection angles between the orientation and spatial frequency gradients as near perpendicular (61-90º) angles (Figure 1L). But, for the 4-feature case, a much greater percentage of pixels had near perpendicular angles than near parallel angles. Thus, removal of a single feature map is predicted, by the Kohonen algorithm, to alter the remaining maps and the spatial relationships between them in several specific ways.

We next tested whether a feature map could be removed experimentally, and whether its removal would impact the layouts of and spatial relationships between the remaining functional maps in the ways predicted by the Kohonen model. This would allow us to test whether the development of feature maps in the real brain proceeds according to similar principles as govern the Kohonen model.

Neonatal monocular enucleation alters the expression of the ocular dominance map

To attempt to remove the cortical map of ocular dominance, we performed monocular enucleation. In postnatal day 0 ferrets, we severed the inputs from one eye to the brain at the level of the optic nerve, and allowed the animals to grow to adulthood. In

adult animals that had been monocularly enucleated at birth, we found that the optic nerve from the enucleated eye had degenerated completely, such that the optic chiasm received input from only one eye (data not shown). Thus, the removal of input from one eye to the brain was complete.

To test whether this manipulation successfully ablated the ocular dominance map, we compared the cortical spatial activation pattern due to monocular stimulation between normal and monocularly enucleated animals. In a normal animal, each eye innervates complementary patches in the primary visual cortex, and these form the basis of the ocular dominance map. The patches can be revealed by intrinsic signal optical imaging. In normal animals, we measured the cortical spatial activation pattern resulting from stimulation of the contralateral eye. The responses to grating stimuli of 4 different orientations were summed, and the resulting pattern was termed the "monocular single-condition map" (Figure 2A). As expected, the spatial pattern in this map was not uniform, indicating that in a normal animal the contralateral eye activates V1 in a patchy manner. To quantify the patchiness, we plotted the light reflectance signal as a function of distance along the medio-lateral axis of cortex (across which ocular dominance columns run in this region of ferret visual cortex), and calculated the standard deviation (divided by the mean level) of this line (Figure 2A). This was done separately for lines at each anterior-posterior position within the imaged region. The average standard deviation of all positions was termed the "modulation index" for that animal; a higher index indicates a more patchy activation of cortex. In animals that had been enucleated at birth, the monocular single-condition map was less patchy (Figure 2B). Across all animals, the average monocular modulation index was significantly lower in the enucleated animals

compared to normal animals (Figure 2D). Although the modulation index did not go to zero in enucleated animals, it did go as low as the degree of modulation resulting from *binocular* stimulation in normal animals (Figures 2C and 2D). The results indicate that single-eye stimulation in an enucleated animal activates the cortex more uniformly than single-eye stimulation in a normal animal, and as uniformly as does binocular stimulation in a normal animal. This suggests that monocular enucleation at postnatal day 0 in the ferret significantly reduces and likely removes the expression of the functional ocular dominance map in cortex. These results, along with previous results (Guillery et al., 1985), suggest that the eye-specific patches found in both LGN and cortex in a normal ferret are no longer present in monocularly enucleated ferrets; thus, the retino-geniculo-striate pathway becomes monocular (Figure 3).

Formation of feature maps in monocular ferrets

Given that we successfully removed the ocular dominance map, we next tested whether the remaining feature maps could still form in these animals. If so, then we wished to determine whether their structures would be altered in the manner predicted by the Kohonen model. In the binocular region of normal ferret V1 as well as in V2, orientation preference is mapped smoothly in orientation "domains" and breaks sharply at "pinwheels" and "fractures" (Figure 4A). In monocular ferrets, in the cortex contralateral to the remaining eye, orientation maps appeared normal in both V1 and V2 (Figure 4B). Further, the distribution of orientation preferences was similar for normal and monocular ferrets, though the bias for orientation preferences near 0 and 90 found in normal ferrets was somewhat less pronounced in monocular ferrets (Figure 4C). Spatial frequency

preference is also mapped in the binocular region of normal ferret V1, in alternating high and low domains (Figure 4D). In monocular ferrets, in the cortex contralateral to the remaining eye, we also find a map of spatial frequency preference (Figure 4E), though the distribution of preferred spatial frequencies shifted upwards compared to normal controls (Figure 4F). Interestingly, in the cortex *ipsilateral* to the remaining eye in monocular animals, we find an orientation map but not a spatial frequency map (Figure 5). It is unclear whether the spatial frequency map did not form, or was too weak to detect. Thus, visual input from the contralateral eye alone is sufficient to form an orientation and spatial frequency map; visual input from the ipsilateral eye alone is sufficient to form an orientation map, but may not be sufficient to form a spatial frequency map.

Another map which of course exists in normal ferret V1 is that of retinotopy, and we also measured the structure of the retinotopic map in normal and monocular ferrets, as well as the relationship between this map and that of orientation (Supplementary Figure 1). However, we found that measurement of the local structure of the retinotopic map with optical imaging is prone to artifacts, such that comparing the structure of this particular map between normal and enucleate ferrets may not be meaningful (Supplementary Figure 2).

Alterations in the structures of individual feature maps in monocular ferrets

Given that the orientation and spatial frequency maps can form in monocular animals without an ocular dominance map, we can determine whether the layouts of the maps change in the manner predicted by the Kohonen model following the removal of a

feature map. The Kohonen model predicted that the removal of a feature map, leaving everything else constant, should result in a higher wavelength of the orientation and spatial frequency maps (see Figure 1). Experimentally, we found that while there was a slight trend for a higher wavelength of the orientation map in monocular ferrets compared to normal ferrets, consistent with the model prediction, neither map wavelength differed significantly between normal and monocular ferrets (Figure 6A-B).

However, we did find an interesting difference in the *gradient*, or rate-of-change, of the orientation map in the monocular ferrets. In a normal ferret (Figure 7A), most of V1 is covered by iso-orientation domains, where orientation gradient is low; these regions are punctuated by orientation pinwheels and fractures, which have a high orientation gradient. A similar layout was observed for the orientation gradient map in monocular ferrets (Figure 7B). But a pronounced difference was that the average orientation gradient over all image pixels of V1 was significantly lower for monocular ferrets than for normal ferrets (Figure 7C-D). While we also found an effect of gender on the orientation gradient within monocular animals, it still held that the orientation gradient was lower in monocular ferrets than in normal ferrets of the same gender (Figure 7C-D; we have data from only female normal ferrets, not male normal ferrets). These results are consistent with the Kohonen model (see Figure 1), which predicted that the removal of a feature map should result in a lower average orientation gradient.

Alterations in feature map relationships in monocular ferrets

A central prediction of the Kohonen model and other dimension-reduction models is that the number of features that are mapped within a cortical area should determine the

spatial relationships between the maps (Swindale, 2004; Carreira-Perpinan et al., 2005). For example, we showed that removal of the ocular dominance map is predicted to have two specific consequences on the spatial relationships between the orientation and spatial frequency maps. First, it should increase the tendency for high orientation gradient regions to avoid high spatial frequency gradient regions (see Figure 1K). Second, it should increase the tendency for gradients of orientation and spatial frequency maps to intersect each other orthogonally (see Figure 1L). We asked whether the experimental removal of the ocular dominance map, caused by monocular enucleation, altered the relationships between the orientation and spatial frequency maps in these two ways.

In normal ferrets (Figure 8A), regions of high orientation gradient (bright red) tend to avoid regions of high spatial frequency gradient (bright green). The relationship between these gradient maps can be illustrated directly by plotting the orientation gradient as a function of the spatial frequency gradient. For each normal animal tested, it can be seen that as the spatial frequency gradient increases, the average orientation gradient decreases (Figure 8C, red lines). The same overall tendency holds for monocular ferrets (Figure 8B-C), but pooling the data within normal and monocular ferrets revealed a difference between the groups in the details of the relationship (Figure 8D). Specifically, within the high spatial frequency gradient regions of V1, the orientation gradient was lower in the monocular ferrets than in normal ferrets. Interestingly, this indicates that the decrease in the average orientation gradient found in monocular ferrets (see Figure 7) does not occur uniformly across the cortex, but rather is most pronounced in the high spatial frequency gradient regions (the same trend held when comparing between normal females and either monocular females or monocular males; Figures 8E-

F). This result is consistent with the Kohonen model, which predicts that removal of a feature map should result in an overall decrease in the orientation gradient, and that the change in the orientation gradient should be non-uniform: there should be a slight increase of the orientation gradient in the lowest spatial frequency gradient regions, and a more pronounced decrease in the highest spatial frequency gradient regions (see Figure 1K).

A related prediction of the Kohonen model is that the removal of a feature map should result in more orthogonal intersection angles between the contours of the remaining maps (see Figure 1). In Figure 9A, we superimpose the contour maps of orientation and spatial frequency from a normal ferret. A slight tendency for contours (or gradients) of the two maps to cross at near perpendicular angles may be visible, though quantifying the relationship shows that it is weak (Figure 8C). We found that in normal ferrets, there was not a significant difference in the percent of image pixels having near perpendicular intersections (61-90º) and near parallel intersections between orientation and spatial frequency gradients (1-30º; Figure 9D). However, in monocular ferrets (Figure 9B), there was a highly significant tendency for more image pixels to have near perpendicular intersection angles than near parallel angles (Figure 9D). The results indicate that when a feature map is removed, the intersection angles between the orientation and spatial frequency gradients become more orthogonal; this is in agreement with the predictions of the Kohonen model (see Figure 1L).

We showed previously that in the normal ferret, the tendency for orthogonal crossings between orientation and spatial frequency gradients is most pronounced in those regions of the cortex where high gradient magnitude regions of these two maps

coincide (see Chapter 1). Orientation and spatial frequency contours from a normal ferret (Figure 9E) and from a monocular ferret (Figure 9F) are displayed only for those regions of cortex where the high gradient regions of orientation and spatial frequency overlap. Close inspection of these maps reveals that the contours of the two maps have a tendency to cross orthogonally within these regions. In Figure 9G, we plot the percent of image pixels having intersection angles within 9 different ranges (0-10º, 10-20º, …, 80-90º), considering only those regions where both the orientation and spatial frequency gradients are within the highest 30th percentile. The individual plots are noisy, because the calculation derives from pixels covering only 9% of the surface area of the imaged region; however, it can be seen that the tendency for orthogonal intersections is higher within these high gradient overlap regions than across the whole V1 (compare Figure 9G to Figure 9C). Also, there was a significantly higher percentage of image pixels having near perpendicular intersection angles within high gradient overlap regions of the orientation and spatial frequency maps, compared to over the whole V1; this was true for both normal and monocular ferrets (compare Figure 9H to Figure 9D). The extent of orthogonal intersection angles, within the high gradient overlap regions, was not significantly different between normal and monocular ferrets (Figure 9H); this is perhaps because the calculation was noisy because of being restricted to only a small percent pixels from the imaged regions.

DISCUSSION

We show in this study that neonatal monocular enucleation in the ferret results in the absence of a functional ocular dominance map in the adult visual cortex. Thus,

following an altered pattern of input to cortex, the number of feature maps that exist in a cortical area can change. Further, the spatial relationships between the remaining feature maps are altered in a manner that is in agreement with the predictions of a dimension-reduction model of cortical organization. Thus, relationships between feature maps are not intrinsically determined; rather, maps can rearrange over the time course of development in a manner that is consistent with optimizing dimension-reduction principles for the numbers of features that are mapped in a given area.

The effects of monocular enucleation on ocular dominance properties in the ferret

The effects of monocular enucleation on the organization of the visual pathway are dependent on when the enucleation is performed as well as the age at which the assays are performed. Enucleation performed at an early age causes profound changes to visual system organization, but some of the effects might not take place until after feature maps are initially established in cortex.

Monocular enucleation of the retina appears to have little effect on patterns of ocular dominance in cortex, when these affects are measured in pre-eye opening ferrets. Ocular dominance columns in the cortex of the ferret develop around P16, well before the age of eye-opening (Crowley and Katz, 2000). Monocular enucleation, when performed between the ages of P7 and P14, does not disrupt the initial establishment of these ocular dominance bands, measured between P17 and P21 (Crowley and Katz, 2000). This suggests that the balance of retinal input, between P7 and P14, does not play an instructive role in ocular dominance column formation.

In contrast, when visual system properties are measured at later ages, significant effects of monocular enucleation are detected on the anatomical properties of the LGN. In adult ferrets that have been monocularly enucleated at P0, geniculate A layers can be distinguished from C layers, but not all LGN layers are present. The layers that are normally innervated by the remaining eye survive and expand while those belonging to the enucleated eye do not survive (Guillery et al., 1985). Thus, by adulthood the LGN architecture which forms the basis for ocular dominance columns has been fundamentally altered.

The cortical effects of monocular enucleation have not been characterized in the adult ferret. But even more subtle imbalances in activity patterns between the two eyes, caused by monocular lid suture during the critical period, can greatly change ocular dominance properties in adult ferret cortex (Issa et al., 1999). In other species, the effects of monocular enucleation have been characterized in the adult cortex. If a monkey is monocularly enucleated during the second fetal month, transneuronal labeling of the remaining eye indicates that it uniformly innervates layer 4 of cortex, rather than innervating ocular dominance patches as in a normal animal (Rakic, 1981). At the level of the LGN, the results of monkey monocular enucleation performed at this age are similar to those of ferret monocular enucleation performed at postnatal day zero (the age at which our enucleations were performed); the retinal input from the remaining eye spreads over the entire LGN rather than remaining restricted to eye-specific layers (Rakic, 1981). Thus, a similar result as is observed due to *prenatal* monocular enucleation in monkeys (i.e. uniform innervation of layer IV of visual cortex by the remaining eye) may be expected to occur due to *postnatal day 0* monocular enucleation

in ferrets, though this must be tested experimentally. The cortical effects of monocular enucleation in the monkey are less pronounced when the procedure is performed at later stages of development (Horton and Hocking, 1998). In cats monocularly enucleated 2 weeks before birth or earlier, it was reported that all neurons from the normally binocular area of V1 could be driven by the single remaining eye (Shook et al., 1985). However, in layer IV of binocular cortex in normal cats, 80% of cells can be driven by both the contralateral and ipsilateral eyes (Shatz and Stryker, 1978). Since an even greater percentage can presumably be driven by one eye only in normal animals, it is not clear whether there is a significant increase in the amount of cells that can be driven by one eye in monocularly enucleated compared to normal cats.

Though the visual cortex of ferrets has not been examined following monocular enucleation, a significant potential for plasticity is expected to exist given that the visual system is immature at the time of birth. At postnatal day zero, the eye-specific layers of the thalamus are not yet distinguishable, and the afferents from the two eyes are still entirely overlapping in the nucleus. Geniculocortical afferents have reached the subplate of cortex but have not yet reached layer 4.

Our physiological measurements indicate a strong effect of P0 monocular enucleation on the functional ocular dominance properties of cortex. The remaining contralateral eye in monocular ferrets activates the superficial layers of cortex significantly more uniformly than the contralateral eye does in normal ferrets. This indicates that our manipulation did flatten the ocular dominance map in binocular visual cortex. Taken together with the previous studies mentioned, it is likely that the effects of monocular enucleation on visual cortex organization that we measured (as well as those

previously measured in LGN) take place not at very young ages, but rather near eye-opening (postnatal day 30) or during the critical period.

Effects of monocular enucleation on other physiological properties of cortex

Some functional consequences of early monocular enucleation have been examined. In cats that were monocularly enucleated 2 weeks before birth, electrophysiological recordings in V1 indicated that cells are still orientation selective, and that a smooth progression of orientation preferences is encountered as the cortex is traversed tangentially (Shook et al., 1985). This indicates that orientation preference is still mapped smoothly, although it was unknown whether the full two-dimensional structure of the map was normal. To our knowledge, the present study was the first to measure this structure, and our results indicate that in the ferret the overall structure is largely unchanged. Thus, the expression of the orientation map in binocular V1 does not appear to depend on binocular input, or on the presence of the ocular dominance map.

One functional difference reported between monocularly enucleated and normal cats is that in the former, cells have smaller receptive fields on average (Shook et al., 1985). Consistent with this observation, a selective loss of contrast sensitivity for lower spatial frequency stimuli, as well as behavioral disruptions in the detection of low spatial frequency stimuli, have been reported in monocular enucleates (Bisti and Trimarchi, 1993; Bisti et al., 1995). Consistent with these reports, we find that the preferred spatial frequency of cells is higher on average in monocular ferrets than in normal ferrets. It is unknown why this occurs; the effect could be adaptive, or could result from the

contralateral and ipsilateral eyes carrying different spatial frequency information in normal animals and therefore the loss of a subset of this input in monocular enucleates.

Possible mechanisms for the development of feature maps and their relationships

The initial establishment of feature maps in visual cortex, with the exception of the direction map, appear resistant to changes in visual activity patterns (Crair et al., 1998; Crowley and Katz, 1999; White et al., 2001b; Li et al., 2006). However, altered activity patterns following eye-opening and during the critical period can greatly alter the structures of maps and provide instructive cues for their development (Wiesel and Hubel, 1963; Crair et al., 1998; Sengpiel et al., 1999; White et al., 2001b; Li et al., 2006).

Less is known about the mechanisms responsible for the specific spatial relationships that exist between feature maps in visual cortex. We envision two possible general mechanisms that could account for the existence of these spatial relationships. First, map relationships could be set up by a process that is not responsive to changes in input patterns during development (at least following some specific developmental age). This would imply that the maps lose the ability to *interact* with each other after that age. For example, the layouts of individual maps could be instructed by the spatial expression patterns of certain patterning molecules, and the relationships between maps could arise from interactions between the molecules responsible for setting up the different individual maps. If these molecules were unresponsive to later changes in the individual maps, caused by altered input patterns, then altering one map would not affect the layouts of the remaining maps.

On the other hand, the mechanisms that set up the relationships between individual maps could retain the ability to respond to changes in inputs and be active throughout some period of development. If this were true, alterations in input patterns that caused a change in the pattern of one map would result in the rearrangement of the other maps as well. Our results support this second proposal—that mechanisms which set up map relationships are responsive to alterations in input activity patterns at or after the age of enucleation in this study, i.e. postnatal day zero in the ferret. Either molecular mechanisms or activity-dependent mechanisms could be responsible. For example, alterations in one map could cause the expression pattern of a molecule to change, and this could in turn change the expression patterns of the molecules with which the first molecule interacts. On the other hand, activity-dependent synaptic modification rules might be responsible for map relationships and remain active throughout development. It appears that monocular enucleation may not affect the initial establishment of the ocular dominance map, but rather may affect the expression of this map at later ages. We suggest that the effects of this manipulation on the remaining maps in cortex, as well, may occur at later stages of development, such as during the critical period and when the animal is receiving patterned visual input.

Previous computational model studies of mapping different numbers of features onto a two-dimensional cortex

A number of groups have recently used computational models to explore the consequences of mapping different numbers of features onto a two-dimensional surface. Swindale (2004) has shown, using the Kohonen algorithm, that the gradient correlations

between retinotopy and other feature maps are predicted to become weaker as more parameters are represented with an area. Our group made a similar prediction, using simulation parameters that closely reproduce the structures maps found in the ferret visual cortex (see Chapter 1). When retinotopy was mapped along with orientation alone, the regions of high retinotopic gradient were clearly correlated with regions of low orientation gradient. However, when ocular dominance and spatial frequency were also mapped onto the same surface, the relationships between the retinotopic and orientation gradients became weaker. It has also been recently shown in studies using the elastic-net algorithm that as additional features are mapped, the orthogonality of the features that are mapped becomes slightly less pronounced and the wavelengths of the remaining maps decrease slightly (Carreira-Perpinan et al., 2005).

We are the first to test the predictions of these dimension-reduction models experimentally, and we show that the removal of a feature map has effects that are consistent those predicted by the models. In the current study, we attempted to simulate as realistically as possible the effects of removing the ocular dominance in the ferret. We use simulation parameters which produce maps that closely resemble those found in ferret, and model the effect of removing just one feature map.

We consider the agreement between our experimental results and the prediction's of models as evidence that during development, the cortex may be trying to optimize similar principles as are driving the models. The Kohonen algorithm and elastic net simulations can both be considered to be driven by the opposing principles (or constraints) of achieving uniform representation of multiple feature combinations, along

with a smooth or continuous representation of each feature. Our results suggest that cortical organization may be driven by these constraints as well.

On the other hand, the biological mechanisms by which these principles are established remain unknown; the mechanisms of the models are in some cases likely biologically implausible. We do not take the agreement between the experimental and model results as evidence that the mechanisms of the model act in the cortex; indeed, the Kohonen and elastic net algorithms each make qualitative predictions that agree with our experimental results, thought each proceed via different mechanisms. Regarding mechanisms, our results do suggest that the principles of coverage and continuity in the visual cortex are not encoded rigidly, but rather can act over the time course of development in response to altered input patterns to optimize cortical organization based on the number of feature maps that exist.

FIGURES

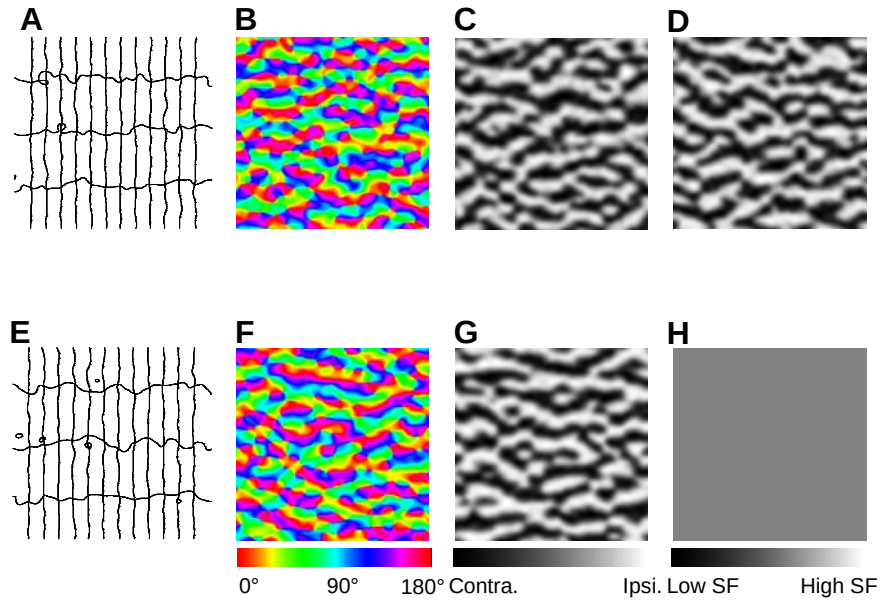
A
B
C
D
E
F
G
H
0°
90°
180°
Contra.
Ipsi.
Low SF
High SF

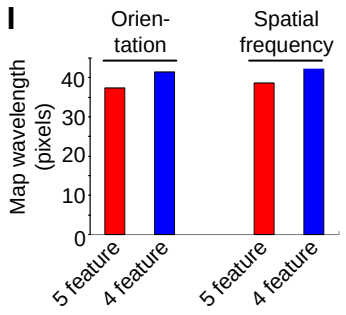
I
Orien-
tation
Spatial
frequency
Map wavelength
(pixels)
40
30
20
10
0
5 feature
4 feature
5 feature
4 feature

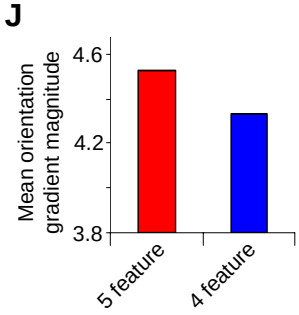
J
Mean orientation
gradient magnitude
4.6
4.2
3.8
5 feature
4 feature

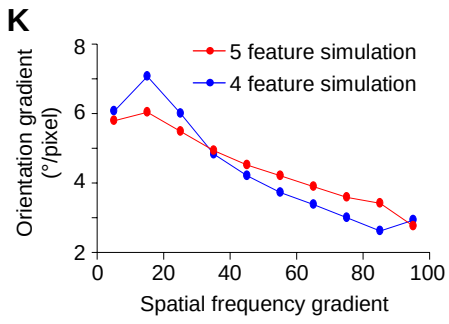
K
Orientation gradient
(°/pixel)
8
6
4
2
0
20
40
60
80
100
Spatial frequency gradient
5 feature simulation
4 feature simulation

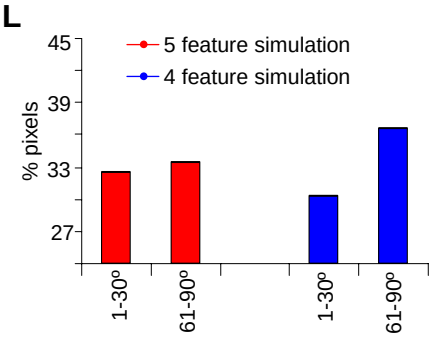
L
% pixels
45
39
33
27
1-30°
61-90°
1-30°
61-90°
5 feature simulation
4 feature simulation

Figure 1

Figure 1. Altering the number of features represented on a 2-D surface is predicted to change the feature maps and their relationships. Using the Kohonen model, we mapped either five (A-D) or four (E-H) features onto a 2-D surface. **(A, D)** The retinotopic map is illustrated by iso-elevation (horizontal in figure) and iso-azimuth (vertical in figure) contours; all contour intervals are identical. Vertical contour lines are more widely spaced than horizontal contour lines, indicating an anisotropy in the visual map magnification factor. This simulates a similar anisotropy found in ferret visual cortex. **(B, E)** The orientation preference map, denoted by color-coding each pixel according to its preferred orientation. **(C, G)** The spatial frequency preference map. **(D, H)** The ocular dominance map; the ocular dominance value of all image pixels was uniform in the 4-feature simulation, to simulate the results of removing the ocular dominance map. **(I)** The wavelengths of the orientation and spatial frequency maps, calculated by determining the frequency with maximum power following 2-D Fourier analysis. **(J)** The mean orientation gradient magnitude over the entire model cortex. The 2-D orientation gradient was calculated at each pixel, and the magnitude of the gradient was averaged over the entire region. **(K)** Image pixels are grouped into ten bins according to their spatial frequency gradient (bin 1: 0-10% of maximum; bin 2: 10-20% of maximum; …) and the mean orientation gradient for each group is indicated. **(L)** The intersection angle between the orientation gradient and spatial frequency gradient at each pixel of the model cortex was calculated; the percent of image pixels that had intersection angles that were near parallel (1-30°) or near perpendicular (61-90°) is indicated.

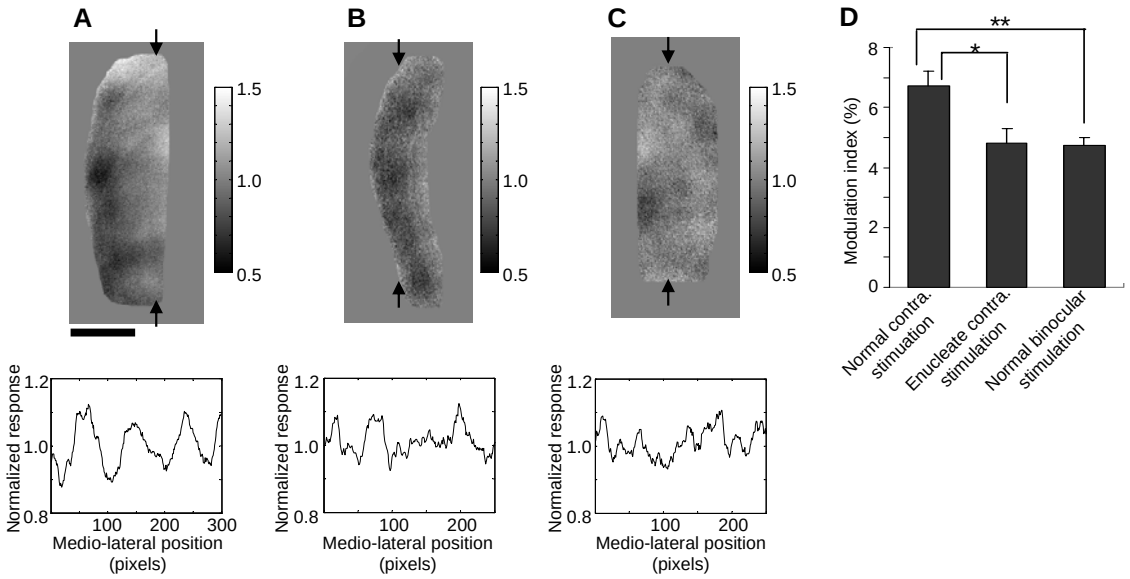

Figure 2. The cortical activation pattern due to monocular stimulation is more spatially uniform in enucleated ferrets than in normal ferrets. (A-B) Maps represent intrinsic signal optical imaging "single-condition monocular" maps, produced by summing the cortical response to monocular presentation of grating stimuli of four different orientations. The plots represent the light reflectance pattern along a vertical line through the corresponding map at the position indicated. The standard deviation of this line, averaged over all positions, is termed the monocular spatial *modulation index* for that animal. The data in (A) comes from a normal ferret; the data in (B) comes from a monocularly enucleated ferret. **(C)** Same as in A-B, except that both eyes were stimulated in a normal ferret. **(D)** The average modulation index for the three groups. Error bars denote the standard error of the mean over 8, 7, and 5 ferrets, respectively. Scale bar in (A) 1 mm, and applies to (A-C).

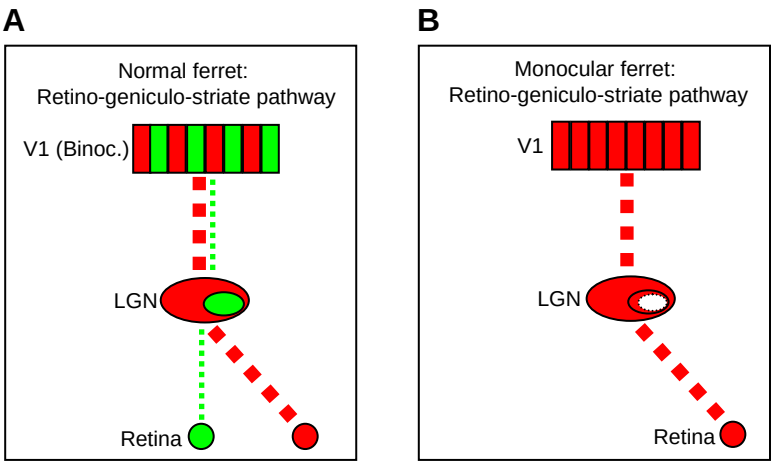

Figure 3. Schematic of the retino-geniculo-striate pathway of normal and monocularly enucleated ferrets. (A) Pathway from normal ferrets. The two eyes project to alternate layers in the LGN and alternate ocular dominance columns within binocular V1. **(B)** Pathway from a ferret that was monocularly enucleated at P0. In the LGN of these animals, it was previously shown with anatomical methods that the eye-specific layer normally belonging to the enucleated eye is absent, whereas the remaining eye layer expands slightly; the remaining eye terminates over a region larger than normal (Guillery et. al, J. Neurosci., 1985). Our results demonstrate that single-eye stimulation in enucleates activates the cortex as uniformly as binocular stimulation in normal animals, suggesting that the physiological ocular dominance map in binocular V1 is weakened or extinguished.

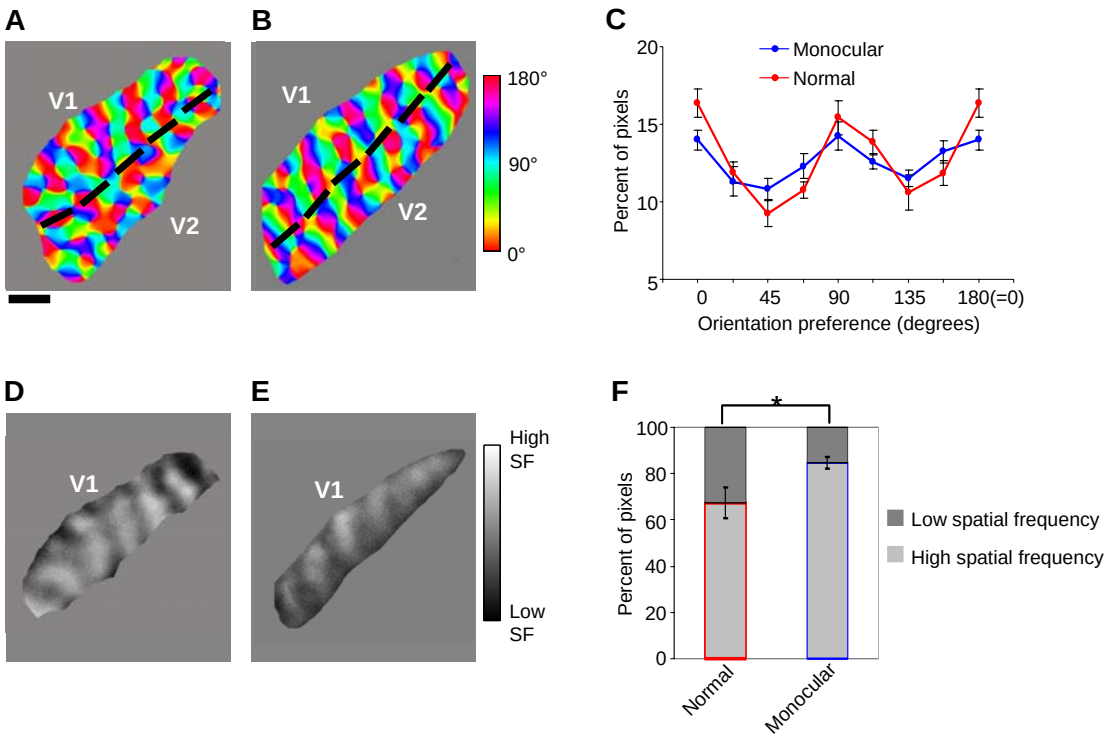

Figure 4. Maps of orientation and spatial frequency form in monocular ferrets. (A-B) Orientation preference maps in V1 and V2 from a normal ferret (A) and from the cortex contralateral to the remaining eye in a monocular ferret (B). Each pixel is color-coded according to its preferred orientation. **(C)** The distribution of preferred orientations within V1. Error bars denote standard error of the mean of 7 normal ferrets and 8 monocular ferrets. **(D-E)** Differential spatial frequency maps in V1 from a normal ferret (D) and from a monocular ferret (E). **(F)** The relative percent of image pixels responding more strongly to either low (0.08 cycles/degree) or high (0.225 cycles/degree) spatial frequency grating stimuli. Error bars denote standard error of the mean over 6 normal ferrets and 8 monocular ferrets. Scale bar in (A) 1 mm, and applies to (A-B, D-E).

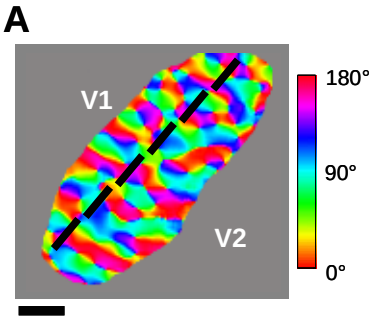

Figure 5. The orientation map forms within V1 and V2 of the cortex ipsilateral to the remaining eye in monocular enucleates. (A) An orientation preference map in V1 and V2 in the cortex ipsilateral to the remaining eye in a monocular ferret. Each pixel is color-coded according to its preferred orientation. Scale bar in (A) 1 mm.

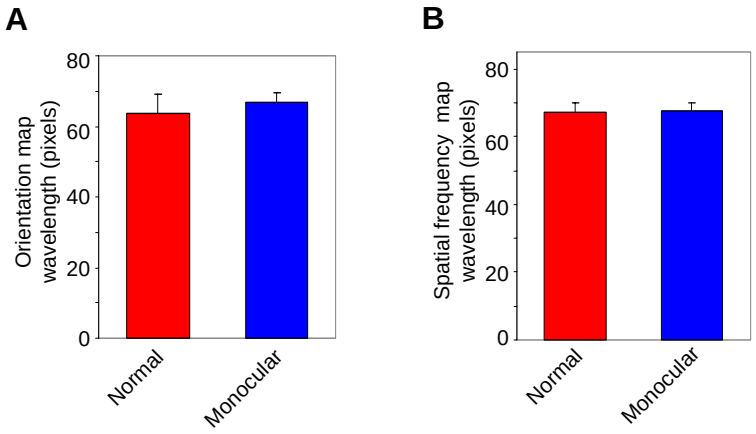

Figure 6. The wavelengths of the orientation and spatial frequency maps in normal and monocular ferrets. (A) The wavelength of the orientation preference map, calculated using 2-D Fourier analysis. Error bars denote standard error of the mean over 4 normal ferrets and 8 monocular ferrets. **(B)** The wavelength of the differential spatial frequency map, calculated using 2-D Fourier analysis. Error bars denote standard error of the mean over 3 normal ferrets and 5 monocular ferrets.

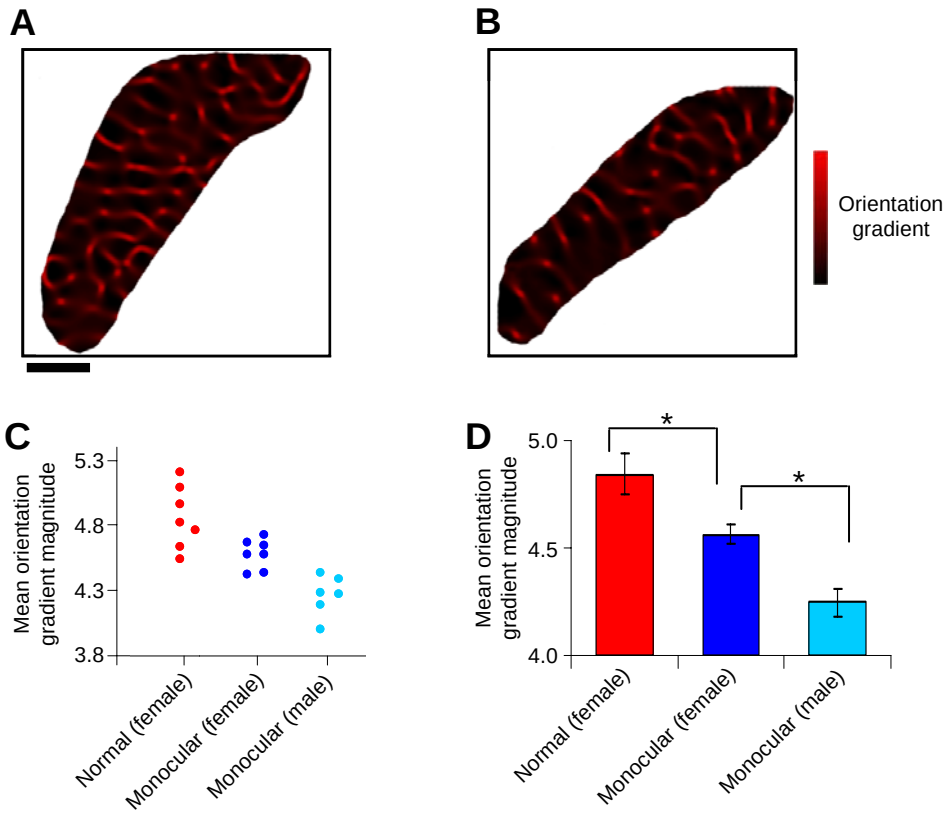

Figure 7. The orientation gradient map in normal and monocular ferrets. (A-B) The orientation gradient map from a normal (A) or monocular (B) ferret, produced by calculating the 2-D orientation preference gradient at each pixel. **(C)** For each ferret, we calculated the mean orientation gradient magnitude over all image pixels of the imaged portion of V1. **(D)** The average of the mean orientation gradient within each group. Error bars denote standard error of the mean over 7 normal female ferrets, 7 monocular female ferrets, and 6 monocular male ferrets. Scale bar in (A) 1 mm, and applies to (A-B).

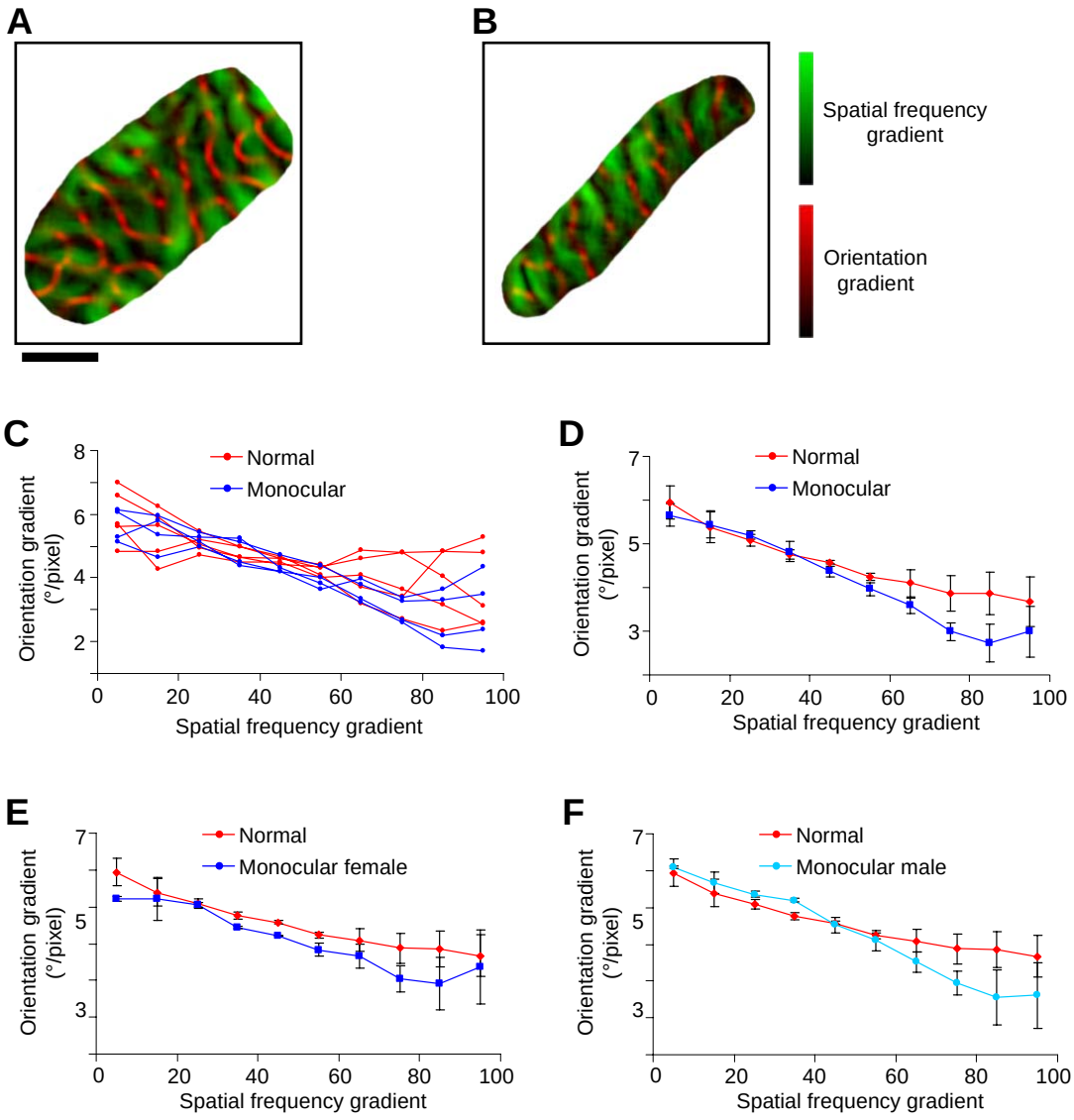

Figure 8. The relationship between the orientation gradient magnitude and the spatial frequency gradient magnitude. (A-B) The orientation gradient map is superimposed on the spatial frequency gradient map. Results are from a normal (A) or monocular (B) ferret. **(C)** For each individual animal, image pixels from V1 are grouped into ten bins according to their spatial frequency gradient (bin 1: 0-10% of maximum; bin 2: 10-20% of maximum; …) and the mean orientation gradient for each group is indicated. **(D-F)** Same as in (C), except each point represents the average over the individual cases within the group. Error bars denote standard error of the mean over 5 normal ferrets (D-F) and either 2 female and 2 male monocular ferrets (D), 2 female monocular ferrets (E), or 2 male monocular ferrets (F). Scale bar in (A) 1 mm, and applies to (A-B).

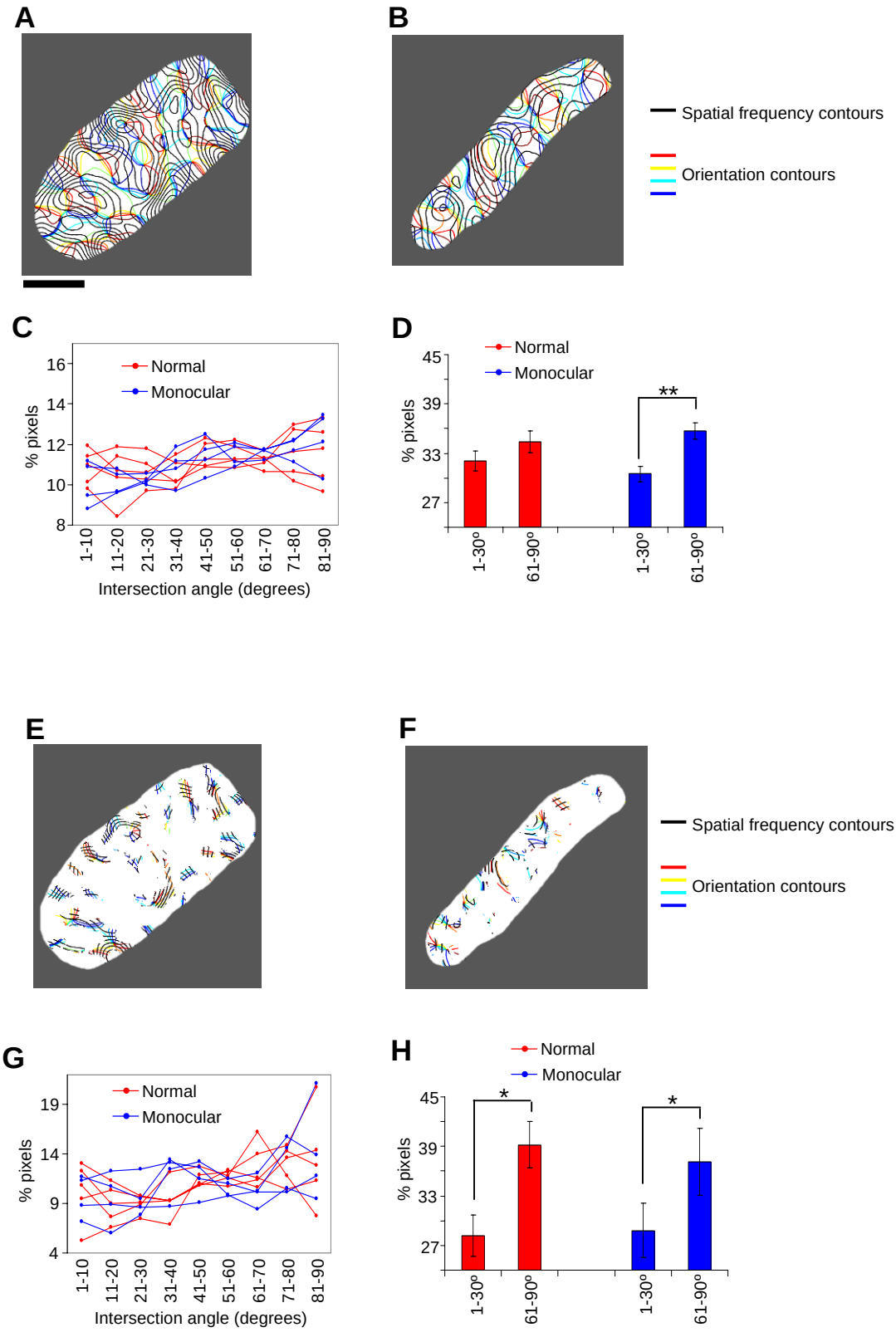
A
B
Spatial frequency contours
Orientation contours
C
Normal
Monocular
% pixels
16
14
12
10
8
1-10
11-20
21-30
31-40
41-50
51-60
61-70
71-80
81-90
Intersection angle (degrees)
D
Normal
Monocular
% pixels
45
39
33
27
**
1-30°
61-90°
1-30°
61-90°
E
F
Spatial frequency contours
Orientation contours
G
Normal
Monocular
% pixels
19
14
9
4
1-10
11-20
21-30
31-40
41-50
51-60
61-70
71-80
81-90
Intersection angle (degrees)
H
Normal
Monocular
% pixels
45
39
33
27
*
*
1-30°
61-90°
1-30°
61-90°

Figure 9

Figure 9. The relationships between the orientation contours (or gradient directions) and the spatial frequency contours. (A-B) Iso-orientation contours are superimposed on iso-spatial frequency contours. Results are from a normal (A) or monocular (B) ferret. **(C)** The percent of image pixels in V1 having intersection angles, between the orientation gradient and the spatial frequency gradient, within the 9 ranges indicated. **(D)** The percent of pixels in V1 having intersection angles between the orientation gradient and the spatial frequency gradient within 1-30 degrees or 61-90 degrees. Error bars denote standard error of the mean over 5 normal ferrets and 4 monocular ferrets. **(E-F)** Iso-orientation contours are superimposed on iso-spatial frequency contours. However, the contours are only shown in those regions of V1 where both the orientation gradient magnitude and spatial frequency gradient magnitude were within the highest 50^{th} percentile of the values in that area. **(G-H)** Intersection angles between orientation gradients and spatial frequency gradients, as in C-D, except considering only the image pixels where both the orientation gradient and spatial frequency gradient were within the highest 30^{th} percentile. Error bars denote standard error of the man over 5 normal ferrets and 4 monocular ferrets. Scale bar in (A) 1 mm, and applies to (A-B, and E-F).

SUPPLEMENTAL DATASET

METHODS

Retinotopic maps. To generate retinotopic maps, we used a periodic visual stimulation paradigm (presented to the contralateral eye) combined with continuous data acquisition optical imaging (Kalatsky and Stryker, 2003). We used either oriented bar stimuli or oriented aperture stimuli. The bar stimuli (see Supplementary Figure 2A) consisted of elongated vertical bright bars (1° width × 30° height) on a dark background, where each bar was separated by 20° in the azimuth dimension. The bars flashed at 3 Hz and shifted their azimuth location by 0.66° every second, such that a bar passed by any given visual field location on the monitor every 30 seconds. For the aperture stimuli (see Supplementary Figure 2G), the background was gray and the stimulus consisted of gratings visible through a vertical aperture. The gratings had a spatial frequency of 0.225 cycles/degree and cycled randomly through 4 different orientations at 4 Hz. Along the horizontal center of the vertical aperture, the contrast of the gratings was 100%, and in moving away from the center, the contrast of the gratings decreased with a Gaussian fall-off until they reached 0% contrast. Each vertical aperture was separated by 24º in the azimuth dimension. The aperture drifted along the azimuth dimension of space at 1.6°/second, such that an aperture passed by any given visual field location on the monitor every 15 seconds. Light-reflectance images were captured at 3 Hz. Each retinotopic stimulus trial consisted of 8-24 cycles of stimulation, after which a blank screen was shown for 25 seconds, and each experiment consisted of 5-15 such trials. The light-reflectance data were averaged in phase over all trials and cycles. Each frame of the averaged response thus represents the activation pattern during a restricted phase of the

stimulus cycle. To obtain the retinotopic single-condition maps, each frame was subtracted from the mean of all the frames and then filtered (Gaussian filter, standard deviation of 0.06 mm). To determine each pixel's preferred receptive field position, we calculated the phase of the Fast Fourier Transform (FFT) at the stimulation frequency, on the time-course response of each pixel (Kalatsky and Stryker, 2003). Since the optical imaging signals follow the stimulation with an unknown lag time, this method provides maps of relative rather than absolute retinotopy. All of our analyses rely only on relative retinotopy values.

RESULTS

Relationships between the maps of orientation and retinotopy

We examined the relationships between the maps of orientation and retinotopy in normal and monocular ferrets. Though there were minor differences in the relationships between the two groups, we found artifacts in the measurement of the retinotopic map that indicate that the comparison may not be meaningful.

In analyzing the retinotopic map, we consider only the azimuth axis of the map, since this represents the high gradient axis of retinotopy, owing to the pronounced anisotropy of visual space representation in the region of ferret visual cortex that was examined (see Chapter 1). We first explored whether there were relationships between the orientation and retinotopic gradient magnitudes. In Supplementary Figure 1A, we superimpose a map of the orientation gradient on a map of the azimuth retinotopy gradient. The same maps, obtained from a monocular ferret, are shown in Supplementary Figure 1B. Unlike the case for orientation and spatial frequency, where a clear correlation

between the gradient maps can be seen, there was no obvious relationship between the gradients of orientation and retinotopy. In Supplementary Figure 1C, we plot the orientation gradient as a function of the retinotopy gradient. A significant amount of variability exists from animal to animal in both normal and monocular ferrets. After averaging over animals, we do not see a clear relationship between the orientation gradient and retinotopic gradient in either group (Supplementary Figure 1D).

We also examined the contour relationships between the maps of orientation and retinotopy in normal and monocular ferrets. In Supplementary Figure 1E, the contours from the orientation map are superimposed on the contours from the azimuth retinotopic map, each obtained from the same region of a normal ferret. A clear spatial relationship between the two maps is visible. Namely, the orientation contours tend to cross the retinotopy contours at near perpendicular intersection angles. This relationship is quantified in Supplementary Figures 1G-H, where we plot the percent of image pixels having intersection angles within 9 different ranges (0-10º, 10-20º, …, 80-90º). Clearly, as the intersection angle range increases, the amount of pixels within that range increases. This result indicates that the orientation and retinotopic maps have a strong correlation in normal ferrets, and was shown previously by our group. The same relationships are illustrated for monocular ferrets in Supplementary Figures 1F-H; the orthogonal relationships between the orientation and retinotopic map contours persist in the monocular animals (while the relationship is slightly stronger in monocular ferrets than in normal ferrets, caution must be taken in comparing the retinotopic and orientation map relationships between normal and monocular animals—see Supplementary Figure 2 below). Thus, it is clear that there is an inter-dependence between the retinotopic and

orientation maps in both normal and monocular ferrets: on average, these maps intersect each other orthogonally. Importantly, this is not evidence for a local co-variation between the gradients of the maps; rather, it appears to arise because the orientation domains are stretched along a specific axis of the azimuth map in both normal and monocular ferrets (see Chapter 1).

Artifacts associated with measuring the local structure of the retinotopic map with intrinsic signal optical imaging

We found possible systematic artifacts in measuring the local structure of the retinotopic map with intrinsic signal optical imaging, which are dependent on the stimulus paradigm employed and the nature of the cortical area examined. In the Fourier method of optical imaging, pioneered by Kalatsky and colleagues for measuring the retinotopic map, the stimulus is a bar that drifts orthogonally to its orientation (Supplementary Figure 2A). To measure the azimuth dimension of visual space, the stimulus is a vertical bar that moves horizontally. The bar drifts over the receptive field of each cortical pixel periodically, leading to a periodic and roughly sinusoidal temporal response pattern for each activated pixel. By performing Fourier analysis on the temporal response pattern for each pixel, the response magnitude of the pixel as well as the azimuth component of its receptive field location (relative to nearby image pixels) can be determined. The response magnitude is given by the amplitude of the Fourier component of the pixel's temporal response profile at the stimulation frequency, and the receptive field location is given by the phase of this Fourier component. Not unexpectedly, we find that the response magnitude of a pixel, due to periodic stimulation with an oriented bar,

depends on the pixel's orientation preference. Specifically, when the stimulus is a vertical bar, the response magnitude is largest for image pixels whose preferred orientation is near vertical (Supplementary Figures 2B-D). More surprisingly, we find that the difference between the response phases (receptive fields) of nearby pixels, i.e. the cortical magnification, also depends on the degree of activation of the pixels in the local region. Specifically, the azimuth retinotopic magnification increases with the degree of activation of the individual pixels (Supplementary Figure 2E). Further, given the observation that pixels whose preferred orientation is near vertical are activated the most strongly (Supplementary Figure 2D), it follows and indeed can be shown that retinotopic magnification is highest for pixels that have near vertical orientation preferences (Supplementary Figure 2F). This relationship could either reflect a real relationship between the azimuth retinotopic map and the orientation preference map, or could derive from an artifact of using a vertical stimulus to measure the azimuth map. We have performed further measurements that support the latter interpretation.

Specifically, we created a stimulus for measuring the azimuth retinotopic map that contains multiple orientation components, rather than simply a vertical component. The stimulus is an aperture within which are flashed gratings of 4 different orientations (Supplementary Figure 2G). Like the vertical bar stimulus used previously, this vertical aperture stimulus drifts horizontally, periodically drifting over each receptive field location. The stimulus robustly activates the cortex and can be used to measure the azimuth retinotopic map. Interestingly however, there is no longer a clear relationship between cortical activation and orientation preference—the relationship is noisy (Supplementary Figure 2J). Further, there is not a clear relationship between the azimuth

magnification and the preferred orientation (Supplementary Figure 2K). Thus, the relationship between azimuth magnification and preferred orientation is different depending on whether it is measured with a bar stimulus or an aperture stimulus. This implies that the retinotopic map measurement is prone to artifacts and that it is difficult to determine the true local structure of the map. The fact that orientation is mapped in domains in the ferret, combined with the fact that the retinotopic map is being measured with an oriented stimulus, are likely what give rise to the artifacts.

It also appears that the presence of the ocular dominance map confounds the measurement of the retinotopic map. In Supplementary Figure 2H, we show a map of ocular dominance from the ferret. We also measured the azimuth retinotopic map in this same region. Importantly, the stimulus was presented to the contralateral eye only, in order to avoid possible confounds arising from misalignment of the optic axes of the two eyes. We find that the response magnitude of a pixel, due to periodic stimulation with the aperture stimulus, depends on the pixel's ocular dominance value. Specifically, the response magnitude increases as the ocular dominance index becomes more contralateral (Supplementary Figures 2H-I, 2L). Further, as noted in the section above, the cortical magnification also depends on the degree of activation of the pixels in the local region. Specifically, the azimuth retinotopic magnification increased with the degree of activation of the individual pixels (Supplementary Figure 2M). Further, given the observation that contralateral-preferring pixels are activated the most strongly (Supplementary Figure 2L), it follows and indeed can be shown that retinotopic magnification is highest for contralateral-preferring pixels (Supplementary Figure 2N).

Thus, the presence of the ocular dominance map causes artifacts in the azimuth retinotopy measurement.

With regard to comparing, between normal and monocular ferrets, the relationships between the azimuth retinotopic map and the orientation map, the previous observations present a particular problem. Namely, our results indicate that the ocular dominance map is present in normal ferrets but absent in monocular ferrets (see Figure 2). If the presence of the ocular dominance map leads to artificial distortions in the measurement of the retinotopic map, then these artificial distortions are expected to be a problem in normal ferrets but not a problem in monocular ferrets (since they do not express an ocular dominance map), even when the same stimulus paradigm is used to measure the map in the two cases. Thus, it may not be meaningful to compare, between normal and monocular ferrets, the local structure of the retinotopic map, or the local relationships between the retinotopic and other maps, at least with the method of intrinsic signal optical imaging.

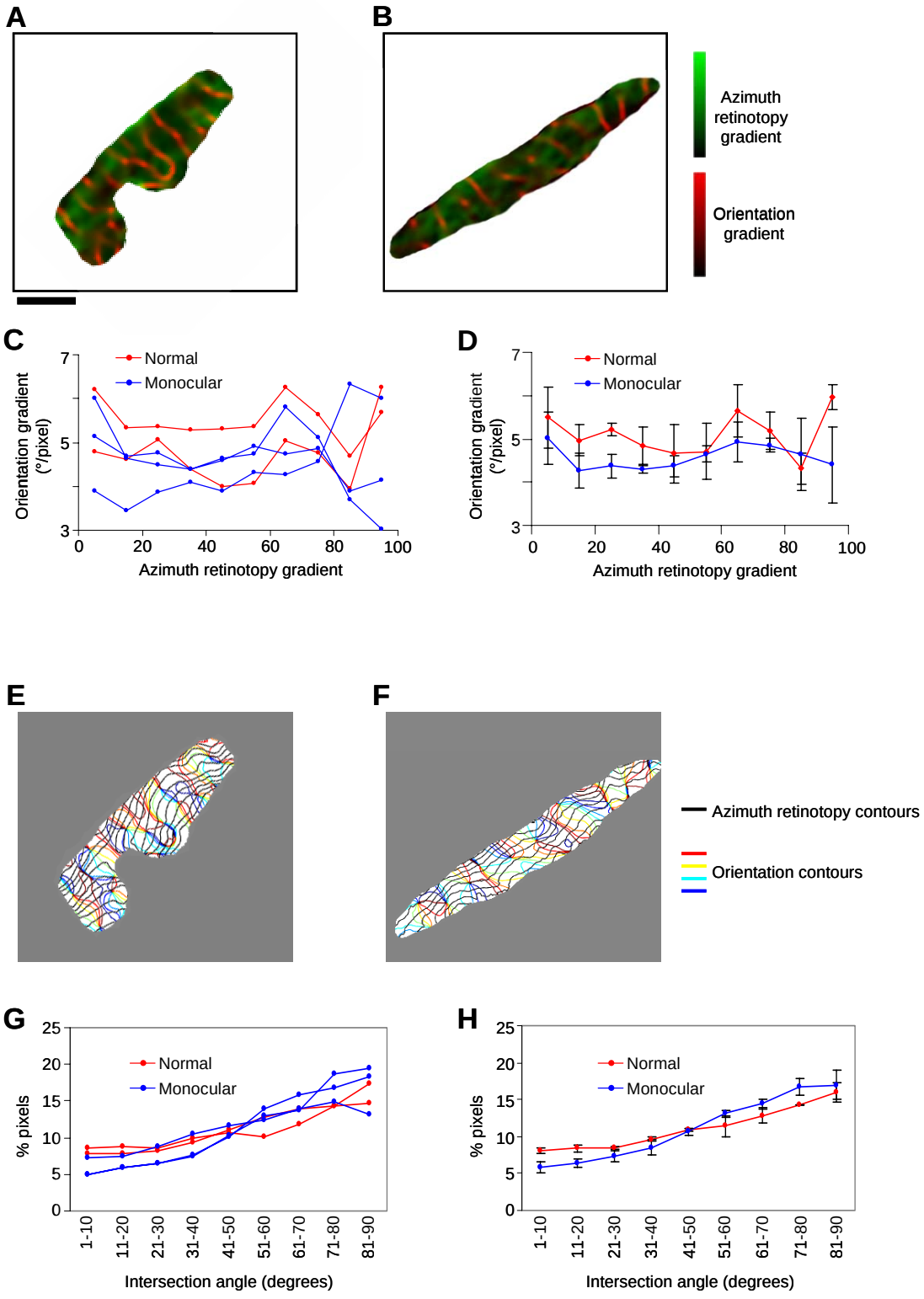

Supplementary Figure 1

Supplementary Figure 1. The relationship between the orientation gradient and the retinotopy gradient. (A-B) The orientation gradient map is superimposed on the azimuth retinotopy gradient map. Results are from a normal (A) or monocular (B) ferret. **(C)** For each individual animal, pixels from V1 are grouped into ten bins according to their azimuth retinotopy gradient (bin 1: 0-10% of maximum; bin 2: 10-20% of maximum; …) and the mean orientation gradient for each group is indicated. **(D)** Same as in (C), except each point represents the average over the individual cases within the group. Error bars denote standard error of the mean over 2 normal ferrets and 3 monocular ferrets. **(E-F)** Iso-orientation contours are superimposed on iso-azimuth contours. Results are from a normal (E) or monocular (F) ferret. **(G)** The percent of pixels in V1 having intersection angles, between the orientation gradient and the azimuth retinotopy gradient, within the 9 ranges indicated. **(H)** Same as in (G), except each point represents the average over the individual cases within the group. Error bars denote standard error of the mean over 2 normal ferrets and 3 monocular ferrets. Scale bar in (A) 1 mm, and applies to (A-B, and E-F).

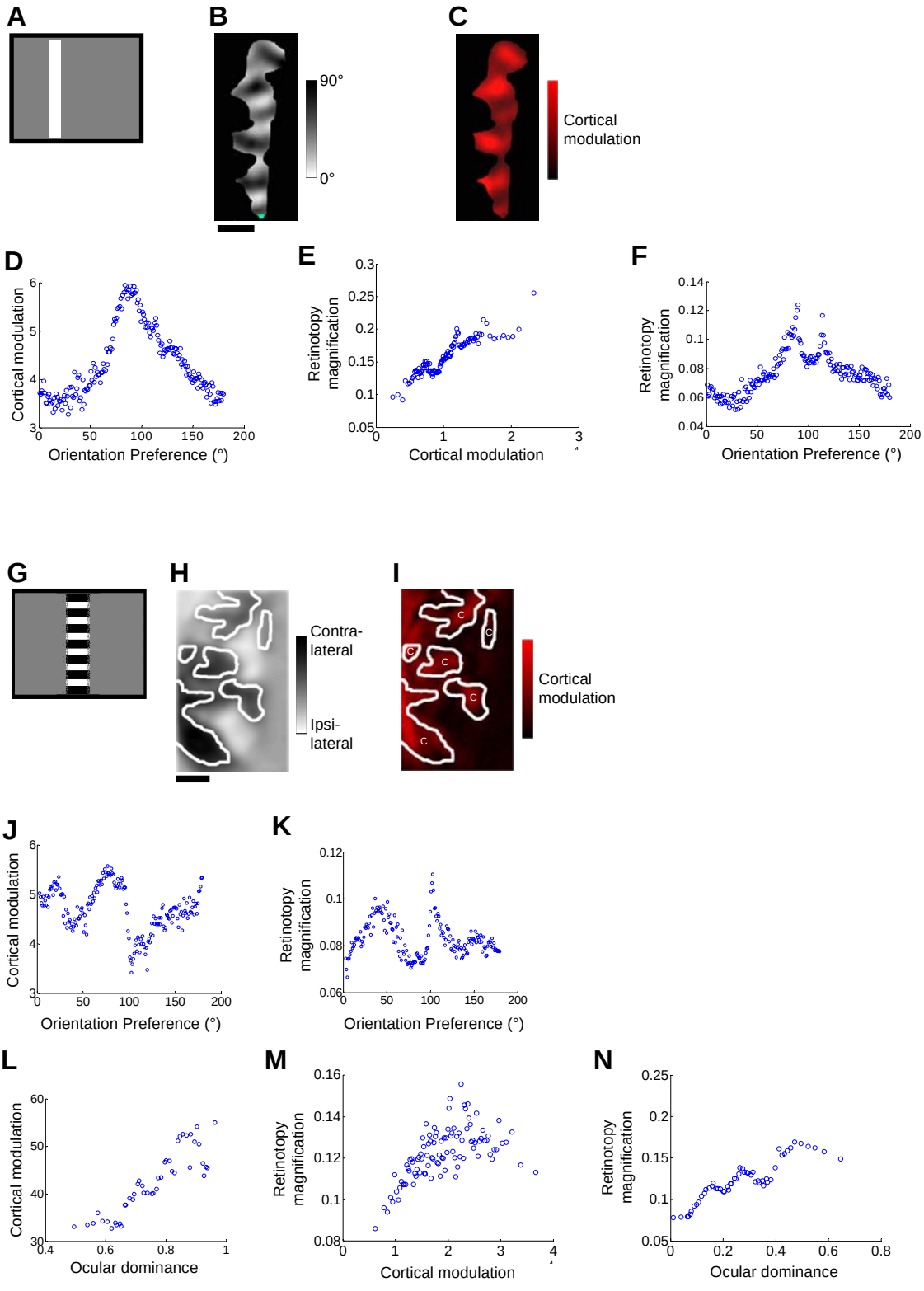

Supplementary Figure 2

Supplementary Figure 2. The map of visual space is affected by the orientation and ocular dominance parameters used to measure it. (A) A schematic view of the vertical bar stimulus used to measure the azimuth dimension of retinotopy. **(B)** A differential orientation map, obtained by subtracting the cortical response to a horizontal (0º) grating from the response to a vertical (90º) grating. **(C)** A map of the cortical modulation magnitude in response to a drifting bar stimulus, showing the magnitude of the Fourier component at the stimulus frequency. **(D)** The pixels from the imaged region were grouped according to their preferred orientation, and the average cortical modulation magnitude for each group was determined. **(E)** The pixels were grouped according to the modulation magnitude, and the average retinotopy magnification for each group was determined. **(F)** The pixels were grouped according to their preferred orientation, and the average retinotopy magnification for each group was determined. **(G)** A schematic view of (a snapshot of) the vertical aperture stimulus used to measure the azimuth dimension of retinotopy. **(H)** An ocular dominance map, obtained by subtracting the cortical response to stimulation of the ipsilateral eye from the response to contralateral eye stimulation. **(I)** A map of the cortical modulation magnitude in response to a drifting aperture stimulus, showing the magnitude of the Fourier component at the stimulus frequency. **(J)** The pixels from an imaged region (different than shown here) were grouped according to their preferred orientation, and the average cortical modulation magnitude due to the aperture stimulus for each group was determined. **(K)** The pixels from an imaged region, same as in (J), were grouped according to their preferred orientation, and the average retinotopy magnification for each group was determined. **(L)** The pixels from the imaged region shown in (H) and (I) were grouped according to their ocular dominance value, and the average cortical modulation magnitude for each group was determined. **(M)** The pixels from the imaged region shown in (H) and (I) were grouped according to the modulation magnitude, and the average retinotopy magnification for each group was determined. **(N)** The pixels from the imaged region shown in (H) and (I) were grouped according to their preferred ocular dominance, and the average retinotopy magnification for each group was determined.

REFERENCES

Baker GE, Thompson ID, Krug K, Smyth D, Tolhurst DJ (1998) Spatial-frequency tuning and geniculocortical projections in the visual cortex (areas 17 and 18) of the pigmented ferret. Eur J Neurosci 10:2657-2668.

Baker TI, Issa NP (2005) Cortical maps of separable tuning properties predict population responses to complex visual stimuli. J Neurophysiol.

Bartfeld E, Grinvald A (1992) Relationships between orientation-preference pinwheels, cytochrome oxidase blobs, and ocular-dominance columns in primate striate cortex. Proc Natl Acad Sci U S A 89:11905-11909.

Basole A, White LE, Fitzpatrick D (2003) Mapping multiple features in the population response of visual cortex. Nature 424:986-990.

Bauer HU (1995) Development of oriented ocular dominance bands as a consequence of areal geometry. Neural Comput 7:36-50.

Bisti S, Trimarchi C (1993) Visual performance in behaving cats after prenatal unilateral enucleation. Proc Natl Acad Sci U S A 90:11142-11146.

Bisti S, Trimarchi C, Turlejski K (1995) Prenatal monocular enucleation induces a selective loss of low-spatial-frequency cortical responses to the remaining eye. Proc Natl Acad Sci U S A 92:3908-3912.

Blasdel G, Campbell D (2001) Functional retinotopy of monkey visual cortex. J Neurosci 21:8286-8301.

Blasdel GG (1992) Differential imaging of ocular dominance and orientation selectivity in monkey striate cortex. J Neurosci 12:3115-3138.

Blasdel GG, Salama G (1986) Voltage-sensitive dyes reveal a modular organization in monkey striate cortex. Nature 321:579-585.

Bonhoeffer T, Kim DS, Malonek D, Shoham D, Grinvald A (1995) Optical imaging of the layout of functional domains in area 17 and across the area 17/18 border in cat visual cortex. Eur J Neurosci 7:1973-1988.

Bosking WH, Crowley JC, Fitzpatrick D (2002) Spatial coding of position and orientation in primary visual cortex. Nat Neurosci 5:874-882.

Buzas P, Volgushev M, Eysel UT, Kisvarday ZF (2003) Independence of visuotopic representation and orientation map in the visual cortex of the cat. Eur J Neurosci 18:957-968.

Carreira-Perpinan MA, Lister RJ, Goodhill GJ (2005) A computational model for the development of multiple maps in primary visual cortex. Cereb Cortex 15:1222-1233.

Crair MC, Gillespie DC, Stryker MP (1998) The role of visual experience in the development of columns in cat visual cortex. Science 279:566-570.

Crair MC, Ruthazer ES, Gillespie DC, Stryker MP (1997a) Relationship between the ocular dominance and orientation maps in visual cortex of monocularly deprived cats. Neuron 19:307-318.

Crair MC, Ruthazer ES, Gillespie DC, Stryker MP (1997b) Ocular dominance peaks at pinwheel center singularities of the orientation map in cat visual cortex. J Neurophysiol 77:3381-3385.

Crowley JC, Katz LC (1999) Development of ocular dominance columns in the absence of retinal input. Nat Neurosci 2:1125-1130.
Crowley JC, Katz LC (2000) Early development of ocular dominance columns. Science 290:1321-1324.
Cynader MS, Swindale NV, Matsubara JA (1987) Functional topography in cat area 18. J Neurosci 7:1401-1413.
Das A, Gilbert CD (1995) Long-range horizontal connections and their role in cortical reorganization revealed by optical recording of cat primary visual cortex. Nature 375:780-784.
Das A, Gilbert CD (1997) Distortions of visuotopic map match orientation singularities in primary visual cortex. Nature 387:594-598.
DeAngelis GC, Ohzawa I, Freeman RD (1993) Spatiotemporal organization of simple-cell receptive fields in the cat's striate cortex. I. General characteristics and postnatal development. J Neurophysiol 69:1091-1117.
Dragoi V, Sharma J, Sur M (2000) Adaptation-induced plasticity of orientation tuning in adult visual cortex. Neuron 28:287-298.
Durbin R, Mitchison G (1990) A dimension reduction framework for understanding cortical maps. Nature 343:644-647.
Engel SA, Rumelhart DE, Wandell BA, Lee AT, Glover GH, Chichilnisky EJ, Shadlen MN (1994) fMRI of human visual cortex. Nature 369:525.
Erwin E, Obermayer K, Schulten K (1995) Models of orientation and ocular dominance columns in the visual cortex: a critical comparison. Neural Comput 7:425-468.
Florence SL, Kaas JH (1992) Ocular dominance columns in area 17 of Old World macaque and talapoin monkeys: complete reconstructions and quantitative analyses. Vis Neurosci 8:449-462.
Friedman RM, Chen LM, Roe AW (2004) Modality maps within primate somatosensory cortex. Proc Natl Acad Sci U S A 101:12724-12729.
Goodhill GJ, Willshaw DJ (1990) Application of the elastic net algorithm to the formation of ocular dominance stripes. Network-Comp Neural 1:41-59.
Guillery RW, LaMantia AS, Robson JA, Huang K (1985) The influence of retinal afferents upon the development of layers in the dorsal lateral geniculate nucleus of mustelids. J Neurosci 5:1370-1379.
Herrmann K, Antonini A, Shatz CJ (1994) Ultrastructural evidence for synaptic interactions between thalamocortical axons and subplate neurons. Eur J Neurosci 6:1729-1742.
Horton JC, Hocking DR (1998) Effect of early monocular enucleation upon ocular dominance columns and cytochrome oxidase activity in monkey and human visual cortex. Vis Neurosci 15:289-303.
Hubel DH, Wiesel TN (1963) Shape and arrangement of columns in cat's striate cortex. J Physiol 165:559-568.
Hubel DH, Wiesel TN (1977) Ferrier lecture. Functional architecture of macaque monkey visual cortex. Proc R Soc Lond B Biol Sci 198:1-59.
Hubener M, Shoham D, Grinvald A, Bonhoeffer T (1997) Spatial relationships among three columnar systems in cat area 17. J Neurosci 17:9270-9284.
Issa NP, Trepel C, Stryker MP (2000) Spatial frequency maps in cat visual cortex. J Neurosci 20:8504-8514.

Issa NP, Trachtenberg JT, Chapman B, Zahs KR, Stryker MP (1999) The critical period for ocular dominance plasticity in the Ferret's visual cortex. J Neurosci 19:6965-6978.
Johnson JK, Casagrande VA (1993) Prenatal development of axon outgrowth and connectivity in the ferret visual system. Vis Neurosci 10:117-130.
Jones JP, Palmer LA (1987) The two-dimensional spatial structure of simple receptive fields in cat striate cortex. J Neurophysiol 58:1187-1211.
Kalatsky VA, Stryker MP (2003) New paradigm for optical imaging: temporally encoded maps of intrinsic signal. Neuron 38:529-545.
Kohonen T (1982a) Self-organized formation of topologically correct feature maps. Biol Cybern 43:59-69.
Kohonen T (1982b) Analysis of a simple self-organizing process. Biol Cybern 44:135-140.
Koulakov AA, Chklovskii DB (2001) Orientation preference patterns in mammalian visual cortex: a wire length minimization approach. Neuron 29:519-527.
Law MI, Zahs KR, Stryker MP (1988) Organization of primary visual cortex (area 17) in the ferret. J Comp Neurol 278:157-180.
LeVay S, Connolly M, Houde J, Van Essen DC (1985) The complete pattern of ocular dominance stripes in the striate cortex and visual field of the macaque monkey. J Neurosci 5:486-501.
Li Y, Fitzpatrick D, White LE (2006) The development of direction selectivity in ferret visual cortex requires early visual experience. Nat Neurosci.
Linden JF, Schreiner CE (2003) Columnar transformations in auditory cortex? A comparison to visual and somatosensory cortices. Cereb Cortex 13:83-89.
Lowel S, Schmidt KE, Kim DS, Wolf F, Hoffsummer F, Singer W, Bonhoeffer T (1998) The layout of orientation and ocular dominance domains in area 17 of strabismic cats. Eur J Neurosci 10:2629-2643.
Mante V, Carandini M (2003) Visual cortex: seeing motion. Curr Biol 13:R906-908.
Mante V, Carandini M (2005) Mapping of stimulus energy in primary visual cortex. J Neurophysiol.
Mrsic-Flogel T, Hubener M, Bonhoeffer T (2003) Brain mapping: new wave optical imaging. Curr Biol 13:R778-780.
Muller T, Stetter M, Hubener M, Sengpiel F, Bonhoeffer T, Godecke I, Chapman B, Lowel S, Obermayer K (2000) An analysis of orientation and ocular dominance patterns in the visual cortex of cats and ferrets. Neural Comput 12:2573-2595.
Obermayer K, Blasdel GG (1993) Geometry of orientation and ocular dominance columns in monkey striate cortex. J Neurosci 13:4114-4129.
Obermayer K, Ritter H, Schulten K (1990) A principle for the formation of the spatial structure of cortical feature maps. Proc Natl Acad Sci U S A 87:8345-8349.
Obermayer K, Blasdel GG, Schulten K (1992) Statistical-mechanical analysis of self-organization and pattern formation during the development of visual maps. Physical Review A 45:7568-7589.
Ohki K, Chung S, Ch'ng YH, Kara P, Reid RC (2005) Functional imaging with cellular resolution reveals precise micro-architecture in visual cortex. Nature 433:597-603.

Ohki K, Chung S, Kara P, Hubener M, Bonhoeffer T, Reid RC (2006) Highly ordered arrangement of single neurons in orientation pinwheels. Nature 442:925-928.
Rakic P (1981) Development of visual centers in the primate brain depends on binocular competition before birth. Science 214:928-931.
Rao SC, Toth LJ, Sur M (1997) Optically imaged maps of orientation preference in primary visual cortex of cats and ferrets. J Comp Neurol 387:358-370.
Redies C, Diksic M, Riml H (1990) Functional organization in the ferret visual cortex: a double-label 2-deoxyglucose study. J Neurosci 10:2791-2803.
Sengpiel F, Stawinski P, Bonhoeffer T (1999) Influence of experience on orientation maps in cat visual cortex. Nat Neurosci 2:727-732.
Sereno MI, Dale AM, Reppas JB, Kwong KK, Belliveau JW, Brady TJ, Rosen BR, Tootell RB (1995) Borders of multiple visual areas in humans revealed by functional magnetic resonance imaging. Science 268:889-893.
Shatz CJ, Stryker MP (1978) Ocular dominance in layer IV of the cat's visual cortex and the effects of monocular deprivation. J Physiol 281:267-283.
Sheth BR, Sharma J, Rao SC, Sur M (1996) Orientation maps of subjective contours in visual cortex. Science 274:2110-2115.
Shook BL, Maffei L, Chalupa LM (1985) Functional organization of the cat's visual cortex after prenatal interruption of binocular interactions. Proc Natl Acad Sci U S A 82:3901-3905.
Sur M, Wall JT, Kaas JH (1981) Modular segregation of functional cell classes within the postcentral somatosensory cortex of monkeys. Science 212:1059-1061.
Swindale NV (1991) Coverage and the design of striate cortex. Biol Cybern 65:415-424.
Swindale NV (1996) The development of topography in the visual cortex: a review of models. Network-Comp Neural 7:161-247.
Swindale NV (2004) How different feature spaces may be represented in cortical maps. Network 15:217-242.
Webster MA, De Valois RL (1985) Relationship between spatial-frequency and orientation tuning of striate-cortex cells. J Opt Soc Am A 2:1124-1132.
White LE, Bosking WH, Fitzpatrick D (2001a) Consistent mapping of orientation preference across irregular functional domains in ferret visual cortex. Vis Neurosci 18:65-76.
White LE, Coppola DM, Fitzpatrick D (2001b) The contribution of sensory experience to the maturation of orientation selectivity in ferret visual cortex. Nature 411:1049-1052.
White LE, Bosking WH, Williams SM, Fitzpatrick D (1999) Maps of central visual space in ferret V1 and V2 lack matching inputs from the two eyes. J Neurosci 19:7089-7099.
Wiesel TN, Hubel DH (1963) Single-Cell Responses In Striate Cortex Of Kittens Deprived Of Vision In One Eye. J Neurophysiol 26:1003-1017.
Wolf F, Bauer HU, Pawelzik K, Geisel T (1996) Organization of the visual cortex. Nature 382:306-307.
Yu H, Farley BJ, Jin DZ, Sur M (2005) The coordinated mapping of visual space and response features in visual cortex. Neuron 47:267-280. Reprinted with permission from Elsevier.